UNIVERSIDADE FEDERAL DE MINAS GERAIS
CTM AND DAIMLER AG
MECHANICAL ENGINEERING POSTGRADUATE PROGRAM

STUDY OF A BEARING TEST BENCH CAPABLE TO SIMULATE WEAR IN DIESEL START-STOP ENGINES

MASTER'S THESIS

Nathália Duarte Souza Alvarenga Santos

Belo Horizonte, MG, Brazil
2019

Nathália Duarte Souza Alvarenga Santos

STUDY OF A BEARING TEST BENCH CAPABLE TO SIMULATE WEAR IN DIESEL START-STOP ENGINES

Thesis presented to the Master's Degree Course of the Mechanical Engineering Graduate Program with emphasis in Energy and Sustainability, of Universidade Federal de Minas Gerais (UFMG), as a partial requirement for obtaining the degree of
Master Degree in Mechanical Engineering

Advisor: Prof. Dr. Ramon Molina Valle

Coadvisor: Thomas Krehahn

Belo Horizonte, MG, Brazil
2019

Santos, Nathália Duarte Souza Alvarenga.
S237s Study of a bearing test bench capable to simulate wear in diesel start-stop engines [manuscrito] / Nathália Duarte Souza Alvarenga Santos. – 2019.
121 f., enc.: il.

Orientador: Ramon Molina Valle.
Co-orientador: Thomas Krehahn.

Dissertação (mestrado) Universidade Federal de Minas Gerais, Escola de Engenharia.

Anexos: 120-121.

Inclui bibliografia.

1. Engenharia mecânica - Teses. 2. Automóveis - Consumo de combustíveis - Teses. 3. Simulação (Computadores) - Teses. I. Valle, Ramon Molina. II. Krehahn, Thomas. III. Universidade Federal de Minas Gerais. Escola de Engenharia. IV. Título.

CDU: 621(043)

UNIVERSIDADE FEDERAL DE MINAS GERAIS
PROGRAMA DE PÓS-GRADUAÇÃO EM
ENGENHARIA MECÂNICA
Av. Antônio Carlos, 6627 - Campus Universitário
31270-901 – Belo Horizonte – MG
Tel.:+55 31 3409.5145
E-mail: cpgmec@demec.ufmg.br

"STUDY OF A BEARING TEST BENCH CAPABLE TO SIMULATE WEAR IN DIESEL START-STOP ENGINES"

NATHALIA DUARTE SOUZA ALVARENGA SANTOS

Dissertação submetida à Banca Examinadora designada pelo Colegiado do Programa de Pós-Graduação em Engenharia Mecânica da Universidade Federal de Minas Gerais, como parte dos requisitos necessários à obtenção do título de **"Mestre em Engenharia Mecânica"**, na área de concentração de **"ENERGIA E SUSTENTABILIDADE".**

Dissertação aprovada no dia 29 de março de 2019.

Por:

Prof. Ramon Molina Valle
Orientador - Departamento de Engenharia Mecânica/ UFMG

Prof. Rudolf Huebner
Departamento de Engenharia Mecânica/ UFMG

Prof. Jose Guilherme Coelho Baeta
Departamento de Engenharia Mecânica/ UFMG

Prof. Fabricio Jose Pacheco Pujatti
Departamento de Engenharia Mecânica/ UFMG

Scanned with CamScanner

AKNOWLEDGMENTS

The following master thesis was written at Daimler AG in Untertürkheim - Germany in the department TP/PEM, Mechanics Core Engine. With this thesis I complete my studies as a master student in the Mechanical Engineering Graduate Program at the Universidade Federal de Minas Gerais – Brazil, representing intense academic growth and discoveries.

My appreciation goes above all to my parents, Milton Antonio and Jacqueline, my brother Rodolfo and my boyfriend Vinícius, for all the encouragement and support. I would like to thank the whole Daimler team, specially my team leader Dr. Jürgen Claus and Daniel Heinz for the opportunity to write this thesis in their department, my supervisor Thomas Krehahn, for the patience, guidance and great support, and Andreas Münker, Stefan Müller, Michele Novelli, Richard Nocke and Andre von Burg for the great help during the whole work.

I would also like to acknowledge the important role of my advisor, Dr. Ramon Molina Valle, for the excellent guidance and for sharing their vast experience and the Federal University of Minas Gerais for its master program, and CAPES for the scholarship.

I am very grateful at CTM - UFMG and Daimler AG for the opportunity to participate in projects of such technological development, so significant and important in my professional and personal growth.

Finally, I would like to thank my fellow postgraduate students for the daily contact, exchange of experiences, advices, study groups and friendship and specially my colleagues Lucimar Amaral, Florian Glenk and Ruth Martins.

ABSTRACT

The growing concern about the environmental impacts of the automobile sector activities has increased governmental regulations regarding fuel consumption and emissions reduction, mainly in Europe, pioneer in the implementation of such regulations. Thereby, the automotive industry has been developing strategies to adapt itself to these new requirements, and in that sense, the use of start-stop systems in the vehicles has been increasing. This system aims to reduce emissions and fuel consumption by stopping the engine at idle conditions, whether at traffic lights or in traffic jams. Such a system, more widely applied for passenger vehicles, has also been introduced for medium duty vehicles such as buses and medium trucks with urban routes. A major challenge in the start-stop implementation, however, is the alteration of the stresses applied to core engine components, such as piston, piston rings and bearings, since the temperature variation and lubrication supply for them is intermittent with the cyclic engine shutdown. As durability tests for such components using common dynamometric test benches are extremely expensive and time consuming, new test strategies have been recently explored. In this work, the main goal was to support the installation of a bearing test bench developed by Daimler AG, simulating the operation of their medium duty MDEG engines, and analyze its first results. The test bench is basically composed of hydraulic cylinders simulating the combustion load and a crankshaft rotated by an electric motor. The first tests, discussed in this work, show the difficulties of developing new test methods, such as problems in the oil conditioning system, the development of an operation program similar to regular engines and the wear measurements, as well as the lack of data acquisition capacity. However, the work shows the great potential of such a test bench after the explored obstacles have been overcome, as a quick and simple way to test bearings, and possibly other core engine components. In addition, the work suggests that the association of this experiment with computational tools can provide even more complete results, further contributing to the development of engines capable to withstand the implementation of start-stop systems.

Keywords: Start-stop, medium-sized engines, bearings, simulation

RESUMO

A crescente preocupação com os impactos ambientais das atividades do setor automobilístico têm aumentado a regulamentação governamental em relação ao consumo de combustível e redução de emissões, principalmente na Europa, pioneira na implementação de tais regulamentações. Dessa forma, a indústria automotiva vem desenvolvendo estratégias para se adaptar a esses novos requisitos, e nesse sentido, o uso de sistemas start-stop nos veículos vem aumentando. Este sistema visa reduzir as emissões e o consumo de combustível, desligando o motor em condições de marcha lenta com o veículo estacionário, seja em sinais de trânsito ou engarrafamentos. Tal sistema, mais amplamente aplicado para veículos de passageiros, também foi introduzido para veículos médios, como ônibus e caminhões médios com rotas urbanas. Um grande desafio na implementação start-stop, no entanto, é a alteração das tensões aplicadas aos principais componentes do motor, como pistão, anéis de pistão e bronzinas, pois a variação de temperatura e o fornecimento de lubrificação para eles é intermitente com o desligamento cíclico do motor. Como os testes de durabilidade de tais componentes usando bancadas dinamométricas comuns são extremamente caros e demorados, novas estratégias de teste têm sido exploradas recentemente. Neste trabalho, o principal objetivo foi ajudar na instalação de uma bancada de testes de bronzinas desenvolvida pela Daimler AG, simulando a operação de seus motores de médio porte MDEG, e analisar seus primeiros resultados. O banco de provas é basicamente composto de cilindros hidráulicos simulando a forca da combustão e um virabrequim acionado por um motor elétrico. Os primeiros testes, discutidos neste trabalho, mostram as dificuldades de desenvolver novos métodos de teste, como problemas no sistema de condicionamento de óleo, o desenvolvimento de um programa de operação similar a motores de combustão e as medições de desgaste, bem como a falta de capacidade de aquisição de dados de teste. No entanto, o trabalho mostra o potencial de tal banco de testes depois de os obstáculos explorados serem superados, como uma maneira rápida e simples de testar bronzinas e, possivelmente, outros componentes principais do motor. Além disso, o trabalho sugere que a associação deste experimento com ferramentas computacionais pode fornecer resultados ainda mais completos, contribuindo ainda mais para o desenvolvimento de motores capazes de suportar a implementação de sistemas start-stop.

Palavras-Chave: Start-stop, motores de médio porte, bronzinas, simulação

ZUSAMMENFASSUNG

Die wachsende Besorgnis über die Umwelteinflüsse der Automobilbranche hat vor allem in Europa als Vorreiter, zu einer Verschärfung der staatlichen Vorschriften in Bezug auf Kraftstoffverbrauch und Emissionsminderung geführt. Dabei hat die Automobilindustrie Strategien entwickelt, um diese neuen Anforderungen einzuhalten. Als eine dieser Maßnahmen hat der Einsatz von Start-Stopp-Systemen in Kraftfahrzeugen zugenommen. Dieses System zielt darauf ab, die Emissionen und den Kraftstoffverbrauch durch abschalten des Motors im Leerlauf z.B., wenn im Stau oder an einer Ampel angehalten wird, zu verringern. Ein derartiges System, dass für Personenkraftwagen weit verbreitet ist, wurde mittlerweile auch für Nutzkraftfahrzeuge mit mittlerer Nutzleistung, wie Busse und mittelschwere Lastkraftwagen mit innerstädtischen Routen, eingeführt. Eine große Herausforderung bei der Start-Stopp-Umsetzung ist jedoch die Änderung der Beanspruchungen auf Motorkomponenten wie Kolben, Kolbenringe und Lagerschalen welche durch Temperaturschwankungen und die veränderte Schmiermittelzufuhr durch das Zykliker Ausschalten des Motors verursacht werden. Da Dauerlauferprobungen für solche Bauteile mit gängigen Prüfständen extrem teuer und zeitaufwändig sind, wurden in der Vergangenheit neue Teststrategien untersucht. In dieser Arbeit das Hauptziel war die Betreuung von der Daimler AG entwickelter Lagerprüfstand Installierung und die Analyse von den ersten Ergebnissen. Bei diesem Prüfstand wird die Verbrennungslast durch Hydraulikzylinder und das drehen der Kurbelwelle durch einen Hydraulikmotor simuliert. Die ersten in dieser Arbeit besprochenen Tests zeigen die Schwierigkeiten bei der Entwicklung neuer Testmethoden. Dabei gab es z. B. Probleme mit dem Ölkonditionierungssystem, bei der Entwicklung eines Betriebsprogramms, welches normalen Motoren ähnelt, sowie einem Mangel an Dateien Akquisitionskapazität. Außerdem traten Probleme bei der Verschleißmessung auf. Die Arbeit zeigt jedoch, dass Potenzial eines solchen Prüfstandes, nach dem Überwinden der untersuchten Hindernisse als schnelle und einfache Möglichkeit, Lager und möglicherweise andere Kernkomponenten des Motors zu testen. Darüber hinaus legt die Arbeit nahe, dass die Verknüpfung dieses Experiments mit moderner Auswertungssoftware noch weiterführende Ergebnisse liefern kann, welche zur Entwicklung von robusten Motoren mit Start-Stopp-Systemen beitragen können.

Schlüsselwörter: Start-Stopp, mittelgroße Motoren, Lagerschalen, Simulation

CONTENTS

AKNOWLEDGMENTS 3
ABSTRACT 4
RESUMO 5
ZUSAMMENFASSUNG 6
CONTENTS 7
LIST OF ABREVIATIONS AND ACRONYMS 9
LIST OF SYMBOLS 9
LIST OF FIGURES 11
LIST OF TABLES 14
1 INTRODUCTION 15
1.1 General Aspects 15
1.2 Research Objectives 16
1.2.1 General Objectives 16
1.2.2 Specific objectives 16
2 LITERATURE REVIEW 17
2.1 Internal Combustion Engines 17
2.2 Tribological systems 22
2.2.1 Engine Friction 22
2.2.2 Lubrication 24
2.2.2.1 Hydrodynamic Lubrication 24
2.2.2.2 Elastohydrodynamic Lubrication 25
2.2.2.3 Boundary Lubrication 25
2.2.2.4 Lubrication Regime 26
2.2.2.5 Engine Oil 28
2.2.3 Cranktrain Components Wear 28
2.3 Bearings 30
2.3.1 Bearing Properties 31
2.3.2 Bearing Geometry 32
2.3.2.1 Bearing Diameter and Bearing Width 32
2.3.2.2 Grooves and Holes 33
2.3.2.3 Bearing Clearance 34
2.3.3 Bearing materials 34
2.4 Start Stop Systems 36
2.5 State of Art 37
2.5.1 Daimler's Start-Stop System 37

2.5.2 RNT evaluation of Start-Stop systems 38
2.5.3 Lubrication in MDEG Engines 48
2.5.1 Recent Development in Bearing Coatings 50
2.5.2 Wear simulation in start stop engine components 52
2.5.2.1 Computational simulation 53
2.5.2.2 Component test bench 54
3 METHODOLOGY 60
3.1 Introduction 60
3.2 TLPP 60
3.2.1.1 Hydraulic cylinder 61
3.2.1.2 Engine shaft 62
3.2.1.3 Electric Motor 62
3.2.1.4 Oil Conditioning 63
3.2.1.5 Connecting rods 64
3.2.1.6 TLPP Automatization 64
3.2.1.7 TLPP Program 66
3.3 Test Materials 67
3.4 Test Planning 68
4 RESULTS AND DISCUSSION 73
4.1 Preliminary Bearing Measurements 73
4.2 TLPP First Program 75
4.3 First Test 78
4.4 Second Test 84
4.5 Lubrication Regime 89
4.6 Wear Calculation 101
4.7 Third Test 102
4.8 New Test Program 107
5 Conclusion 111
6 Suggestions for future research 112
7 REFERENCES 113
ANNEX 1 120
A370 120
G488 120

LIST OF ABREVIATIONS AND ACRONYMS

ATS	After Treatment System
Al-Sn	Aluminum-Tin
BDC	Bottom Dead Center
CO_2	Carbon Dioxide
CO	Carbon Monoxide
CPU	Central Processing Unit
CI	Compression Ignition
CB	Conrod bearing
CMM	Coordinate Measuring Machine
Cu-Pb	Copper-lead
DFP	Diesel Particle Filter
FM	Federal Mogul
HC	Hydrocarbon
HLA	Hydraulic Launch Assistant
HTHS	High Temperature - High Shear
ISS	Idle Start-Stop
ICE	Internal Combustion Engine
Pb	Lead
Pb-based	Lead based
Pb-free	Lead free
MB	Main bearing
MR	Measurement Regulation
MDEG	Medium Duty Engine Generation
MoS_2	Molybdenum disulfide
NO_x	Nitrogen Oxides
PAI	Polyamide-Imide
PM	Particulate Matter
PEEK	Polyether Ether Ketone
PES	Polysulfones
PMC	Process Management Calculator
RNT	Radionuclide-technique
Sn	Tin
Sn-Ni	Tin-Nickel
TLPP	Triebwerkslager Puls Prüfstand - Engine Bearing Pulse Test Bench
SCR	Selective Catalytic Reduction
SAE	Society of Automotive Engineering
SI	Spark Ignition
CDPE	Steering Committee for Conservation and Management of the Environment and Natural Habits
TDC	Top Dead Center
VII	Viscosity Index Improvers
VM	Viscosity Modifiers
WHO	World Heath Organization
ZDDP	Zinc Dialkyldithiophosphates

LIST OF SYMBOLS

ω	Angular engine speed	rad/s
R_q	Asperity heights	mm
F_b	Bearing friction coefficient	-
D_b	Bearing diameter	mm
L	Bearing width	mm
P_b	Bearing pressure	bar
f	Coefficient of friction	-
β	Connecting rod angle	°
l	Connecting rod length	mm
F_{cr}	Connecting rod load	N
α	Crankshaft angle	°
c	Diametric bearing clearance	mm
N	Engine rotation	rpm
F	Friction force	N
F_g	Gas force in the cylinder	N
p_g	Gas pressure in the cylinder	bar
h_o	Minimum oil film thickness	mm
ω_b	Limit sliding bearing speed	rad/s
W	Normal load	N
v	Oil cinematic viscosity	mm²/s
ρ	Oil density	kg/mm³
μ	Oil dynamic viscosity (absolute)	Pa
l_2	Oscillating length of the connecting rod	mm
m_{os}	Oscillating masses	kg
F_{mos}	Oscillating masses force	N
A_p	Piston Area	mm²
D	Piston Diameter	mm
δ	Ratio between minimum lubricant film thickness and the bearing clearance	-
ψ	Relative bearing clearance	-
ε	Relative eccentricity	-
F_{crb}	Resultant load applied in the con rod bearing	N
F_p	Resultant load applied in the piston	N
m_p	Set of piston masses	kg
d	Shaft diameter	mm
u	Shearing velocity	m/s
a_1	Sommerfeld factor 1	-
a_2	Sommerfeld factor 2	-
S	Sommerfeld number	-
h	Thickness of the oil film	mm
Q	Wear rate	mm³/m
K	Wear coefficient	mm³/Nm

LIST OF FIGURES

Figure 2.1 - Loads and forces on an internal combustion engine, Credits: (Manual, 2000) 18
Figure 2.2 - Polar diagram of the forces for a conrod bearing, Credits: (Manual, 2000)19
Figure 2.3 - MDEG Conrod, Credits: Adapted (Global, 2018)..... 19
Figure 2.4 - Schematic distribution of forces in the cranktrain, Credits: (Nebelsiek, 2017) 21
Figure 2.5 - Load Distribution in a Crankshaft, Credits: Adapted from (Ltd, 2019) 22
Figure 2.6 - The Dependence of Surface Roughness and the Plasticity Profile of Surface Interaction, Credits: Adapted from (Hutchings e Shipway, 2017)..... 23
Figure 2.7 - Action of Oil Film in Plain Cylindrical Bearing, Credits: Adapted from (Rogowski, 1953) 25
Figure 2.8 - Cylindrical Bearing Dimensions, Credits: Adapted from (Rogowski, 1953) 26
Figure 2.9 - Types of Bearings in an Engine (Mahle, 2009)..... 31
Figure 2.10 - Geometric deviations in the bearing-crankshaft assembly: (a) conical grinding of journal, (b) conical housing bore, (c) excessive axial clearance, (d) tumble of crankshaft, Credits: (Manual, 2000). 32
Figure 2.11 - Bearing oil holes and grooves in different bearing types: a) Connecting Rod Bearing and b) Main Bearing, Credits: Adapted from (Mahle, 2009). 33
Figure 2.12 - Oil groove types in the bearings, Credits: (Tambellini et al., 2007)..... 34
Figure 2.13 - Bearing types: a) bimetallic b) trimetallic (Tambellini et al., 2007) 35
Figure 2.14 - Wear measurement with RNT 38
Figure 2.15 - Load distribution in bearings due to combustion, Credits: Adapted from cycle word (World, 2018) 39
Figure 2.16 - Engine start varying t1 and t2, Credits: Adapted from (Antriebstechnik, 2013) 40
Figure 2.17 - Ramps a) A and b) B for engine start, Credits: Adapted from (Antriebstechnik, 2013) 41
Figure 2.18 - Bearing wear considering different engine start conditions, Credits: Adapted from (Antriebstechnik, 2013)..... 43
Figure 2.19 - Influence of oil temperature on bearing wear pattern, Credits: Adapted from (Antriebstechnik, 2013)..... 44
Figure 2.20 - Influence of standstill time on conrod bearing wear pattern, Credits: Adapted from (Antriebstechnik, 2013)..... 45
Figure 2.21 - Influence of the rotational speed and load on con rod bearing wear pattern, Credits: Adapted from (Antriebstechnik, 2013)..... 46
Figure 2.22 - Bearing wear speed over number of engine starts, Credits: Adapted from (Antriebstechnik, 2013) 47
Figure 2.23 - MDEG lubrication circuit..... 48
Figure 2.24 - Lubricant flow rate as a function of engine speed..... 49
Figure 2.25 - Oil pressure build up after different stand still times, Source: Daimler Database 50
Figure 2.26 - FM Tin galvanic bearing coating, Credits: (Powertrain, 2010)..... 51
Figure 2.27 - FM IROX® bearing coating, Credits: (Powertrain, 2016)..... 51
Figure 2.28 - MIBA Synthec® bearing coating, Credits: (Manual, 2000). 52
Figure 2.29 - FM Bearing coating IROX II®, Credits: (Powertrain, 2016). 52
Figure 2.30 - Principle of a "Pin-on-disc" test for wear resistance, Credits: (Clausthal, 2018) 54

Figure 2.31 - Slider bearing test rig LP06 of the MIBA-Bearing Group, Credits: (Priestner et al., 2012) 56
Figure 2.32 - Bearing test rig, Credits: Adapted from (Katafuchi e Kasai, 2009) 56
Figure 2.33 - FM Stress Test, Credits: (Häring, 2018). 57
Figure 2.34 - FM Nautilus test, Credits: (Häring, 2018) 58
Figure 2.35 - FM Nautilus test rig, Credits: (Häring, 2018). 58
Figure 3.1 - TLPP Concept, Credits: (Nebelsiek, 2017) 61
Figure 3.2 - Actual TLPP configuration with an overview of the hydraulic cylinder 61
Figure 3.3 - Load measurement 62
Figure 3.4 - Engine shafts a) cranked MDEG series 6-cylinder shaft and b) uncranked TLPP shaft 62
Figure 3.5 - Assembly of the Electric Motor in the Test Bench 63
Figure 3.6 - Connecting rod types in TLPP: a) series con rod for cylinder 1, 4 and 6 and b) dummy con rod for cylinder 2, 3 and 5 64
Figure 3.7 - Conrod temperature measurement 64
Figure 3.8 - Test bench equipment automatization scheme 66
Figure 3.9 - Cylinder pressure and angular speed behavior during engine start, Credits: (Nebelsiek, 2017) 67
Figure 3.10 - Shell Oil Blue, 0W-20 oil viscosity dependence of temperature 68
Figure 3.11 - Bearing position for measurements 69
Figure 3.12 - CMM Measuring Tip, Credits: (Hexagon, 2018) 69
Figure 3.13 - Probe Testing Unit, Credits: (Retter, 2018) 70
Figure 3.14 - Wall thickness bearing measurement positions 70
Figure 3.15 - Machine MarSurf VD 140, Credits: (Mahr, 2019) 71
Figure 3.16 - Surface's biggest depth difference 71
Figure 4.1 - Wall thickness with horizontal measurements 74
Figure 4.2 - Wall thickness with longitudinal measurements 75
Figure 4.3 - TLPP program - Real engine start, Credits: Adapted from (Nebelsiek, 2017) 76
Figure 4.4 - First TLPP Program 77
Figure 4.5 - Wanted, Signal and Real Load Curves 78
Figure 4.6 - Bearings after test 1 79
Figure 4.7 - Profile of Upper Main Bearing 1 – Test 1 81
Figure 4.8 - Profile of Lower Main Bearing 1 – Test 1 82
Figure 4.9 - Profile of Lower Conrod Bearing 1 – Test 1 82
Figure 4.10 - Profile of Upper Conrod Bearing 1 – Test 1 83
Figure 4.11 - Profile of Upper Main Bearing 2 – Test 1 83
Figure 4.12 - Profile of Lower Main Bearing 2 – Test 1 84
Figure 4.13 - Bearings after test 2 85
Figure 4.14 - Profile of Upper Main Bearing 1 – Test 2 87
Figure 4.15 - Profile of Lower Main Bearing 1 – Test 2 87
Figure 4.16 - Profile of Upper Conrod Bearing 1 – Test 2 88
Figure 4.17 - Profile of Lower Conrod Bearing 1 – Test 2 88
Figure 4.18 - Profile of Upper Conrod Bearing 5 – Test 2 89
Figure 4.19 - Load and Rotation Variation during a power stroke, Credits: Adapted from (Nebelsiek, 2017) 90
Figure 4.20 - Rotation and Load recordings 92
Figure 4.21 - Estimation of Load Distribution in the Lower Main Bearings 92
Figure 4.22 – Second TLPP Program 103
Figure 4.23 - Bearings after test 3 103

Figure 4.24 - Conrod bearing profile before test 105
Figure 4.25 - Conrod bearing profile after test 1 106
Figure 4.26 - Conrd bearing profile after test 2 106
Figure 4.27 - Conrod bearing profile after test 3 107
Figure 4.28 - TLPP program - Simplified engine start, Credits: Adapted from (Nebelsiek, 2017) 108
Figure 4.29 - Engine cycle with Rotational Speed Plateaus, Credits: (Nebelsiek, 2017) 108
Figure 4.30 - Simplified TLPP Test Program 1 109
Figure 4.31 -Simplified TLPP Test Program 2 110
Figure 7.1 - Bearing A370 Composition 120
Figure 7.2 - Bearing G488 Composition 121

LIST OF TABLES

Table 3.1 - Bearing set for validation tests..... 67
Table 4.1 - Wear measurement of the first test 80
Table 4.2 - Wear measurement on the second test 86
Table 4.3 - Energy Application in EST Bearings during Start, Credits: (Nebelsiek, 2017) 90
Table 4.4 - Rotation Comparison in the Conrod Bearings – Before Test 1 93
Table 4.5 - Rotation Comparison in the Conrod Bearings – Before Test 1 94
Table 4.6 - Rotation Comparison in the Conrod Bearings – After Test 1 95
Table 4.7 - Rotation Comparison in the Main Bearings – After Test 1..... 96
Table 4.8 - Rotation Comparison in the Conrod Bearings – Before Test 2 97
Table 4.9 - Rotation Comparison in the Main Bearings – Before Test 2 98
Table 4.10 - Rotation Comparison in the Conrod Bearings – After Test 2 99
Table 4.11 - Rotation Comparison in the Main Bearings – After Test 2..... 100
Table 4.12 - Dimensional Wear Coefficient for Loaded bearing in the first and second test..... 101
Table 4.13 - Wear results of the third test..... 104
Table 7.1 - Bearing A370 Composition..... 120
Table 7.2 - Bearing G488 Composition..... 121

1 INTRODUCTION

1.1 General Aspects

The council of Europe, composed by member of the European Union and other European countries is the first and largest European political organization and the first intergovernmental organization to become aware of environmental problems. In 1962 it has set up a pioneer committee responsible of environmental protection called the Steering Committee for Conservation and Management of the Environment and Natural Habits (CDPE).

Since its creation it has issued a wide range of resolutions and recommendation to governments based on studies carried out by experts. One of the Committee's concerns is the environmental management, whose main problem is reconciling economic development and protection of the environment. The strategy around this problem is to adopt an integrated approach in agricultural, industrial and urbanization, aiming actions to be all embracing, coordinated and long term effective (Meyer, 1990).

According to the World Health Organization (WHO), urban air pollution is responsible for more than two million premature deaths each year and pointed as cause of pulmonary and cardiovascular diseases due to their inhalation (Medeiros De Araújo Nunes *et al.*, 2010). As a response to this treat to global health their air pollution guidelines are constantly updated, forcing governments to the same (Others, 2006).

The transport section represents big impact in air pollution since it is responsible for 20% of carbon dioxide CO_2 emissions (De Carvalho, 2011), alongside with carbon monoxide CO, hydrocarbon HC and nitrogen oxides NO_x and particulate matter PM (Kerimov e Mektiev, 1978; De Oliveira Aguiar *et al.*, 2015). With that concern in mind Europe introduced in 1970 its first exhaust emissions standard for passenger cars (Faiz *et al.*, 1996).

The next big change in the European vehicle emission control was made in 1992 and named the European Pathway. It consists of six stages of increasingly stringent emission control requirements, starting with Euro 1/I in 1992, and progressing through to Euro 6/VI. With its standards first presented in 2015 with the intention to be accomplished in 2018. The G-20 countries are responsible for 90 percent of global vehicle sales, and 17 out of the 20 members have chosen to follow the European regulations. A number of Asian and Latin American countries currently have Euro 2/II, 3/III, and 4/IV standards in force (Williams, 2016).

To meet this new emission standards and the market demand for lower fuel consumption, the automotive industry has been researching and incorporating strategies such as engine downsizing, weight lightening and low-rolling-resistance tires, improving vehicle aerodynamics and also considering hybridization and electrification of vehicles. One of the simplest measures found by vehicle manufactures is the stop-start technology, a low-cost solution in which the internal combustion engine is automatically switched off when the vehicle is stationary and restarted upon driver's demand or when needed. By this measure, especially in city traffic, in which the engines spend a great amount of time idling, the wasted energy from idling is reduced, decreasing considerably fuel consumption, and consequently emission rates (Fonseca *et al.*, 2011).

Thereby, since 2011 Daimler AG implemented the start-stop system in their light duty engines and decided, in 2013, to implement the start/stop system in the MDEG (Medium Duty Engine Generation) engines (Daimler, 2011; Nebelsiek, 2017). The start-stop system can be also seen as a step to introduce hybrid systems (Fonseca *et al.*, 2011),

in which an electric engine actuates at low speed and idle conditions whereas the internal combustion engine operates at high speed and longer distances. The switch from an engine to the other also demands quick start and stop of the internal combustion engine.

Despite the advantages of the start/stop and hybrid systems, the increased number of engine starts exposes the engine to more load transients and higher loads and alters the engine operation temperature, influencing on several core engine parts such as crankshaft, connection rods and bearings, which have presented in the early development stages unacceptable wear (Nebelsiek, 2017). Thereby, the research and development of a core engine adapted to these new systems have been made necessary.

1.2 Research Objectives

1.2.1 *General Objectives*

This work aims to support the installation of a component test developed to analyze the wear of the some MDEG (Medium Duty Engine Generation) engine parts which are most impacted by start-stop conditions, such as conrod and main bearings of and analyze its first results.

1.2.2 *Specific objectives*

- Follow the installation of the test bench, supporting with the initial difficulties;
- Development of first test operation programs;
- Determine operation parameters (Lubrication, temperature, materials);
- Evaluate wear in main and conrod bearings.

2 LITERATURE REVIEW

This chapter introduces the basic concepts of a compression ignition engine, the load profile on its mechanical elements, mainly in the connecting rod and main bearings, explains engine friction and principals of lubrication, gives an overview of how an engine can be affected with the start-stop system recently introduced in the MDEG engines and of the recent research on engine wear, in order to construct the necessary knowledge background to understand the hereby research and its results analysis. Most of the contents in this chapter can be traced to a known reference source. However, as this work is conducted inside an industry, some of the content are not related to a particular source, as they are considered common knowledge of the company or intern research.

2.1 Internal Combustion Engines

Internal combustion engines are thermal machines in which the conversion of chemical energy into thermal is done by burning or oxidizing a mixture of air and fuel in a combustion chamber inside the engine (Heywood, 1988; Van Basshuysen e Schäfer, 2004). One way to distinguish engines is by their ignition method. They can be either Spark Ignited (SI), in which the air fuel mixture admitted in the combustion chamber is ignited with a spark, or Compression Ignited (CI), in which the ignition of the fuel occurs spontaneously due to high temperatures caused by great air compression rates in the chamber, common used with Diesel, other similar oils and some gaseous fuels (Heywood, 1988). However, currently, the best classification among engines is by the dominant flame propagation regime, whether the premixed type or the diffusion type. In pre-mixed flame propagation regimes, it is possible to use all air present in the combustion chamber, which are more characteristic of the SIsystems. For this regime, combustion occurs rapidly, so it is possible to achieve very high specific potencies. In diffusion flame propagation regimes, more characteristic of the CI cycles, the thermal efficiency increases with the reduction of the engine load, there being no problems of anomalous combustion with the increase of the level of turbo-feeding (Baêta, 2006).

In a reciprocation engine, the energy produced by the fuel combustion is transformed in useful work as the combustion gases press a piston that moves back and forth transmitting power through a connecting rod and crank mechanism to the drive shaft. The majority of engines operate on what is known as a four-stroke cycle, in which each cylinder requires four strokes of a piston (corresponding to two crankshaft's revolutions) to complete the sequence of events, which produces one power stroke (Heywood, 1988). The four strokes are generally:

- **Intake:** The intake stroke starts with the piston at Top Dead Center (TDC) and ends with the piston at Bottom Dead Center (BDC). The descending movement of the piston with open inlet valves draws fresh air into the cylinder for natural aspirated engines. For supercharged engines the air is forced into the cylinder by a compressor.
- **Compression:** As valves close, the air inside the cylinder is compressed to a small fraction of its initial volume by the ascending movement of the piston. For CI engines, toward the end of this stroke fuel is injected and encounters air at pressure and temperature above its ignition point, and combustion is initiated, rapidly increasing cylinder pressure.

- **Power:** Also called the expansion stroke, the power stroke starts with the piston at TDC and ends at BDC as the exhaust gases from combustion push the piston down and force the crank to rotate.
  In the diesel engine combustion process, fuel vapor is produced within the combustion chamber during the injection spray, as the fuel drops encounter a high temperature environment. The fuel drops sprayed into the already high temperature combustion chamber flow into an already formed flame, vaporizing and initiating g the combustion process. After the flame initiation, the fuel still being injected flows into the flame. As the combustion chemical reaction takes place preferably where the temperatures are highest; just enough air flows from outside to reach stoichiometric with the fuel and release the fuel's complete combustion energy enter the flame. The combustion products diffuse away from the diffusion flame on the outside into the surrounding air, expanding the volume of the combustion chamber and moving the piston downwards (Heywood, 1988).
- **Exhaust:** In the exhaust stroke the burned gases are expelled with the ascending movement of the piston as the exhaust valves are opened. Just after TDC the exhaust valves close and the cycle starts again (Heywood, 1988).

Mainly during combustion, due to the dynamic gas and inertia forces, several engine components such as bearings present constant load application, which changes its direction and magnitude continuously. Loads and mass forces on the piston of a Diesel 4-stroke engine causing dynamic bearing loads are presented in Figure 2.1.

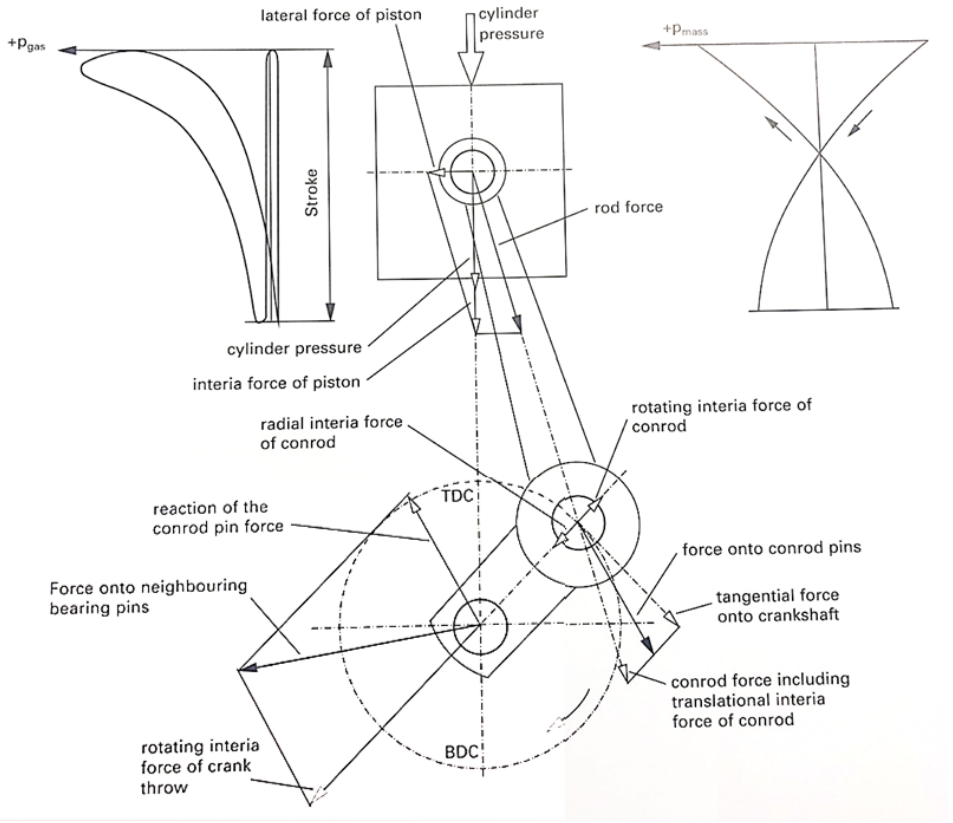


Figure 2.1 - Loads and forces on an internal combustion engine, Credits: (Manual, 2000)

Figure 2.2 exemplifies the typical bearing forces on a conrod big end bearing, presenting the load patterns according to the crankshaft angle. The load components of the bearing load during the engine operation are extremely difficult to measure. However, as Figure 2.2 shows, the main load on the bearing occurs near TDC, during the power stroke. Thereby, the calculations to estimate the load applied on the bearing can take only the combustion output into consideration (Manual, 2000).

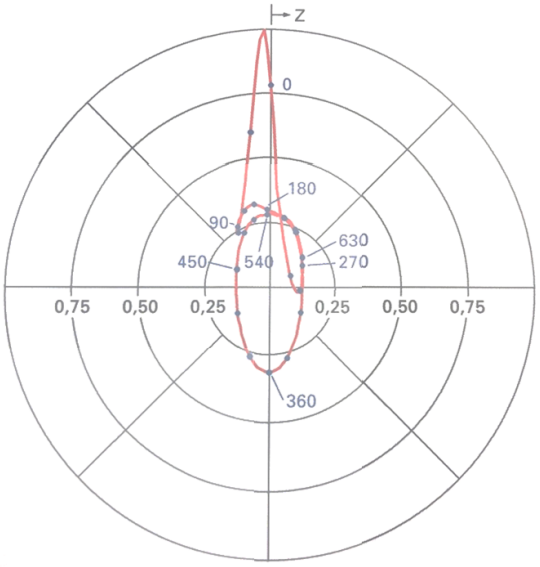


Figure 2.2 - Polar diagram of the forces for a conrod bearing, Credits: (Manual, 2000)

The MDEG conrod bearings, for constructive reasons have its big end rotated 45° in relation to the main rod, as shown in Figure 2.3, to facilitate its assembly. Therefore, the main load, occurring on TDC, is in degree 0° for the rod and 45° for the upper conrod bearing. Thus, it is expected that bearings assembled in a MDEG conrod have at 45° the highest load application, and consequently, the most wear. The main bearings are assembled, as usual, perpendicular to the load application, so for them, the highest load application, and consequently, the most wear, occur at 90°.

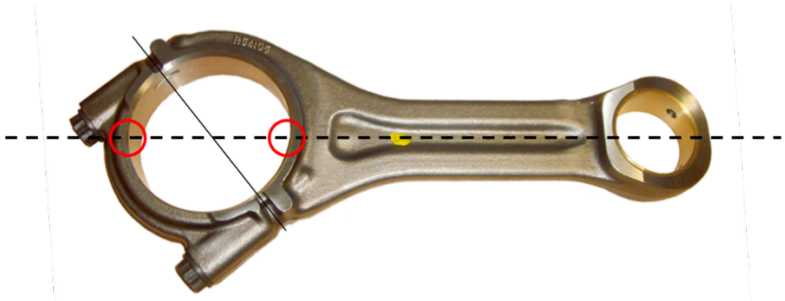


Figure 2.3 - MDEG Conrod, Credits: Adapted (Global, 2018)

The resultant load in a bearing during combustion after simplifications is composed of gas forces in the cylinder, the inertia force of the piston assembly masses and the inertia force of the connecting rod, both in the small and big ends (Uicker *et al.*, 2011). The load the combustion gases make in the piston, F_g, can be determined by Equation 2.1, in which p_g is the gas pressure in the cylinder and A_p is the area of the piston, given by Equation 2.2, in which D is the piston diameter.

$$F_g = p_g . A_p \qquad 2.1$$

$$A_p = \frac{\pi D^2}{4} \quad 2.2$$

The load caused by the gas pressure opposes the rotational movement of a set of oscillating masses, such as the piston, the piston rings and a portion of the connecting rod, generating a counteracting oscillating masses force F_{mos}, presented in Equation 2.3. This load is significantly influenced by the instantaneous crankshaft angular speed ω, the angle between crankshaft and conrod, α, shown in Figure 2.4, the set of oscillating masses, m_{os}, and connecting rod length, l. The crankshaft angle α describes the offset to TC (0º), in which the gas forces act on the piston (Affenzeller e Gläser, 2013). In the MDEG engines this angle varies between 2 to 10º (Nebelsiek, 2017).

$$F_{mos} = m_{os}.\frac{s}{2}.\omega^2.[cos(\alpha) + \lambda cos(2\alpha)] \quad 2.3$$

Equation 2.4 relates m_p, the masses of the piston package, l, the oscillating length of the connecting rod l_2 and the parameter m_{os} used in the Equation 2.3.

$$m_{os} = m_p + m_p.\frac{l_2}{l} \quad 2.4$$

Equation 2.5 presents the relation between the crankshaft angular speed in rad/s, ω, and N, the engine rotation in rpm.

$$\omega = 2\pi N \quad 2.5$$

The resultant of the combustion gas load on the piston and the counteracting oscillating masses load is the applied on the piston, F_p. This relation is shown in Equation 2.6

$$F_p = F_g - F_{mos} \quad 2.6$$

The connecting rod angle β indicates the current angle in which the connecting rod is in relation to the axis of the piston raceway. By the relations shown in Equation 2.7, the connecting rod load can be estimated by this angle and the load acting in the piston.

$$F_{cr} = \frac{F_p}{cos(\beta)} \quad 2.7$$

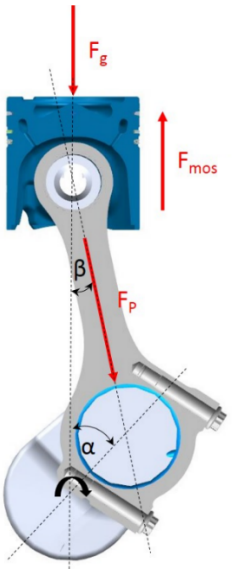


Figure 2.4 - Schematic distribution of forces in the cranktrain, Credits: (Nebelsiek, 2017)

The load in the connecting rod can also be considered as the load in the upper conrod bearings, F_{crb}. This load is the main responsible for the wear in these bearings. By knowing the combustion pressure in the cylinder, this load and so the way it varies during the engine operation can be calculated.

The knowledge of the load pattern incident on the bearing during engine start is a very important step of this research, as it directly influences bearing wear, whose analysis is the aim of this work. In the situations studied, the F_{mos} can be neglected, as it represents in average 0.3% of the whole gas forces in the cylinders due to its low angular speed in idle conditions. Also, as the angle between crankshaft and conrod is so small, its influence can be neglected. Then, with these simplifications and also disregarding friction losses due to the piston and conrod movements, the load in the conrod can be considered the load produced from the combustion gases, as presented in Equation 2.8 (Nebelsiek, 2017).

$$F_g = F_p = F_{cr} = F_{crb} \tag{2.8}$$

The load applied in the main bearings is much more complicated to estimate and although several studies have been focused in using mathematical models and computational analysis to simulate crankshaft stresses (Jung *et al.*, 2009; Salvinder *et al.*, 2016; Sun *et al.*, 2016). However, as this is not the focus of this work, the load actuating in the lower main bearings can be estimated by basic concepts of structural analysis, considering the balance of normal and shear stress and bending moments and disregarding the presence of energy losses between conrod and crankshaft, as shown in Figure 2.5. The simplifications suggested in the Figure 2.5 are to consider the crankshaft a regular beam and the lower main bearing positions as simple bearing supports, instead of an area of load distribution (Leet *et al.*, 2014).

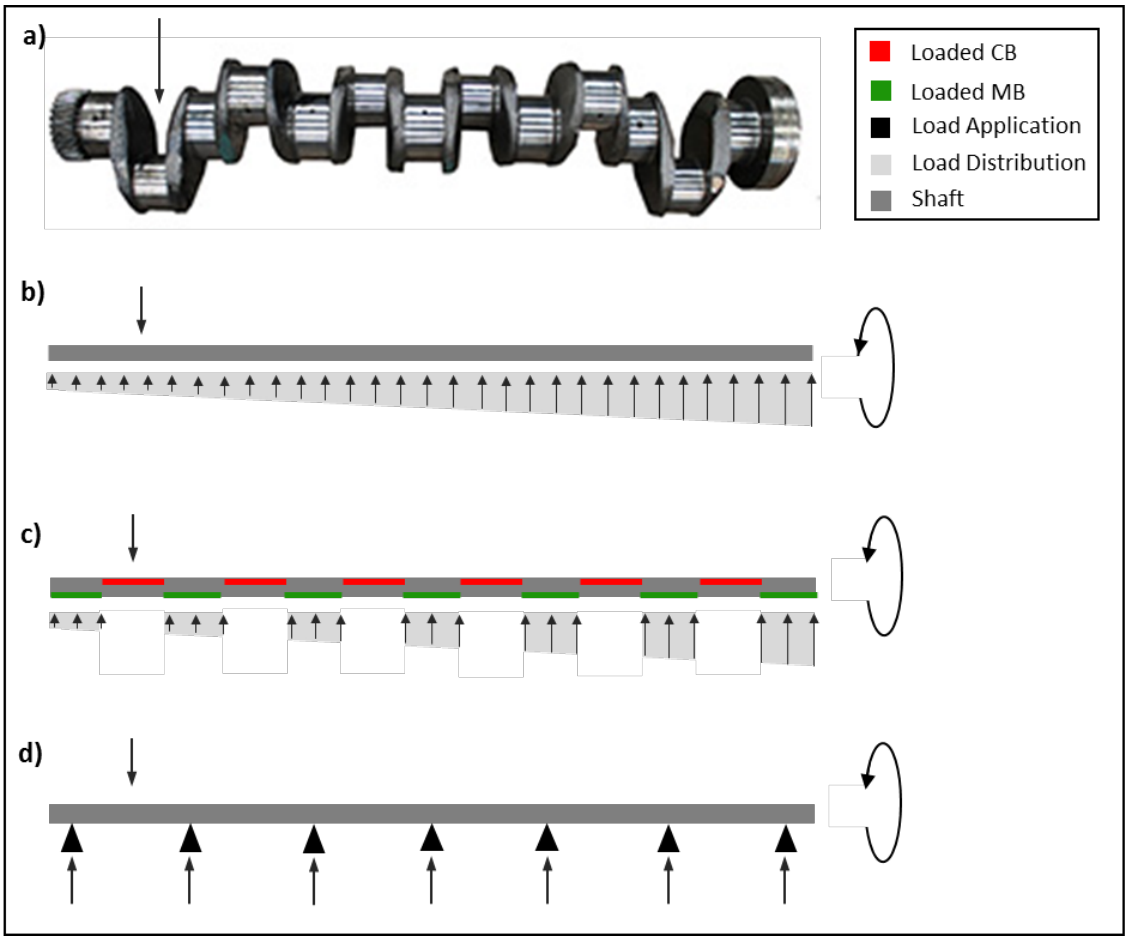


Figure 2.5 - Load Distribution in a Crankshaft, Credits: Adapted from (Ltd, 2019)

2.2 Tribological systems

Tribology is defined as the science and technology of interacting surfaces in relative motion and of the practices related thereto. This science embraces the scientific investigation of all types of friction, lubrication and wear (Zum-Gahr, 1987). Reciprocating engines contain several tribological systems, one of them being the crankshaft-bearings systems, main focus of this present research. In order to understand this particular system and the friction, lubrication and wear involved, these three topics will be better explained in the following subsections.

2.2.1 *Engine Friction*

Friction is the resistance to motion and rises from interaction of solids at the real area of contact, being a case of energy dissipation and characterizes an engineering system, being not an intrinsic material property (Zum-Gahr, 1987; Bowden e Tabor, 2001). The total friction loss in an engine can be divided into pumping and mechanical friction. As in average, 70% of the total friction is mechanical, this particular matter should be studied in deep. The greatest cause of mechanical friction is the sliding friction between piston and cylinder wall. The remaining fraction is due to bearings and to auxiliaries such as fans, pumps and magnetos (Rogowski, 1953).

According to (Bowden e Tabor, 2001), the sliding friction force arises from two sources: the adhesion force developed at the asperity contacts and the deformation

force needed to plough the asperities of the harder surfaces to the softer (Hutchings e Shipway, 2017).

Even highly polished mechanical components present, in some level, surface roughness. When two surfaces interact, the profile of their asperities and the level in which they are pressed against each other determine the intensity of the contact. When these surfaces slide over each other, the less contact the irregularities have, due to good surface polishing or less pressure, the higher the elastic profile of the deformation. On the other hand, as shown in Figure 2.6, the more irregularity contact, the higher the plastic deformation (Hutchings e Shipway, 2017).

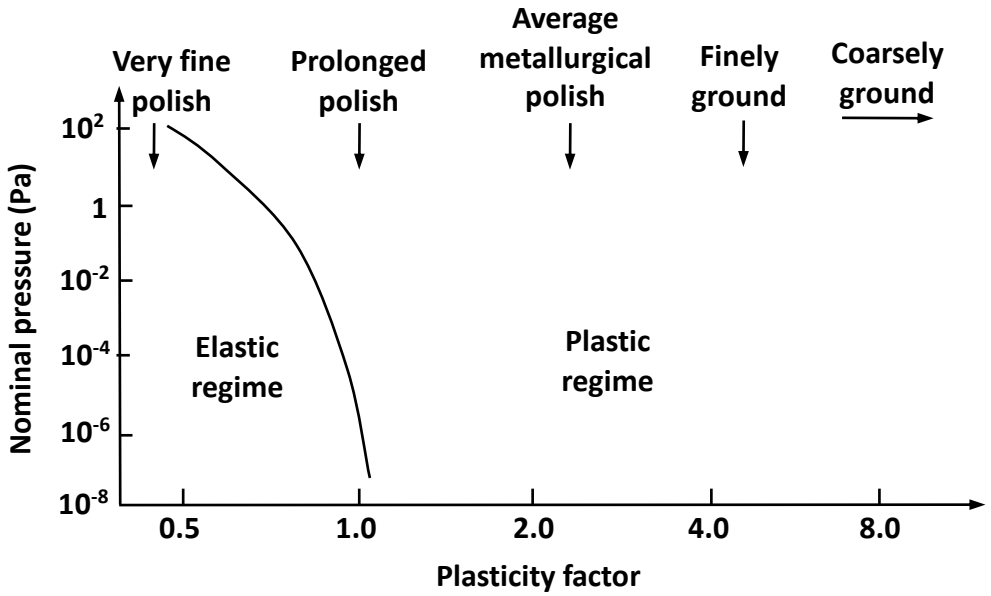


Figure 2.6 - The Dependence of Surface Roughness and the Plasticity Profile of Surface Interaction, Credits: Adapted from (Hutchings e Shipway, 2017)

As such, the type of deformation occurring during sliding has great influence on the friction force. In this way, the friction force, F, the load acting normal to the surfaces influencing adhesion, W, and the coefficient of friction, f, determined by technical features of the contact, can be related by Equation 2.9 (Rogowski, 1953).

$$f = \frac{F}{W} \qquad 2.9$$

Pure rolling consists of the movement of a disklike or circular object along a surface with punctual contact between them. The friction in this case is normally static. For sliding to occur, the static friction has to be overcome, but normally the static friction force is higher than the dynamic friction force, present when the sliding movement is already established. Hence, the static friction coefficient is higher than the dynamic one (Hutchings e Shipway, 2017).

When two unlubricated surfaces slide over each other f is practically constant over all range of loads and rubbing velocities and depends principally upon the materials of which the surfaces are made and the mechanical roughness of the surfaces. It varies among different materials and sometimes during the sliding process, mainly due to work-hardening and junction growth, effects caused by plastic deformation intrinsic to the process which alter the surfaces' characteristics (Rogowski, 1953; Hutchings e Shipway, 2017).

Equation 2.9 suggests that a good way to decrease friction force is to lower *f* by interposing the two sliding surfaces with a film of material with low shear strength, such as lubricants and bearings made with special materials and coatings (Hutchings e Shipway, 2017).

2.2.2 *Lubrication*

The purpose of lubrication is to minimize friction force and energy loss due to surface sliding by separating moving surfaces with a layer of material with lower shear strength than the surfaces themselves. Although in some cases the lubricant may not completely separate the surfaces, lubrication can reduce irregularity contact or the strength of their junctions. Thereby, to a greater or lesser extent, lubrication can decrease friction and wear (Zumbühl, 1946; Rogowski, 1953; Hutchings e Shipway, 2017). According to this description and considering various potential lubricant materials, four types of lubrication can be defined:

- **Hydrodynamic:** Condition in which the surfaces are separated by a lubricant film thicker than their asperity heights and the hydrostatic pressure of the film causes little elastic distortion of surfaces;
- **Elastohydrodynamic:** Condition in which the lubricant film is relatively thin, local pressures are high and, therefore, elastic deformation of the surfaces cannot be neglected;
- **Boundary:** Condition in which considerable irregularity contact occurs and lubrication cannot totally prevent junction and wear;
- **Solid:** Condition in which solid materials of low shear strength are used instead of fluid or semi-fluid films to separate sliding surfaces.

As all these lubrication conditions are constantly seen between sliding surfaces and coexist in the same contacts during engine operation, each of them will be explained and discussed in detail.

2.2.2.1 Hydrodynamic Lubrication

Hydrodynamic lubrication occurs when surfaces are closed matched in dimensions so that they can be separated by only a relatively small gap compared to the area, such as opposed planes and plain bearings and shafts. With this geometry the surfaces can be completely separated by an oil film and the friction is only caused due to the resistance to shear of the oil film, requiring significantly smaller forces to be overcome (Zumbühl, 1946; Rogowski, 1953). The hydrodynamic friction does not depend on the normal load, *W*, and thus, is practically independent of the roughness of the parts or of the material of which they are made (Rogowski, 1953).

When a shaft turns in a bearing, some of the lubricant adheres to the shaft and is carried around with it making the clearance under the shaft smaller than on the entering side and causing a certain eccentricity. Viscous resistance to the return flow of this oil builds up the hydrodynamic oil pressure, keeping surfaces from contact, as shown in Figure 2.7 (Hutchings e Shipway, 2017). As load in the bearing decreases or the rotational speed increases, the shaft and its housing tend to be concentric, and with load increase or decrease in rotational speed the eccentricity increases (Hutchings e Shipway, 2017).

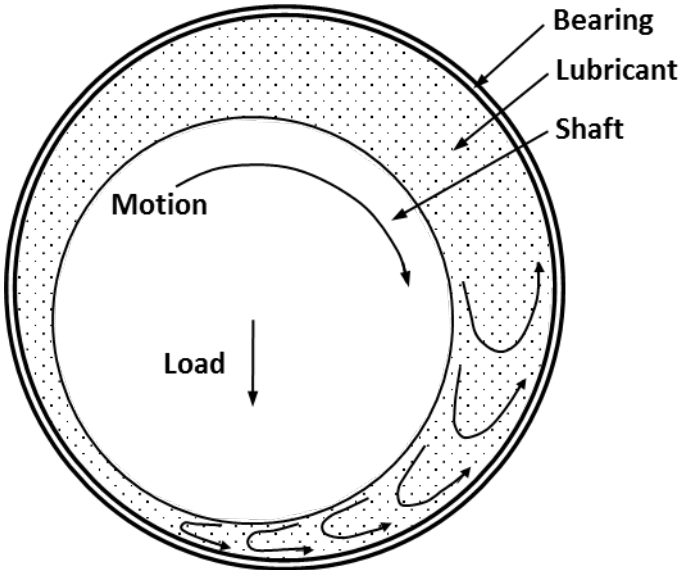


Figure 2.7 - Action of Oil Film in Plain Cylindrical Bearing, Credits: Adapted from (Rogowski, 1953)

The viscous friction load on bearings in this case depends upon the oil viscosity, engine speed, the size and the geometry of the bearing, but not upon the loading for wedge flow conditions. The normal load influences only when it tends to squeeze out the oil film and reduce the oil film thickness, *h*, what is common on big-end connecting rod and main bearings subjected to large cyclic loading by the varying force of the piston, such as during engine start (Hutchings e Shipway, 2017).

2.2.2.2 Elastohydrodynamic Lubrication

Elastohydrodynamic lubrication occurs when the contacting surfaces are counter formal, involving nominally lines or point contacts. This local contact increases local pressure that will be generally much higher than the hydrodynamic pressure. At this condition, the film thickness is 1-5μm, which is a small percentage of the bearing clearance and also a lot smaller than the size of several particles transported by the lubricant (Manual, 2000). Under this condition, the lubricant viscosity on pressure and the elastic deformation on surfaces play important roles. The contact area and pressure distribution are modified due to elastic deformation of the surfaces and the effect of film thickness on normal load is very slight, whereas sliding velocity and viscosity have higher impact. To analyze and calculate parameters under this condition, numeric solutions are necessary (Hutchings e Shipway, 2017).

2.2.2.3 Boundary Lubrication

At extremely high loads or low sliding speeds the hydrodynamic forces of the lubrication are insufficient to maintain a fluid film between surfaces, leading to film breakdown and direct contact between asperities. At this condition, high friction and wear will occur unless boundary lubrication is applied. By some authors, this condition is also called “inefficient lubrication” (Czichos, 1976).

2.2.2.4 Lubrication Regime

The lubrication regime between bearings and crankshaft variate intensively during engine operation and especially during an engine start due to the variation in the load patterns. In the highest loaded points the fluid film can break, especially if the rotation is not high enough, promoting direct contact between shaft and bearing, increasing wear rates and damaging both shaft and bearing surfaces (Nebelsiek, 2017). This regime can be roughly estimated by calculations taking into consideration the pressure applied in the bearing, lubrication and bearing geometric patterns.

The pressure made over a bearing, in special, can be calculated as the normal load applied in the bearing per unit of projected area, as shown in Equation 2.10, where D_b and L are respectively the diameter and length of a cylindrical bearing, presented in Figure 2.8 (Rogowski, 1953).

$$P_b = \frac{F_b}{LD_b} \tag{2.10}$$

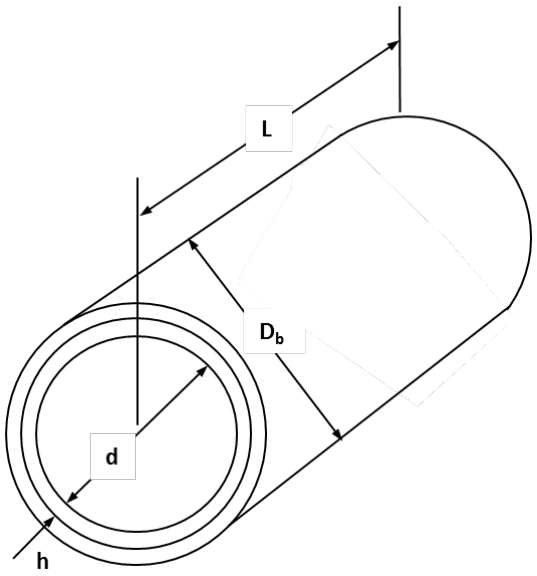


Figure 2.8 - Cylindrical Bearing Dimensions, Credits: Adapted from (Rogowski, 1953)

The Figure 2.8 presents also the shaft diameter, d, and the average lubricant thickness, h. The difference between bearing and shaft diameter is the bearing clearance, c, corresponding to the double of the average lubricant thickness. The relative bearing clearance, ψ, is given by Equation 2.11 (Nebelsiek, 2017).

$$\psi = \frac{D_b - d}{D_b} \tag{2.11}$$

Equation 2.12 determines the dynamic viscosity, μ, as a function of the cinematic viscosity, ν, and of the oil density, ρ.

$$\mu = \rho\nu \tag{2.12}$$

The Sommerfeld number for rotation, an indicator of the eccentricity of the shaft within its housing, can also help to determine the lubrication regime and is given by

Equation 2.13, in which ε is the relative eccentricity given by Equation 2.14 and a_1 and a_2 are given by Equation 2.15 and 2.16. The eccentricity, ε, is dependent on the average lubricant thickness, h, as well as the minimum lubricant film thickness, h_0, and the relative lubricant film thickness, δ, is the ratio between minimum lubricant film thickness and the bearing clearance (Affenzeller e Gläser, 2013).

$$S = \left(\frac{L}{D_b}\right)^2 . \frac{\varepsilon}{2(1-\varepsilon^2)^2} . \sqrt{\pi^2(1-\varepsilon^2)+16\varepsilon^2} . \frac{a_1(\varepsilon-1)}{a_2+\varepsilon} \qquad 2.13$$

$$\varepsilon = 1 - \delta \qquad 2.14$$

$$a_1 = 1{,}1642 - 1{,}9456\left(\frac{L}{D_b}\right) + 7{,}1161\left(\frac{L}{D_b}\right)^2 - 10{,}1073\left(\frac{L}{D_b}\right)^3 + 5{,}0141\left(\frac{L}{D_b}\right)^4 \qquad 2.15$$

$$a_2 = -1{,}000026 - 0{,}023634\left(\frac{L}{D_b}\right) - 0{,}4215\left(\frac{L}{D_b}\right)^2 - 0{,}038817\left(\frac{L}{D_b}\right)^3 - 0{,}090551\left(\frac{L}{D_b}\right)^4 \qquad 2.16$$

Knowing the pressure applied between the counter surfaces, geometric characteristics of the bearing, given by the Sommerfeld number and the relative bearing clearance, and lubrication specifications, a limit sliding bearing speed, ω_b, can be calculated, as shown in Equation 2.17.

$$\omega_b = \frac{P_b \psi^2}{\mu S} \qquad 2.17$$

The limit sliding bearing speed represented the minimum speed in which the hydrodynamic pressure built by the lubrication film can withstand the load applied in the counter surfaces. Hence, comparing the limit sliding bearing speed with the actual bearing angular speed, ω, the following can be concluded:

$\omega_b < \omega \quad \rightarrow$ Hydrodynamic lubrication
$\omega_b > \omega \quad \rightarrow$ Elastohydrodynamic lubrication / Boundary Regime

Although this method gives just a rough estimative of the lubrication regime, and cannot distinguish Elastohydrodynamic and Boundary lubrication, this analysis can already indicate the occurrence of counter body contact and help to explain wear during engine operation.

2.2.2.5 Engine Oil

Engine oils have two main functions: to control engine temperature by transferring heat through conduction as it flows through the engine and lubrication. It can also absorb shock loads, reduce noise and by having some additives added, can prevent corrosion, and also be a cleaning agent.

A lubricant consists of a mixture of base oils (80–95%) and a mixture of lubricant additives. Either the choice of base oils and additives are determinant to the lubricant properties desired in a particular operation. The viscosity of an oil must be well determined as it has to be sufficient to prevent film seizure at highest loads and lower speeds but not excessive, which could result in high friction losses and interfere with the oil flow through piping (Rogowski, 1953).

Viscosity is highly dependent on temperature and pressure and is normally higher at low temperatures and high pressures and to rate how the oil viscosity is affected by temperature and weather changes viscosity index are used. Oils are graded by SAE (Society of Automotive Engineering) through the resolution SAE J300 with indexes close to zero as they assimilate themselves with naphthenic oil, highly influenced but temperature variation and close to 100 when then are similar to paraffin-base oil, almost unchanged. For winter grade oils the dynamic viscosity is measured at different cold temperatures, and the lower the viscosity grade, the lower the temperature the oil is tested and for non-winter grade oils, the kinematic viscosity is measured at a temperature of 100 °C. The higher the viscosity, the higher the SAE viscosity grade is (Bates, 1986).

However, for the design and development of engine moving parts such as bearings, camshafts, pistons and liners, the knowledge of lubricant characteristics with the temperature is incomplete and more important are the characteristics of an oil as the engine runs at high speed. Hence, another lubricant viscosity classification by SAE J300 was specified, with viscosity measurements at temperatures of 150°C and shear rate of approximately 106 Hz, condition more similar to an actual engine operation, in which oil particles are deformed, stretched and sheared. These test results are designed to ensure the oil quality and properties at operating temperatures and that the oil film strength is sufficient to minimize wear. The viscosity measured under such conditions is called High Temperature-High Shear (HTHS) viscosity (Zadorozhnaya *et al.*, 2016).

2.2.3 *Cranktrain Components Wear*

Wear, as well as friction, is not an intrinsic material property, but a characteristic of the engineering system, and represents material dissipation. It can be determined as the progressive loss of material from a solid body surface due to mechanical action, normally related to relative motion of surfaces or its contact with a solid, liquid or gaseous counter body (Materials, 1969; Normung, 1979). It is rarely catastrophic, but beyond representing energy loss and reduction of operating efficiency, it may result in dimensional changes of components or surface damage, causing secondary problems such as vibration or misalignments. Moreover, the generation of wear debris, mainly in systems with small clearances, may be more damaging than the component dimensional changes (Barwell, 1979).

Independently of any special wear mode, the type of mechanical contact is very important for all wear losses, mainly during immediate contact between solid surfaces, without any interfacial medium such as adsorbed layers, oxides, lubricants, dirt, etc. (Zum-Gahr, 1987).

The normal force between asperities determine the contact among asperities and is directly related to surface wear. The number of asperity contacts can increase with the normal load, also altering the contact character. When the contact of asperities is independent of the normal load, the increase of normal load increases deformation of each contact, and may change the contact from elastic to plastic (Archard, 1953).

Wear can be caused by several mechanisms of energetic and material interactions between the elements of a tribosystem. The main wear mechanisms studied in this work will be the sliding and abrasive wear. The sliding wear is the surface damage caused by relative motion between two smooth solid surfaces in contact under load. The load creates adhesive junctions among surface asperities and the relative motion between surfaces lead these junctions to be torn away and form new irregularities and cause progressive loss of material. This wear mechanism is highly influenced by the contact between surfaces, elastic of plastic or totally separated by lubrication, and material properties (Zum-Gahr, 1987).

The abrasive wear is the most rapid form of wear and it is basically the surface loss of material by the passage of particles of equal or greater hardness. It normally involves both plastic flow and brittle fracture and has difficult prevention, precisely because several wear mechanisms can be involved in the contact between the surface and particles. Normally, the application of a hard material or hard coating is used to solve this problem. Ceramic and polymeric materials can be sufficient hard and homogeneous and, because of that, are constantly used to coat softer materials as steels and non-ferrous metals in order to prevent such wear (Stachowiak *et al.*, 1994).

Even though sliding wear is harder to avoid, due to its systematic presence, it can be estimated, what is extremely important to the design of a component, as it predicts the component lifetime and reduce economic losses caused by component failure or reposition during an equipment operation. Extrapolations using the actual system can be made by measuring the wear during some time of equipment operation and extrapolated to predict the component lifetime. This technique, however, may not be accurate as wear rates in some systems are not constant throughout time. They can decrease after a running-in period (normally in lubricated systems where sliding wear is dominant) or they may increase after an initial incubation period (if the material coating is removed due to wear and the wear behavior of the lower layer is different).

Wear can be also estimated theoretical or empirical equations relating wear rate to the operating variables such as load and speed. A simple model for wear brought by Holm and Archard suggests that the amount of material removed from sliding body is dependent on the sliding distance and the nominal pressure (load divided by the nominal contact area over the contact region. The model can roughly estimate wear, as presented in Equation 2.18, which relates wear rate, Q, which is the volume removed per unit sliding distance, to the normal load, W. In this equation H_S is the hardness of the softer surface between the two and K is a dimensionless wear coefficient dependent on the state of lubrication and further material properties.

$$Q = \frac{KW}{H_s} \qquad 2.18$$

In general, there is no direct correlation between wear rate and coefficient of friction (Stachowiak *et al.*, 1994). It is important to highlight that, not only this equation presents only a wear estimation, the parameters needed for the calculation can vary along

the process and in the same material. Thus, better wear estimations are obtained either by simulations or experimental tests that can better represent the reality.

This equation, however, presents for engineering applications a valuable means of comparing the severity of wear processes in different wear systems for different materials. Specifically, the quantity K/H_S or the symbol k (mm^3/Nm) is called the dimensional wear coefficient and represents the volume of material removed by wear (mm^3) per unit of normal load (N) per distance slid (m) and is very helpful to compare wear rates in different materials (Hutchings e Shipway, 2017).

The wear estimation can be also made using component test in which wear is estimated thought simulations of conditions which are expected in the component service, method particularly frequent to predict wear in bearings, varying loads, speeds, temperatures and states of lubrication. Test conditions used to accelerate wear production must be done with caution to ensure that the wear mechanism is not changed and other relevant operating conditions remain the same (Stachowiak *et al.*, 1994).

2.3 Bearings

Bearings are used to increase the functional strength of a moving connection between two components. Plain bearings, specifically, are necessary to separate surfaces that present relative sliding movement in relation to the other. This spacing is provided by a viscous lubricating film, which creates a pressure field that withstands external loads with proper design of the surfaces and their relative movement. Most plain bearings used in automotive engines are shown in Figure 2.9 and can be listed as:

- Connecting rod bearing for the large connecting rod eye,
- Connecting rod bushings for the small connecting rod eye,
- Main bearings,
- Fitting or guide bearings,
- Thrust washers.

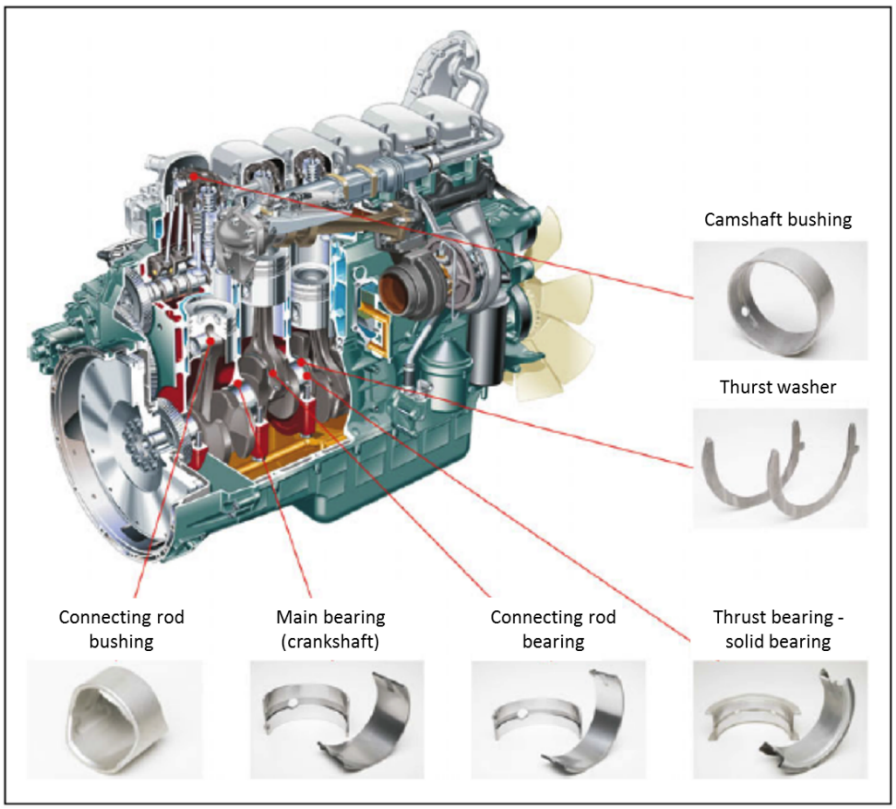


Figure 2.9 - Types of Bearings in an Engine (Mahle, 2009)

In the present work, only the main and connecting rod bearings will be studied.

2.3.1 *Bearing Properties*

The right choice of bearing material is based on the engine profile of application and material properties. The bearing load profile can describe the mechanical and tribological requirements of the bearing. The material selection is always the result of a compromise between all properties, which are often of opposite nature. The main properties desired in a bearing are listed hereafter.

- **Resilience:** Ability to endure mechanical loads permanently without developing fatigue cracks;
- **Wear Resistance**, mainly under the conditions of mixed lubrication regime and in the presence of foreign particles circulating with the lubricant;
- **Compatibility (Seizure Resistance):** Ability of the material to resist physical joining the journal in the limit lubrication area, where bearing and journal materials come to a direct contact;
- **Embeddability:** Ability of the material to absorb hard particles on the sliding surface and circulating in the lubricant oil;
- **Conformability:** Ability to compensate and accommodate misalignments prevenient of geometric variations in local contacts of the journals, housing or bearings, as shown in Figure 10;
- **Corrosion Resistance:** Ability to resist corrosion caused by weak organic acids and strong mineral acids derived from fuel combustion products and

weak organic acids, formed as result of the oxidation of lubricating oil (Mahle, 2009);

- **Cavitation Resistance:** Ability to withstand impact stresses caused by collapsing cavitation bubbles, which are formed as a result of sharp and localized drops of pressure in the flowing lubricant (Tambellini *et al.*, 2007; Mahle, 2009);

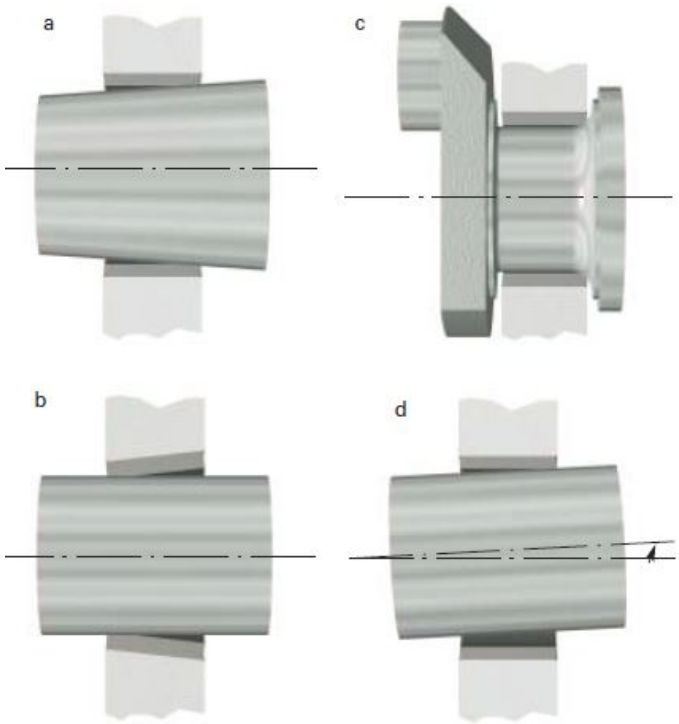


Figure 2.10 - Geometric deviations in the bearing-crankshaft assembly: (a) conical grinding of journal, (b) conical housing bore, (c) excessive axial clearance, (d) tumble of crankshaft, Credits: (Manual, 2000).

These properties can be evaluated during or after service trials, but can also be individually tested by several procedures. Contact stresses, thermal conditions, sliding speeds and chemical environment are determinant in any wear test. As such, it is important to guarantee that the testing conditions and wear and lubrication regimes represents the real operation conditions (Mahle, 2009).

2.3.2 *Bearing Geometry*

Several constructive parameters have to be taken into consideration during bearing design. The most important ones are listed and explained in the following subsections.

2.3.2.1 Bearing Diameter and Bearing Width

The width/diameter ratio L/D affects the operating characteristics of the bearing. At a given projected plain bearings bearing surface, the higher L/D ratio bearing experiences lower oil film pressures, greater minimum oil film thicknesses and, thus, more favorable stress conditions (Gmbh, 2009; Mahle, 2009). Bearings can be mainly divided into two categories regarding its width:

- **Thick-walled bushes and shells:** This design is used when the housing has a low stiffness. Thus, it is possible to maintain the functionality of the bearing without a strain in a housing. Thick-walled slide bearings are usually made of a single material or made of a maximum of 2 components (support body + bearing material).
- **Thin-walled bushes and shells:** This type reaches its desired end position only by the pressed or strained seat in the housing. It should be noted here that, at every operating point, the tension is high enough to prevent the bearings from turning. When not installed, thin-walled bearings are neither dimensionally stable nor round. In contrast to thick-walled bearings, these can consist of up to 4 different materials (Nebelsiek, 2017).

2.3.2.2 Grooves and Holes

Through grooves and holes, as shown in Figure 2.11, the lubricating oil gets from the oil canals to the bearing surface. To help the oil distribution between bearing and shaft, sometimes groves and milled canals are machined in the bearings. The groves can be built in the partial or total area of the bearing, as show in Figure 2.12. Regardless of their important role in lubrication, they are undesirable in stressed areas because they increase the maximum oil film pressure and reduce the minimum oil film thickness. When receiving high loads, there is an increased risk of contact of the sliding parts or of cavitation damage of the bearing material. Thereby, oil hole and grooves are placed only in the upper main and lower con rod bearings, the ones suffering lower loads, mainly due to the compression stroke (Mahle, 2009; Nebelsiek, 2017).

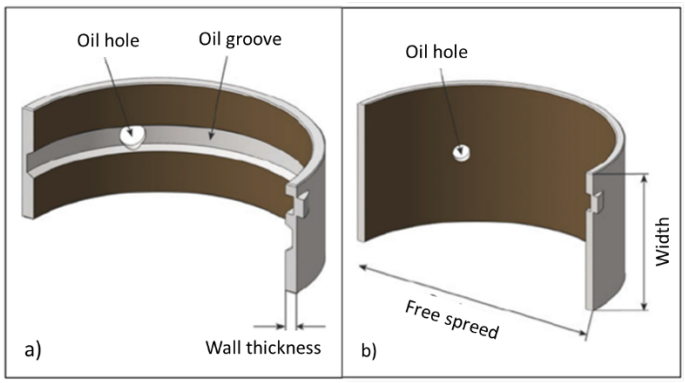


Figure 2.11 - Bearing oil holes and grooves in different bearing types: a) Connecting Rod Bearing and b) Main Bearing, Credits: Adapted from (Mahle, 2009).

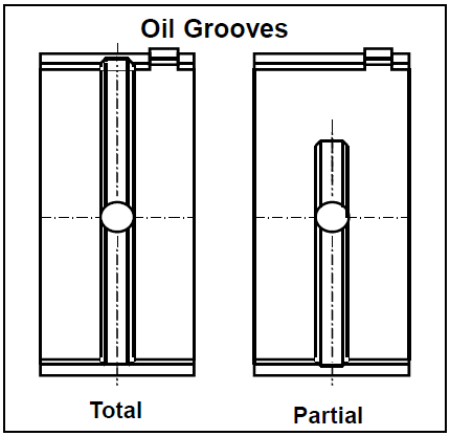


Figure 2.12 - Oil groove types in the bearings, Credits: (Tambellini *et al.*, 2007).

2.3.2.3 Bearing Clearance

The bearing clearance has a double effect on the properties of the oil film. On the one hand, with a small clearance the loads are better distributed, since the bearing journal curvature almost corresponds to the bearing curvature and produces a lower maximum oil film pressure. On the other hand, small clearances cause greater heat generation, which reduces the oil viscosity (Mahle, 2009). The lower clearance limits are 0.6% of the shaft diameter for conrod bearings and 0.75% for main bearings (Manual, 2000).

2.3.3 *Bearing materials*

The material selection for mechanical components, in general, take several factors into consideration, such as costs, corrosion resistance, mechanical properties such as strength, stiffness and toughness, and also tribology. Metals are the most common choice of materials for this kind of application as their composition and microstructure are largely standardized and have easily predicted properties. Nonmetallic materials are less well standardized and their properties tend to vary more widely.

For both metallic and non-metallic materials, unlike physical and mechanic properties, tribological properties of materials are difficult to be expressed by numbers and quantities. Hence, for components such as bearings, in which tribology plays an important role, the selection of materials and surfaces is less quantitative and more dependent on generalized rules and previous experiments.

Ceramics can exhibit very low wear coefficients, but present some drawbacks as their mechanical properties may not be adequate for the component demands, their fabrication in some special shapes can be unpractical and severe wear can lead to surface fracture. Some of these disadvantages can be overcome by using the material in form of coatings. These and other hard coatings, surface work hardening procedures, rough surfaces in general and diffusion layers of very low ductility can confer good surface wear resistance as they present low solubility with other materials and present limited junction growth. Polymers are normally used in bearing materials, mainly under marginal or dry lubrication. The most common polymers used in tribological applications are the nylons (polyamides), acetal, Polyether Ether Ketone (PEEK) and Polysulfones (PES).

For the material selection it is also important to consider the type of lubrication used during the bearing operation. Bearings have normally a steel backing and a bearing lining of a few hundred micrometers in thickness applied on top. Considering

that bearings in start-stop operation will remain long with boundary lubrication or in direct contact with the shaft, they can be considered marginally lubricated. In this application, bronze leaded alloys were very common before the concern with health impacts. Lead presents a great lubricant capacity, especially important in boundary lubrication regimes, and can increase conformability and embeddability but, as its content increases it decreases the load capacity. Copper and tin alloys are also a very common alloy base for linings (Hutchings e Shipway, 2017).

Modern bearing design tends to consider different materials and alloys and their respective load limits, obtained through simulations, test bench and engine tests. The limits set for main and conrod bearings are overestimated for safety reasons, considering possible misalignments. Depending on the test results for each material and application, it is decided if a bearing just with a lining is capable of withstanding the given operation, or other material layers are need. Thus, bearings can be distinguished into bimetallic and trimetallic bearings, as shown in Figure 2.13 (Gmbh, 2009; Mahle, 2009):

- **Bimetallic bearings:** They are normally used for bushings and thrust washers and usually consist of a steel supporting shell coated with a lining of aluminum, bronze alloy or white metal. Their tribological performance is determined by the bearing lining itself (Gebretsadik *et al.*, 2015);
- **Trimetallic bearings:** They have also a steel supporting shell coated with an aluminum or bronze alloy lining. However, an intermediate layer with thickness varying from 1-4µm is deposited on the top of the lining as a diffusion barrier. Finally, an overlay with a thickness of some tenths of microns is electroplated or sputtered on the top, what improves most of the required tribological properties, such as friction, seizure resistance, conformability and embeddability (Grün *et al.*, 2011). Due to the material variety used, the trimetallic bearings have more load capacity, achieving optimal combination of individual properties. The sputters variables are under development to endure the new engine concepts, with different load capacities (Tambellini *et al.*, 2007).

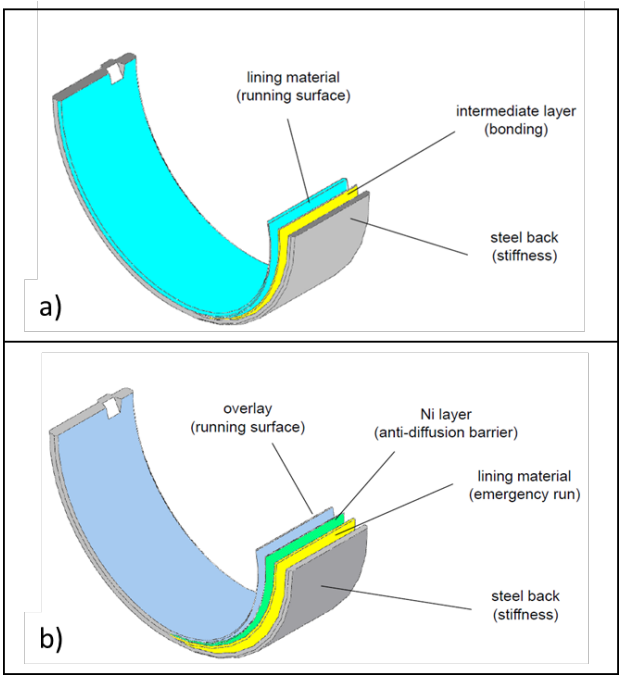


Figure 2.13 - Bearing types: a) bimetallic b) trimetallic (Tambellini *et al.*, 2007)

2.4 Start Stop Systems

One of the major challenges faced by vehicle manufacturers is the increasing fuel prices and stricter regulations on emissions and CO_2, motivating technological improvements such as downsizing, low-rolling-resistance tires, aerodynamic improvements and vehicle electrification (Rueger, 2008; Canova e Sala, 2009). However, the presence of electric vehicles in the near future is difficult to be established due to lack of infrastructure and high prices (Ozdemir e Mugan, 2013). As a compromise, hybrid systems, that combines the power source of the internal combustion and electric engine (Rizzoni *et al.*, 1999; Martinez *et al.*, 2011), become widespread and slowly introducing the electric concept, basic being divided in three developing stages (Baumann *et al.*, 2000; Salmasi, 2007; Van Berkel *et al.*, 2012):

- **Micro hybrid:** The electric engine is only used to store energy (Regenerative Braking) and to switch off the engine in idle conditions, restarting it upon driver's demand or when needed (Start-Stop);
- **Mild hybrid:** The electric engine has more capacity and can help to accelerate the engine or store energy from the engine break, in addition to working as a start-stop, but cannot run the vehicle alone;
- **Full hybrid:** The electric engine can power the car alone for some time at mild speed. In this configuration, the electric motor is used for low speed city traffic and to recover kinetic energy of the ICE during braking, and the ICE is used only for higher speeds (Chan, 2007), optimizing the operations of the power sources (Fang e Qin, 2006; Gurkaynak *et al.*, 2009).

The engine stop-start is a simple and low-cost strategy to reduce the energy waste when vehicle is stationary, what has been increasing with the urban vehicle fleet growth and leads to more time at traffic lights and in traffic jams. It is estimated that the energy spent in idle conditions can account for up to 10% of total fuel consumption (Rueger, 2008) and that in well-developed idle stop systems, the fuel economy is estimated to be between 7 and 9% (Floraday, 2009).

In order to guarantee good drivability, special methods should be adopted to promote a quick switch between the two engines, and specially, a quick internal combustion engine start (Kataoka e Tsuji, 2005). The start-stop operation in that sense can cause additional vibration and noise (Kuang, 2006), affecting on passenger comfort and increasing torque gradients during engine start (Fonseca *et al.*, 2011), what can be extremely damaging for core engine parts.

However, even at regular torque gradients, the tribological context of the start-stop operation is less well understood beyond of lubricant starvation between contacting surfaces, such as piston and cylinder and crankshaft, piston and bearings, and local temperature rise (Ryk *et al.*, 2002; Kagohara *et al.*, 2009). The friction and wear behavior of counter bodies during a constant range of lubrication regimes, from boundary condition at the stroke end, where reversal velocity inhibits formation of an Elastohydrodynamic film, to Elastohydrodynamic lubrication in the mid-stroke region and Hydrodynamic lubrication during continuous operation (Dowson *et al.*, 1962; Taylor, 1985; Taylor, 2003; Hamrock *et al.*, 2004). Even though this regime transition occurs during all engine starts, the frequency of its occurrence in start-stop systems provokes a regular disruption of the Elastohydrodynamic film, leading to a greater degree of asperity

contact and possibly higher frictional energy loss and wear damage of the surfaces (Walker *et al.*, 2013).

The research of these new tribological conditions are extremely important in order to guarantee that the fuel economy achieved by idle stop of hybrid operations is not harmed by increase in friction losses or cause irreversible damage in several engine parts. In this new context, engine tests simulating the constant idle stop and even component tests to evaluate the damage on the most affected parts, such as piston, cylinder walls and bearings are being developed (Walker *et al.*, 2013). These tests are important both for engine designers and component manufacturers, which can respectively determine the new life shelf of various engine components and research new technologies to reduce friction and wear, such as low friction coatings based on diamond-like carbon or molybdenum-based composites, surface finishing to reduce asperity contact and surface texturing by laser techniques, altering the lubricant flow in contact zones, which have presented so far positive friction and wear (King, 2012).

2.5 State of Art

After presenting in the previous subsections all the necessary concepts for the understanding and accomplishment of this research, the present subsection describes the latest developments in the field, trying to make the current research a sequence of the research already done.

2.5.1 *Daimler's Start-Stop System*

The Daimler hybridization process has been introduced in passenger vehicles in a form of start-stop systems since 2011 (Daimler, 2011). With the start-stop system developments, the main impacts on the ICE were the sharp drop in operation temperatures, change of oil properties, increase of start numbers, and also, the increase in the torque gradient during engine start. These latest developments have altered the wear behavior of the internal combustion engine, leading to an intensive research of new materials and lubricants before its commercial release.

The truck department also followed to passenger vehicle trend, however, the only MDEG engines already released for commercial use were buses from the FUSO line, developed for the Japanese market. The idle start-stop (ISS) system of these engines is designed for 200,000 starts and is released for operation only when the following conditions are fully fulfilled:

- The engine should only stop automatically at idle speed;
- A range of coolant temperature of the engine is determined temperatures. If the coolant is too low, the engine stop will lead to a delay in the engine warm-up, increasing thermal losses of the engine and possibly jeopardizing some engine parts. If the coolant temperature is too high, it is considered that the engine is already at its full operation potential and the engine stop would lead to decrease of this potential;
- The fuel temperature has to be below certain temperature so that it does not change its properties in the injection line when stagnant during engine stop, increasing the probability of its gluing in the injection line or worsening the combustion quality;
- A range of oil temperature is also determined. When the oil is too low, the engine stop could lead to pumping problems when the engine is once again started. On

the other hand, a certain temperature the oil viscosity strongly decreases, increasing wear substantially in case of a new engine start.

Even if these conditions are fulfilled, the system will not be available when certain parallel operation are ongoing such as emission particle filtration or emission catalytic treatments. No determination of the minimum stopping time for the engine to be switched off is determined. However, it is well known that if the engine standstill time is too small, the energy spent to start the engine again is higher than the energy saved during the shutdown, thus characterizing an invalid stop. The Japanese market, however, is under different environmental laws, uses different suppliers and materials for the engine construction, and also demands different engine operation. Thus, despite aiming for a similar engine operation, the start-stop systems in Europe need further research. Keeping the market demands in perspective for hybrid engines, the start-stop concept is also used, demanding mainly higher torque gradients at ICE start and more wear resistant engine components.

2.5.2 *RNT evaluation of Start-Stop systems*

The radionuclide-technique (RNT), developed in 1958 by the Universität Karlsruhe, is a method of using radiation for tribological studies in internal combustion engines (Herkert, 1975). With this method, a layer of up to 100 µm of the studied component is radioactively activated, not requiring for its handling additional protective measures or adherence to strict radiation protection regulations. Then, by the "concentration measurement procedure", the concentration of the radioactive particles resulting from the component wear located in their transporting medium, what is normally the lubrication oil, can be detected. These particles are detected by a sensor that measures their radiation emission when the oil with the particles is collected, as shown in Figure 2.14. From this, the worn mass, depth or wear speed can be calculated by using the calibration data of the measuring system and by considering further relevant system data, such as the half-life of the radioactive nuclide of the wear particles (Scherge *et al.*, 2003).

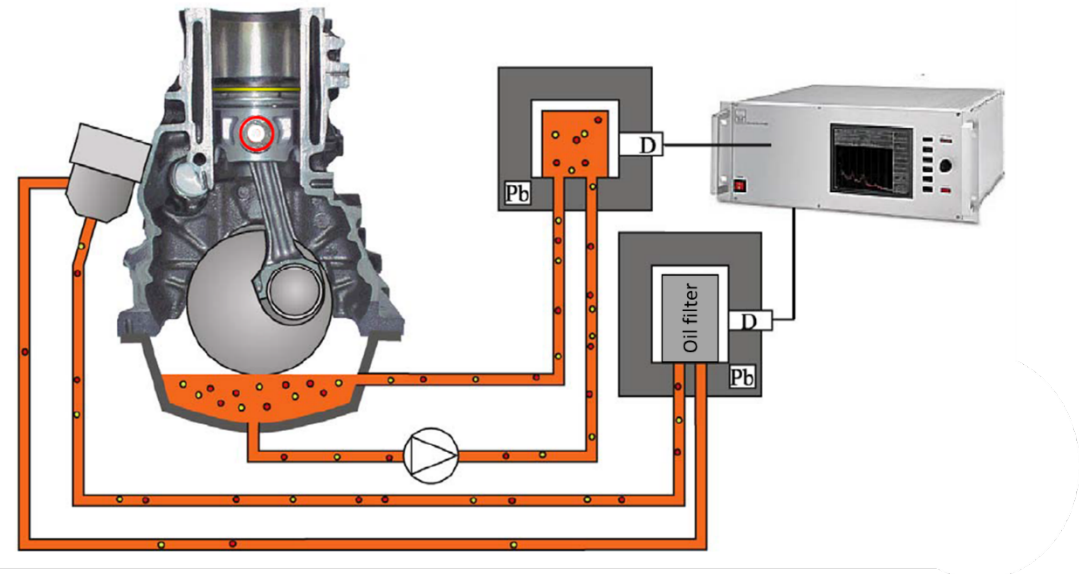


Figure 2.14 - Wear measurement with RNT

In 2013, a study at Daimler AG Medium Duty department was conducted to analyze wear in some engine components affected by start-stop conditions with the RNT

method to consider the use of the ISS in MDEG engines, more specifically, in FUSO buses. For this application the engine is expected to withstand up to 235,000 starting operations. In this study, the wear of the main bearings (MB) and con rod bearings (CB) was investigated under different boundary conditions, i.e. the use of Shell HTHS with viscosity of 3.5 mPa and Idemitsu oil (used in Japan, with significantly lower viscosity) and at different temperatures (Antriebstechnik, 2013).

The loads acting on con rod and main bearings are generated by combustion in the cylinders. The increased cylinder pressure during combustion leads to a downward piston movement, which is converted to crankshaft rotation by the connecting rod, the link between piston and crankshaft. The upper conrod bearing shell is the first bearing to support the combustion load, and since the crankshaft is supported also by the engine housing and respective main bearings, they react to the load transmitted. Since the downward movement of the conrod also pushes the crankshafts down, the lower main bearings shells are the most loaded, as shown in Figure 2.15. Hence, the most important bearings shells to be considered are the upper conrod and lower main bearings, since if their wear is acceptable, the wear in the lower conrod and upper main bearings will be consequently lower. Normally, because of this load pattern, the upper conrod and lower main bearings are made of more wear resistant materials, or at least special coatings.

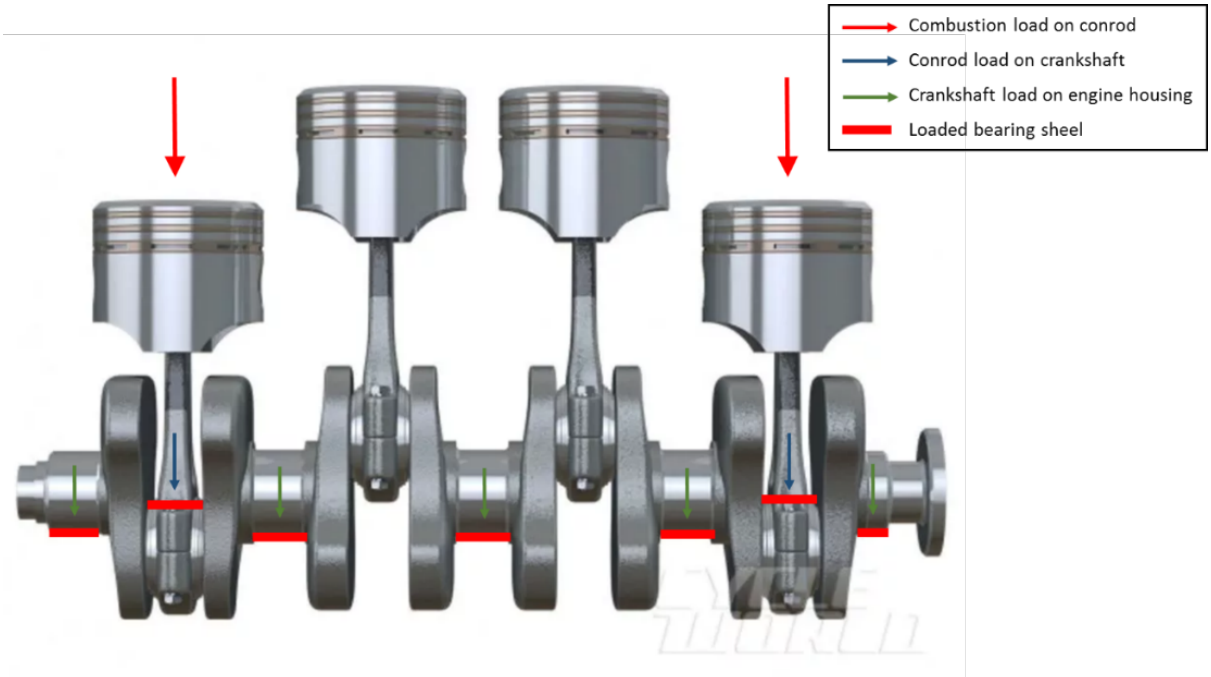


Figure 2.15 - Load distribution in bearings due to combustion, Credits: Adapted from cycle word (World, 2018)

In regular durability tests not considering start-stop operation, the upper main bearings presented sufficiently low wear. At more severe conditions, such as fast engine starts with higher rotational speeds and higher loads, the wear rates obtained were significant higher, but not inadmissible with the oil with higher viscosity. The lower main bearings also presented low wear rates even with a heavily loaded engine. In start-stop operations, however, the regular bearing wear is unacceptable, which leads to research regarding the use of new bearing materials.

Several tests were conducted varying t1 and t2, respectively the time the engine takes to reach the idle condition and the time within which the speed is increased

from idle to rated speed, as shown in Figure 2.16. Also varied were the ramp programs, A and B, presented in Figure 2.17.

Figure 2.17 shows the clutch actuation during an engine start. As a rule, the clutch is required to be activated during start, so that the load application is relieved and the engine components are less damaged. However, to simulate more severe load application conditions, as soon as the engine is started, the clutch is decoupled to force the increase of the axial load on the shaft, in order to hinder the fluid film biult up between the shaft and the bearing and increase the wear of these components

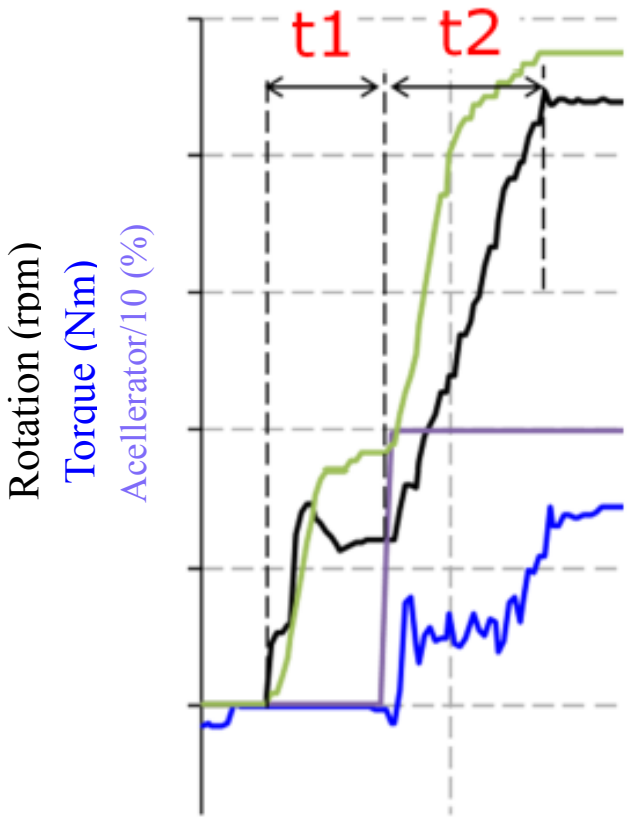


Figure 2.16 - Engine start varying t1 and t2, Credits: Adapted from (Antriebstechnik, 2013)

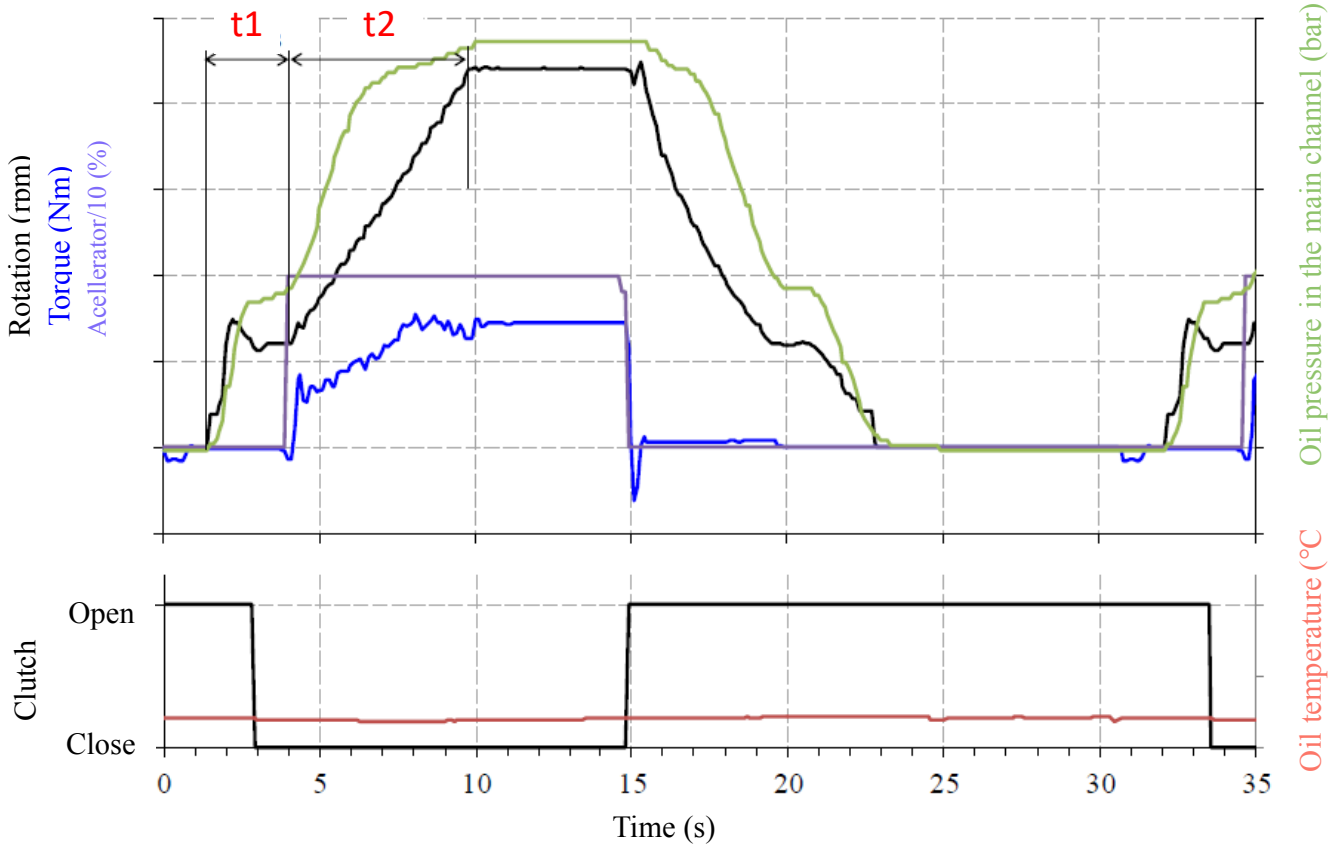


Figure 2.17 - Ramps a) A and b) B for engine start, Credits: Adapted from (Antriebstechnik, 2013)

First of all, tests with oil in the oil pan with approximately 82% of the highest possible engine temperature for MSS were made in the main bearing shells, as shown in Figure 2.18. These results consider average wear in bearing surface by calculating the worn particle amount found in the lubrication oil. In the wear axis the wear is presented as a percentage of the highest wear obtained in the tests it is known, however, that bearings do not present homogeneous wear in its surface, and it is normally increased with increase load application. In general, the upper and lower main bearing shells presented slightly higher wear for ramp A in all conditions, what can be explained by the higher engine torque applied between 5 and 15 seconds of operation. Very different results were obtained, and even though the lower main bearings have special wear resistant coatings, they presented from 2x to 12x higher wear in the same conditions when compared to the upper main bearings. A fast motor start for the upper main bearings leads to significantly higher wear rates at the upper main bearing compared to the load connection after 2.5 or 4 s. This happens because, during start, the engine is under boundary or Elastohydrodynamic lubrication conditions, in which the increase of sliding speed brought by rotational speed increase leads to increased wear. The influence of time t2, within which the speed is increased from idle to rated speed, is negligible on the other hand.

For the lower main bearings, higher t1 increases wear because the lower engine rotation is not enough to overcome the lubricant inertia, leading to boundary condition between lower main bearing and crankshaft, and hence, increased wear. Differently, lower t2 increases wear for the same reason of the upper main bearings, fast

rotational speed increases the sliding speed between counter bodies at boundary or elastohydrodynamic conditions, increasing wear. The wear in all t1=4s conditions presented unacceptable wear, suggesting that the whole coating layer in these bearings were worn out. It must be considered, that the wear was calculated based on a number of starts lower than 100,000, and the wear pattern presented by these tests may not represent the wear pattern during the whole test, as different layers, with different composition and microstructures could be affected.

A maximum wear depth up to which an uncritical operation can be ensured cannot be clearly defined, as it depends on many factors, which must be assessed individually. Even if a coating is completely worn out of a bearing and the underlying bearing material starts to be compromised, it would still be possible to run the engine properly. It all depends on this layer's properties and if it presents low sliding restriction, allowing rotational moving without sharply increasing the friction load, and not increasing drastically the bearings wear rates.

The conrod bearing wear tests were conducted similarly to the main bearings and the results are presented in Figure 2.19. As the loaded main bearing shells presented such greater wear when compared to the unloaded, only the upper main bearings were than considered. The upper conrod bearings presented relatively higher wear when compared to the lower main bearings, due to their more direct contact with combustion loads. They also presented higher wear for higher t1 and lower t2, for the same reasons. The wear difference among these start conditions are not as influential as in main bearings, because as the conrod bearings are the first bearings to receive the combustion load, to build a fluid film in all conditions is harder, leading to more counter body contact and more wear. In all conditions, the upper conrod bearings presented significantly higher wear for ramp A.

As ramp A induced more severe wear pattern in all conditions, it was the only ramp considered in further wear investigations. In these studies, the oil temperature is also notably influential in wear rates, as shown in Figure 2.19. The increase of the oil temperature in the main gallery from 78 to 100% of the highest engine temperature leads to a doubling of the wear rates, and at the highest engine temperature possible, the MSS function deactivated.

The influence of the standstill time between engine operations was researched and its results are presented in Figure 2.20. A longer standstill time has significantly higher influence on wear increases for all bearings, as it gives time for the lubricant film to be disrupted and increase counter body contact in the following start, even though contributing to slightly decrease oil temperature, increasing its viscosity. However, since all standard start-stop tests have a standstill time of less than 30 s, the wear increase due to standstill time is of no concern.

The influence of the overrun time, that is, the time the engine keeps rotating after the end of combustion, was studied and the results show that this parameter presented no significant effect on start-stop wear, so extended lag can be used to reduce the number of engine starts.

The rotational speed and engine load also shown to be influential for wear patterns, as shown in Figure 2.21. These two parameters, however, presented more impact on the loaded bearing shells than on the unloaded ones. For the upper conrod bearing shells the rotational speed increase seemed to impact more the wear pattern than for the lower main bearing shells. These results were already expected, since the loaded shells are more likely to have a fluid film disrupted, and with more asperity contact between counter bodies wear is more likely and is significantly increased by increasing relative sliding speed.

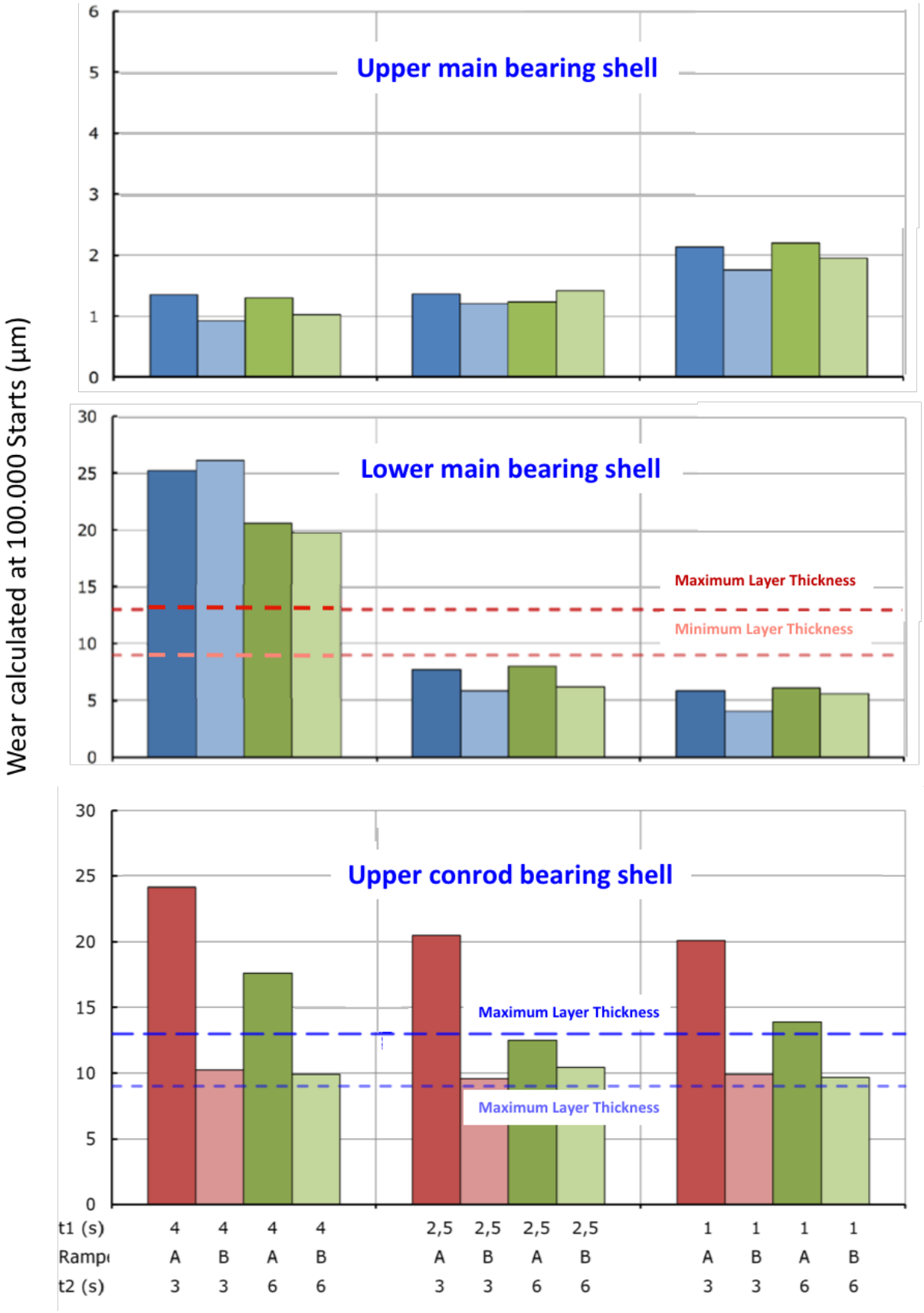


Figure 2.18 - Bearing wear considering different engine start conditions, Credits: Adapted from (Antriebstechnik, 2013)

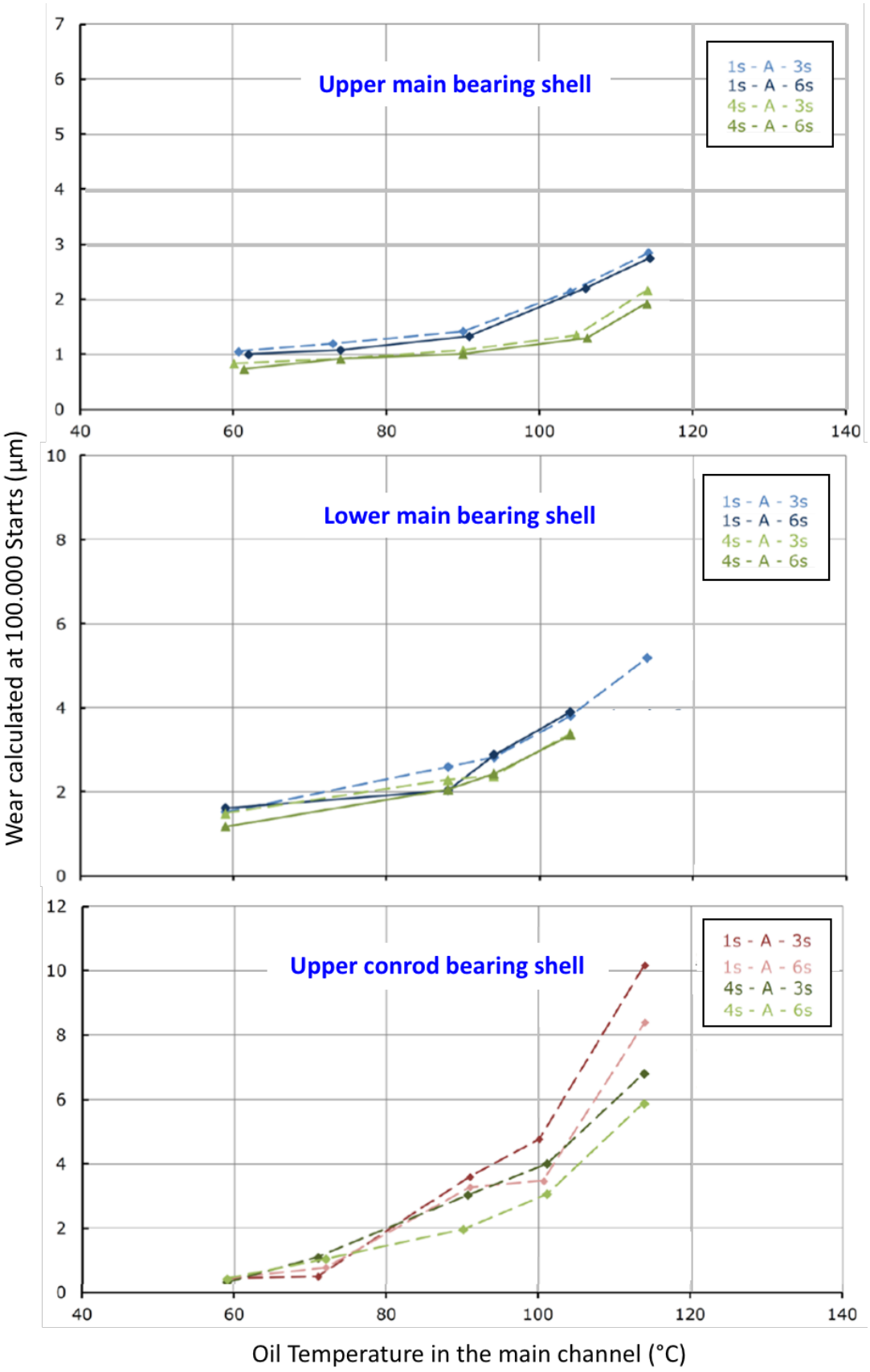


Figure 2.19 - Influence of oil temperature on bearing wear pattern, Credits: Adapted from (Antriebstechnik, 2013)

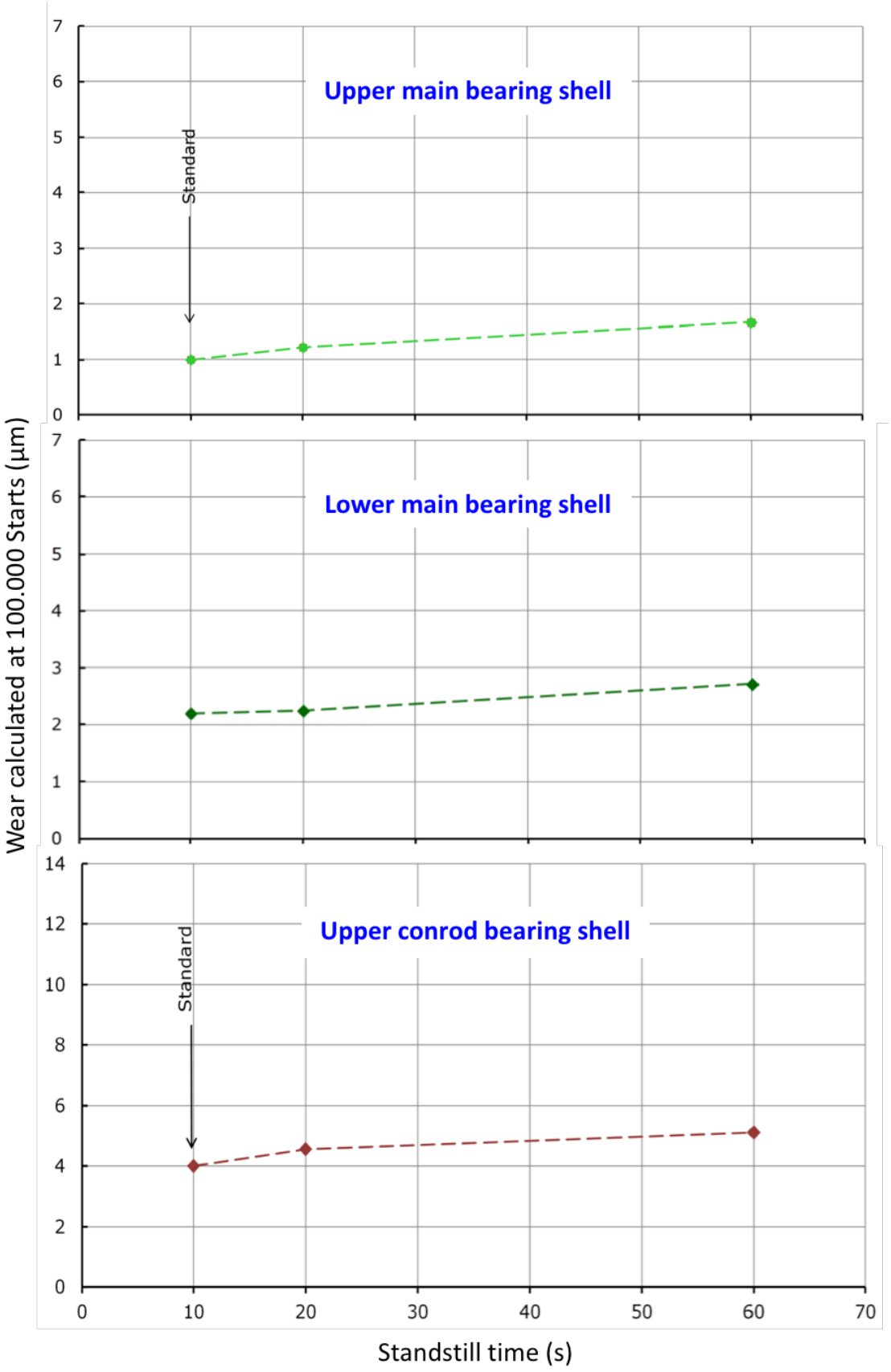


Figure 2.20 - Influence of standstill time on conrod bearing wear pattern, Credits: Adapted from (Antriebstechnik, 2013)

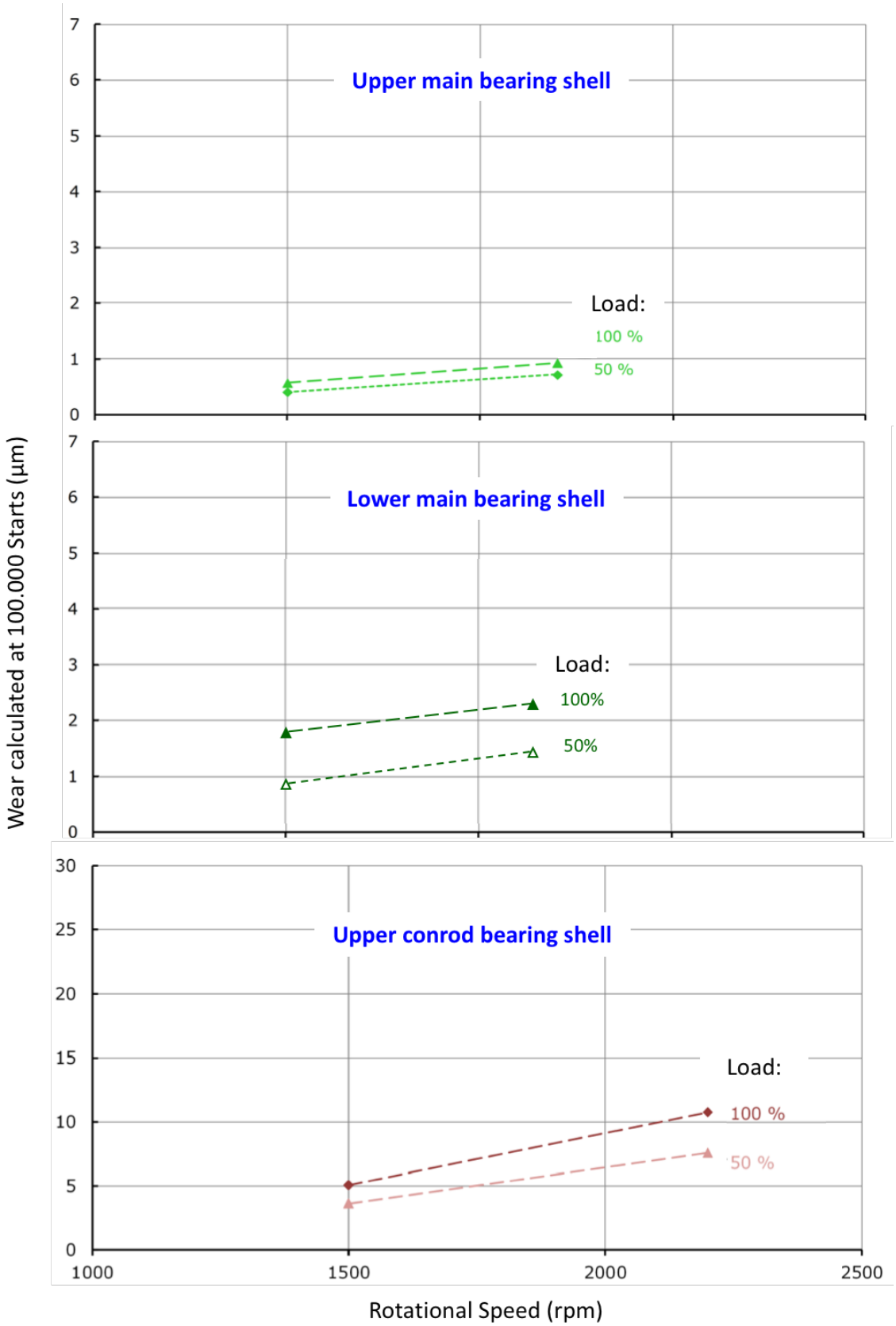


Figure 2.21 - Influence of the rotational speed and load on con rod bearing wear pattern, Credits: Adapted from (Antriebstechnik, 2013)

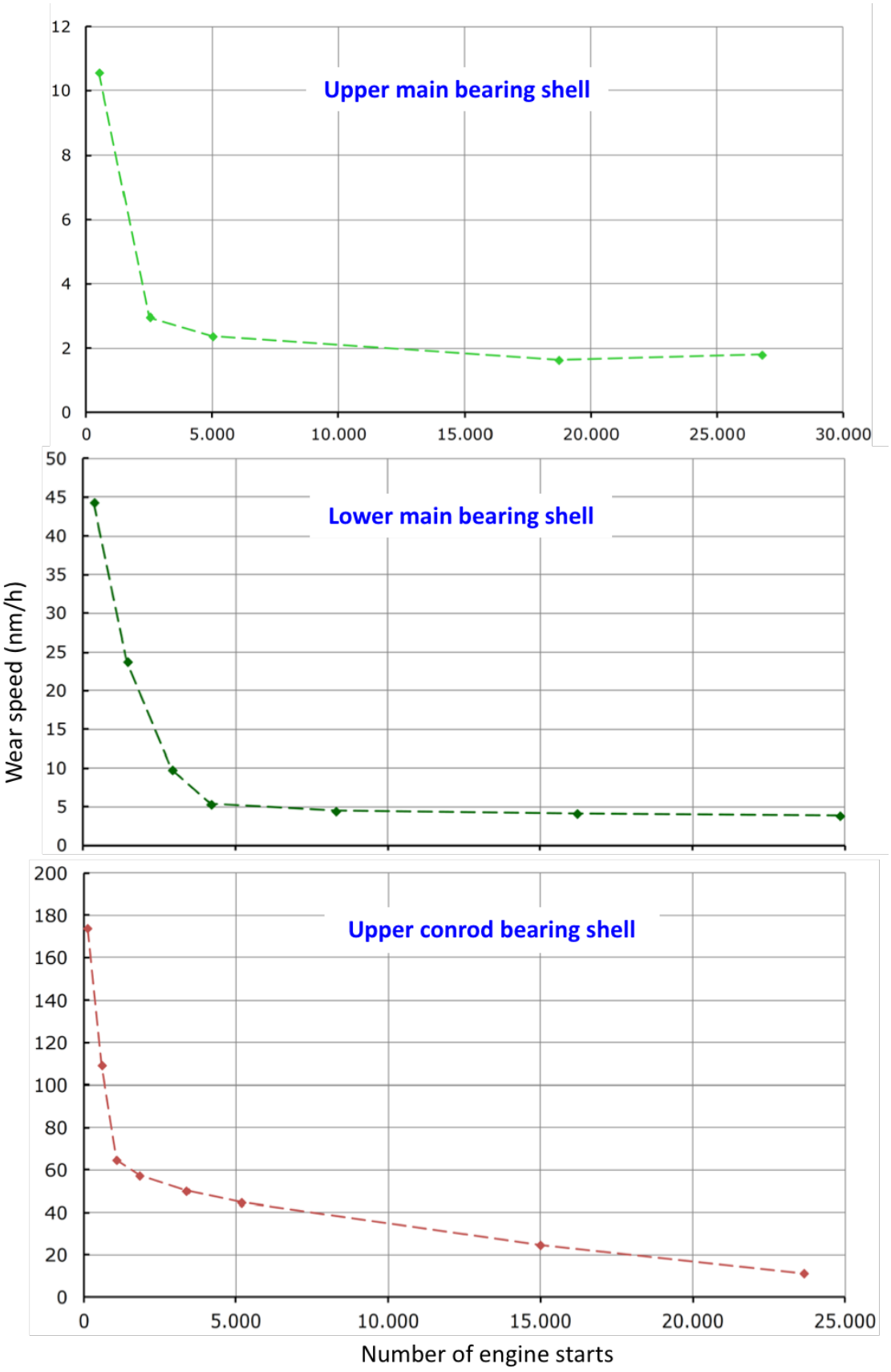


Figure 2.22 - Bearing wear speed over number of engine starts, Credits: Adapted from (Antriebstechnik, 2013)

At last, another very important relation discovered during this research was the approximated bearing wear speed considering the number of engine starts, shown in Figure 2.22. The Figure 2.22 presents a sharp drop of wear speed during the first 4,000-5,000 engine starts, suggesting the complete wear of the first bearing coating and the reach of the layer below it, when wear speed tends to stabilize and reach a constant value. Even though the lower main and upper conrod bearings are constituted of the same materials and coatings, the higher loads experienced by the upper conrod bearings justify its different wear pattern and longer time for wear speed stabilization.

In general, the studies proof that the unloaded bearing shells are sufficient for start-stop conditions, by the loaded bearings, mainly the upper conrod bearings, can be extremely damaged if several operational conditions such as low starting time until idle, long time from idle to rated speed, high loads or rotational speed, high lubricant oil temperatures, and long standstill time between engine starts are frequently chosen during engine lifetime, appointing to the need of more wear resistant bearing materials, and/or, lubricant alterations.

2.5.3 *Lubrication in MDEG Engines*

The oil circuit in a MDEG engine follows basically the path shown in Figure 2.23. The oil in the oil sump is integrated in an oil suction device and controlled by the oil pump. After passing through the pump, the oil passes through the oil-cooler to regulate its temperature, to the filter and then, after passing the main oil gallery, it is first directed to the piston cooling channels, where oil is sprayed in the cylinder liners. Then the oil is directed to overhead camshaft lubrication and the complex rear gear drive. After that it is directed to further systems through the integrated oil circuit. It is important to notice that after the oil pump the oil is directed to the oil filter module and from there, a channel between cylinders 1 and 2 connected to the main oil gallery is fed and then, these main and conrod bearings are the first supplied with lubrication. From the main oil gallery, the oil is also directed to the back of the engine, suppling the flywheel and cylinder head oil circuit, being distributed to pistons, liners and the other conrods and main bearings from the back to the front.

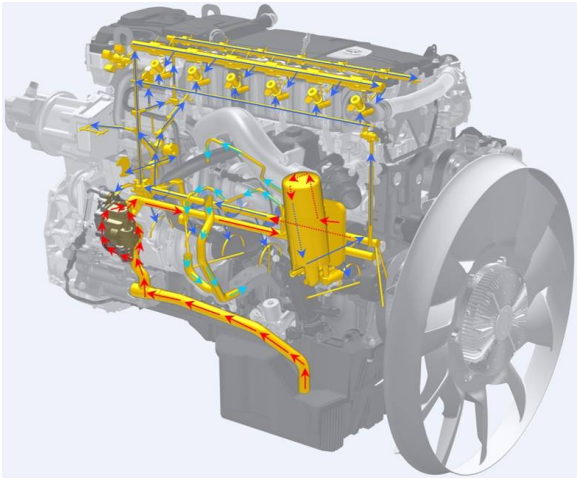


Figure 2.23 - MDEG lubrication circuit

The oil pump is a regular gear pump connected to the crankshaft, and hence, increases the oil pressure as the crankshaft rotates faster. However, as most positive displacement pumps, at faster crankshaft speeds, the pressure oil delivered by the oil

pump may be more than enough, what can even lead to component damage, such as cavitation. Thus, the oil pump has a pressure relief valve located at the oil pump outlet that open when the oil pressure reaches a certain value, as shown in Figure 2.24.

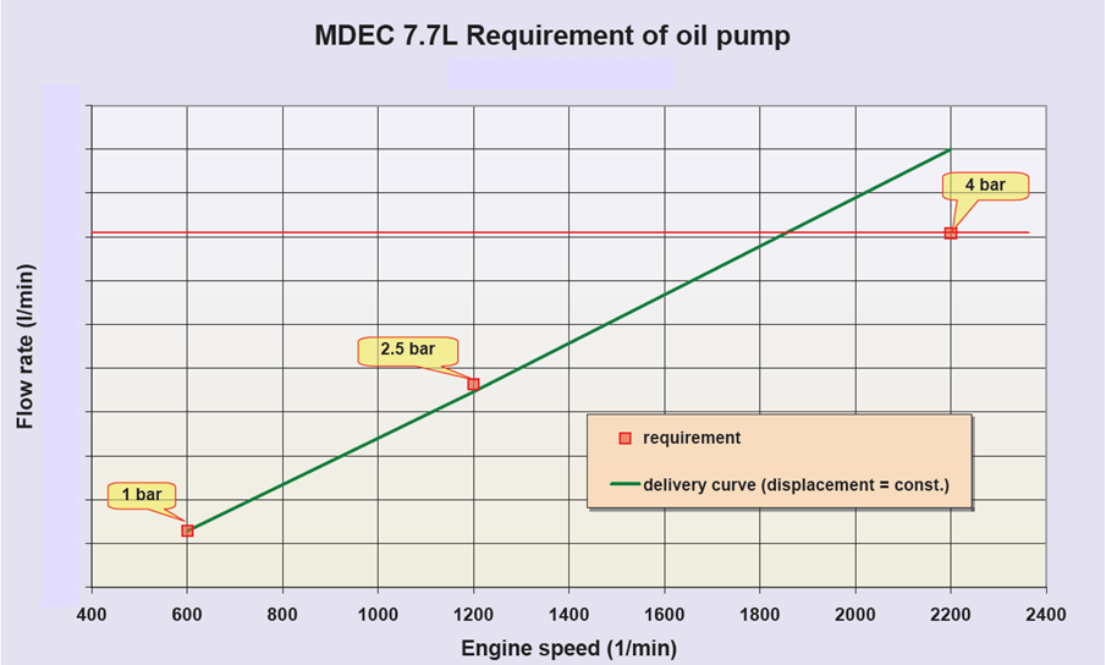


Figure 2.24 - Lubricant flow rate as a function of engine speed

The oil film builds up is a complicated parameter to be measured without tools capable of measuring surface contact between counter bodies. Normally, for simple comparisons and qualitative analysis of oil film build up, the time it takes for the oil in the main gallery to reach a certain set pressure is measured for different engine conditions, different temperatures and oil types for a set pressure to be built in the main oil pipeline. For the same oil and same operation conditions when the oil temperature was set at 23°C, it took 4.5s to reach 1 bar and when it was at 100°C, it took only 1.25s, as shown in Figure 2.25. That happened due to the higher viscosity of the oil in lower temperatures, demanding more energy on the oil pump to reach the set oil pressure, what is possible as the engine rotation is higher, increasing also the rotation and energy delivered to the pump.

Another important parameter is the standstill time before engine start, as shown in Figure 2.25. The figure shows that when the standstill time is longer, more time is taken for the oil pressure to be build, and that happens because, as longer the standstill time, the more the oil can be drained back and empty the oil distribution channels, demanding more time for it to be filled once again.

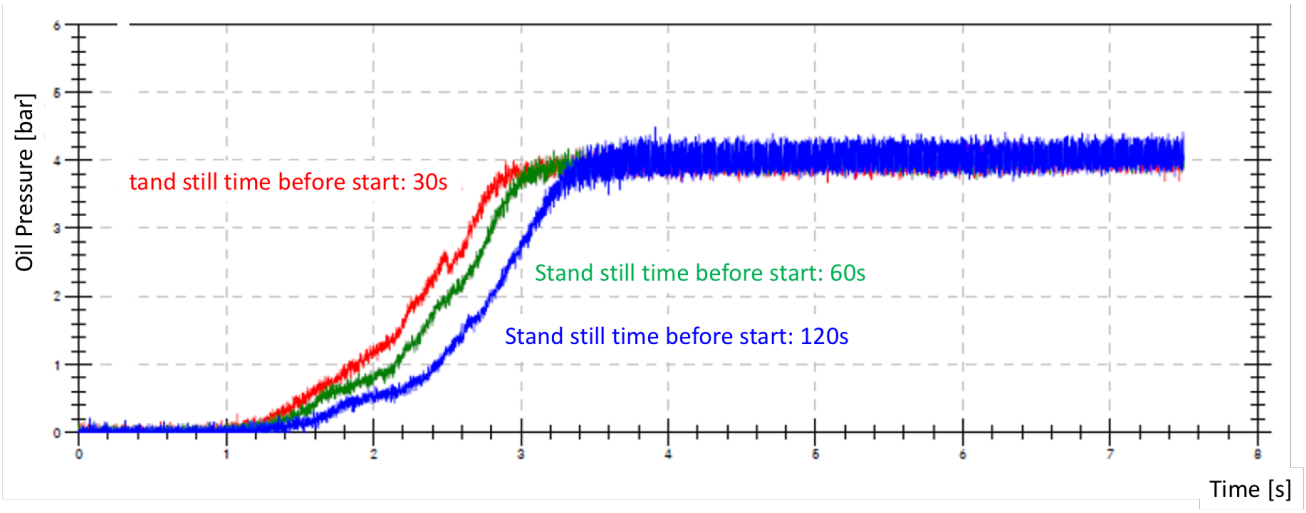


Figure 2.25 - Oil pressure build up after different stand still times, Source: Daimler Database

2.5.1 *Recent Development in Bearing Coatings*

Among the various materials investigated for use in engine bearings, lead (Pb) containing materials such as copper-lead (Cu–Pb) based linings and overlays have been often used in the past due to the low friction characteristics and excellent conformability and embeddability behavior of lead (Pratt, 1973). However, environmental concerns regarding the widespread use of lead has entailed manufacturing restrictions and lead-free (Pb-free) materials are being developed lately (Becker, 2004). Various Pb-free bearing materials are suggested by bearing manufacturers. For instance, Al–Sn based overlays have been developed and have presented better wear resistance when compared with lead based (Pb-based) material (Grün *et al.*, 2011). These tin-based materials also have presented high resistance to cavitation and corrosion damages and excellent conformability and embeddability for engine tribological applications (Zhang *et al.*, 2016). The most attention, however is being given to Polyamide-Imide (PAI), an amorphous thermoplastic with high mechanical strength, high resistant against diesel fuel and chemical components in the engine oil and thermal degradation has being extensively studied and it is believed to be further improved by incorporating solid lubricants. In recent studies, bearing materials PAI based overlay containing graphite and MoS_2 exhibited better friction and wear properties than Pb-based and aluminum-tin (Al–Sn) based materials (Gebretsadik *et al.*, 2015), and same excellent seizure behavior as Pb-based coatings (Gebretsadik *et al.*, 2017) appointing the benefits of further study in with this material.

Other recent concern regarding bearing material selection are the increasingly severe the loading and lubrication conditions. Recently, a tin galvanically coated bearing from Federal Mogul was developed as an intelligent material. The operation condition induces diffusion of tin (Sn) in the tin-nickel (Sn-Ni) layer, thinning the sliding layer and increasing the concentration of hard particles by load increase, as shown in Figure 2.26. This technology increased by 25% the bearing load resistance and also increased the bearing resistance to wear (Powertrain, 2010).

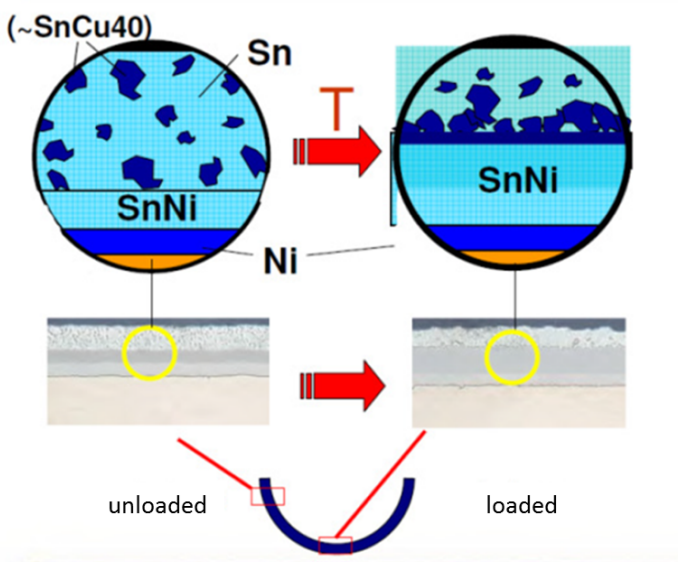


Figure 2.26 - FM Tin galvanic bearing coating, Credits: (Powertrain, 2010)

Then, according to the market demands, to withstand more wear, seizure and fatigue, FM developed a polymeric bearing cover named IROX®, as shown in Figure 2.27 (Powertrain, 2016).

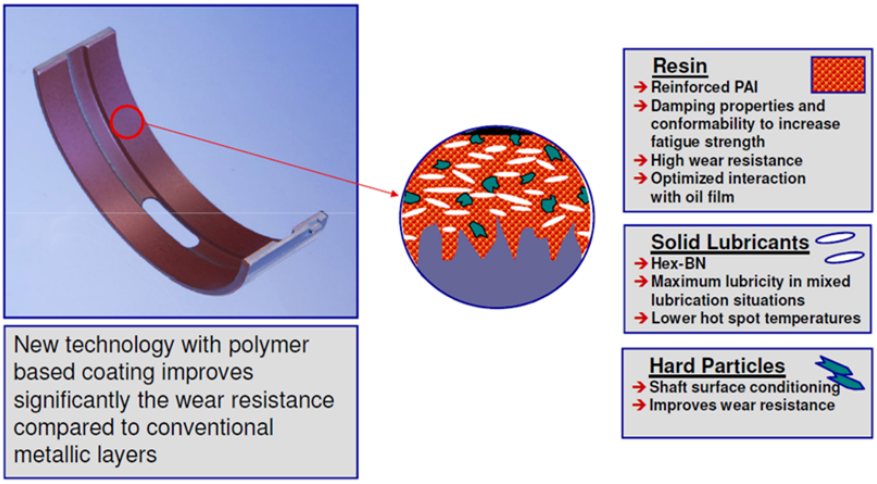


Figure 2.27 - FM IROX® bearing coating, Credits: (Powertrain, 2016).

Simultaneously, MIBA developed a polymeric bearing cover called Synthec®, chemically composed by 32% PAI (Duratron polyamide-imide), 23% graphite and 45% Molybdenum disulfide (MoS_2), as shown in Figure 2.28 (Manual, 2000).

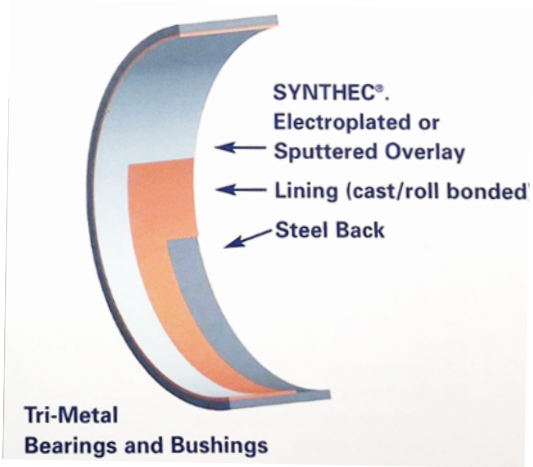


Figure 2.28 - MIBA Synthec® bearing coating, Credits: (Manual, 2000).

Seizure tests developed by FM based on load increase and minimal lubrication have being used to test bearing coating materials in bearing development. In a "Stress Test", IROX® withstood the severe load applications, but concerns regarding start-stop operations lead FM to develop a new test program simulation this specific operation conditions, called "Nautilus test", in with IROX® failed. After that, FM developed the IROX II® coating with some coating developments such as MoS_2 as solid lubricant and mixed oxides for micro reinforcements to improve seizure properties of the bearing, as shown in Figure 2.29. Only bearings with IROX II® polymeric cover passed the Nautilus test, proving its suitability for start-stop and possibly hybrid use (Häring, 2018).

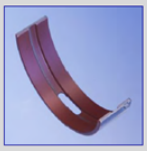
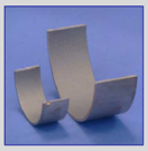
	IROX® - PC-11		IROX® 2 - PC-15	
				
Binder	PAI		PAI	
Solid Lubricants	Hexagonal BN		MoS_2 + Hexagonal BN	Im-proved Seizure Properties
Micro-reinforcem.	Fe_2O_3		Mixed Oxides	
Hard particles	SiC	Wear Resis-tance	None	
Pretreatment	Blasting (Korundum)		Blasting (Korundum)	

Figure 2.29 - FM Bearing coating IROX II®, Credits: (Powertrain, 2016).

2.5.2 *Wear simulation in start stop engine components*

The start-stop systems are relatively new in the automotive market, and so is the development of parts for the engines with this new technology. Normally to test new engine components, the component is assembled in an engine and a special durability test is developed to submit the part to extreme operation scenarios. Another approach is to assemble an engine component in a vehicle, submitting the component to real driving conditions. Despite presenting extremely realistic and reliable results, the two approaches

are extremely costly and time consuming, mainly for the engine parts presenting great compliance issues and still in an early development stage.

As several core engine components have been presenting unacceptable wear after the implementation of start-stop system trials, special and simplified tests aiming to simulate the load charge pattern in this core engine parts are being developed, among them computer simulation and component test benches can be highlighted.

2.5.2.1 Computational simulation

Several simulation models to predict friction and wear have been also recently developed and physically relevant factors have to be considered in order to obtain an accurate program, and frequently, these simulations models acquire their base premises in experimental tests. Most of the studies are limited to investigating the operational characteristics of the system and just cover their applications as simple mechanisms. The majority of studies in this area, due to the difficulties regarding wear and friction investigation, just cover simple wear mechanism, and even studies that go further on these initial developments are limited to develop wear predictions based on dry joints only (Nikolic *et al.*, 2012; Olyaei e Ghazavi, 2012; Xu e Han, 2016). Some studies also tried to study wear considering lubrication, but with engines running at constant speed and disregarding combustion forces, external torque and other real engine parameters (Daniel e Cavalca, 2011; Wu *et al.*, 2012). Furthermore, the majority of studies considered a direct switch from full film to boundary contact skip the Elastohydrodynamic lubrication phase, and consequently, asperity interactions.

Simulation studies including this phase into consideration were conducted integrating vibration and wear analysis techniques and updates on profile and wear rates (Haneef *et al.*, 2017). To obtain more reliable simulation results, test rigs are extremely important, as they are appropriate to obtain primary data for simulation, as well as providing validation of simulation methods with a direct comparison of measured and simulated results (Priestner *et al.*, 2012). The influence of surface adaption caused by running-in wear on bearing friction is considered to be an important input data (Bartel *et al.*, 2012). The wear process not only changes surface roughness, but alters the surface geometry, what consequently alters the contact pressure between bearing and lubricant and may cause misalignments (Fillon e Bouyer, 2004; Sun *et al.*, 2014).

Moreover, wear profiles are important to friction simulation as friction is dependent on the nature of asperity contact between counter bodies. Hence, the use of realistic surface shapes and its real structural elastic deformation under load can lead to better friction estimations. To simulate an accurate bearing wear profile during engine operation, bearing shell surfaces are measured for wear after test runs (Priestner *et al.*, 2012). The measured wear depths were averaged for all performed identical test runs and used as database for several friction prediction simulation programs (Allmaier *et al.*, 2011; Allmaier *et al.*, 2012)

The results obtained from this simulation model are compared to measurements performed on the slider bearing test rig LP06 of the MIBA-Bearing Group. This test rig, using the “Pin-on-disc” test concept, applies a static load to a rotational bearing and was used prior to simulation program development to model bearing wear profiles and after simulation results to validate the simulation and acquire specific operating conditions such as load, temperature, shaft speed and oil characteristics during test, providing a solid base to further simulation programs to forecast bearing friction (Priestner *et al.*, 2012; Allmaier *et al.*, 2013).

2.5.2.2 Component test bench

Many different tests have been used to study sliding wear either to examine the mechanism by which wear occurs or to simulate practical applications and provide useful data regarding friction coefficients and wear rates. For both cases it is very important to reproduce and measure variables which can influence wear, as minor changes in conditions can lead to radical changes in the dominant wear mechanism and influence on its rate. Wear under sliding conditions depends on the distance slid, but also on the sliding velocity and the duration of the test, as they respectively affect the rate of friction energy dissipation and temperature, and contact pressure transitions can alter the lubricant regime. The testing temperature is also very important to be controlled as it influences the mechanical properties of the materials and can affect chemical processes. The atmospheric composition should also be ideally controlled as it can contain reactive components such as water vapor and oxygen, which can influence on wear rates

Wear is then measured either by removing the specimen at intervals and weighing or measuring it, or by continuously measuring its position with electrical or mechanical transducer and deducing the wear from its change in dimensions. Several geometrical arrangements can be employed in wear tests and the most common are asymmetric, in which the two sliding bodies will experience different wear rates (Hutchings e Shipway, 2017). One of the most popular and simple test of wear resistance is the "Pin-on-Disc" test, presented in Figure 2.30. The test is non-standardized and consists basically of a specimen pressed against a rotating disc with fixed rotation and a defined load. The test can be run dry or lubricated and after a determined number of cycles the worn volume of the testing block is determined. The wear resistance depends, in particular, on the hardness of the material. Therefore, trimetallic galvanized bearings cannot be compared to bimetallic bearings because their overlays are very soft (Mahle, 2009). To better understand the wear mechanisms in this test, torque, friction coefficient lubricant and specimen temperatures can be measured (Clausthal, 2018).

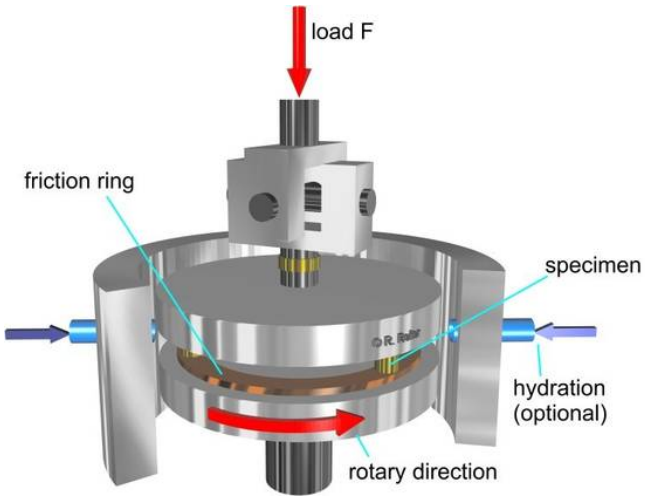


Figure 2.30 - Principle of a "Pin-on-disc" test for wear resistance, Credits: (Clausthal, 2018)

The recent reduction of oil film thickness and use of lower viscosity oils to decrease friction losses have led to an increase of counter body contact during the engine dynamic operation (Taylor, 1998; Priest e Taylor, 2000; Tung e Mcmillan, 2004). That situation concerns mainly piston rings, liners and bearings. To evaluate journal bearing wear under this new triboconditions a test similar to the “Pin-on-disc” test was conducted

by Bovington (Bovington *et al.*, 1999). A static load was applied to a journal bearing and friction torque was measured for a wide speed range. In this study different lubrication regimes were identified and tests were conducted with several engine oils, with different formulations.

In more specific cases, (Walker *et al.*, 2013), concerned with the influence of start-stop systems in the piston sliding tribology, developed a component test bench using a cylinder liner and a piston ring attached to a high frequency reciprocation test machine. Lubricating oil was fed between the both surfaces through a feed hose attached to the loading head, both surfaces were heated to a temperature of 100°C prior to sliding and the conditioning phase was followed according to ASTM: G171. A load of 5N was applied to the contacting surfaces, followed by acceleration to the test frequency of 23 Hz at a stroke length of 25 mm. The load was incrementally increased by 5 N at 60 s intervals until it reached 150 N, and then decreased in the same manner to 5 N.

After the conditioning phase, the load was increased to 150 N, initiating a start–stop program consisting of 60s and 23 Hz sliding intervals followed by 35 s stop, simulating the average period of vehicle start-stop described by the European Urban Cycle. Tests were stopped at three test intervals of 87, 225 and 495 min, duly cooled and cleaned before weighted to determine mass loss and proceed to further investigations. In order to compare the start–stop system to normal engine operation, an uninterrupted test was carried out under the same conditions at 23 Hz, but without velocity interruption for the same test length intervals. Five tests were conducted, the first to determine if satisfactory running-in conditions were achieved from the conditioning phase and then two repetitions of the first test segment for the interrupted and uninterrupted test to validate similar friction behavior.

As previously mentioned, a bearing test rig based on the “pin-on-disc” test was used not only to acquire base wear and friction parameters, but to validate computer simulation models. The test rig, presented in the Figure 2.31, has a mechanism that consists of a test conrod connected to a hydraulic actuator and the drive shaft in contact with the bearings tested driven by an electric motor. Associated to this test rig is an oil conditioning system capable of regulating the oil temperature within the range of 50-170°C. The maximal dynamic load applied in the bearings were of 500kN, in a frequency range of 0–100Hz. The measurements collected in this test ring are the temperatures of oil and of the back side of the bearing shell tested, the frictional torque and the contact voltage between the drive shaft and the bearing which is an indicator for the presence and intensity of asperity contact. The test runs had a duration of up to 15 h and all measurements were acquired and averaged over the whole run time for further analysis (Priestner *et al.*, 2012).

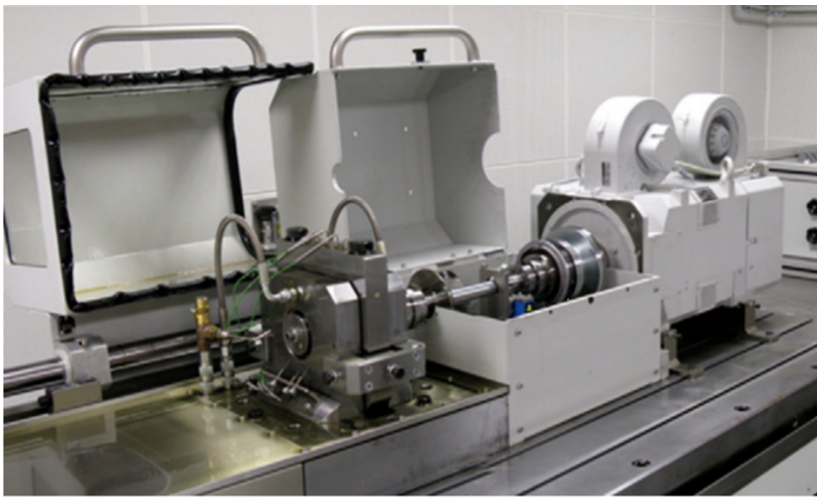


Figure 2.31 - Slider bearing test rig LP06 of the MIBA-Bearing Group, Credits: (Priestner *et al.*, 2012)

Concerns with the lubricant oil viscosity reduction and its impact on automotive plain bearings, an Idemitsu Kosan test rig shown in Figure 2.32, was developed both to study and improve bearing reliability as to test a variety of oil base stocks. In this test apparatus oil is supplied through an oil supply port and the load applied in the bearings fluctuates in the same way as in actual engines. Two tests were conducted, both with the shaft speeds fluctuating among 500, 1000, 2000 and 3000 rpm and oil temperatures 60, 80 and 100°C. In the first test, the static load increased from 1 to 10 kN by increments of 1 kN and in the second, the 8 kN static load varied ±3kN. The friction forces generated were measured. The apparatus was used to evaluate the performance of plain bearings with a variety of engine oil base stocks. In this study it was appointed that not only contact between the shaft and the plain bearing occurs more readily when using lower viscosity base, but that this contact is more likely to occur with highly refined base stocks than with low-refined base stocks among base stocks with the same low viscosity (Katafuchi e Kasai, 2009).

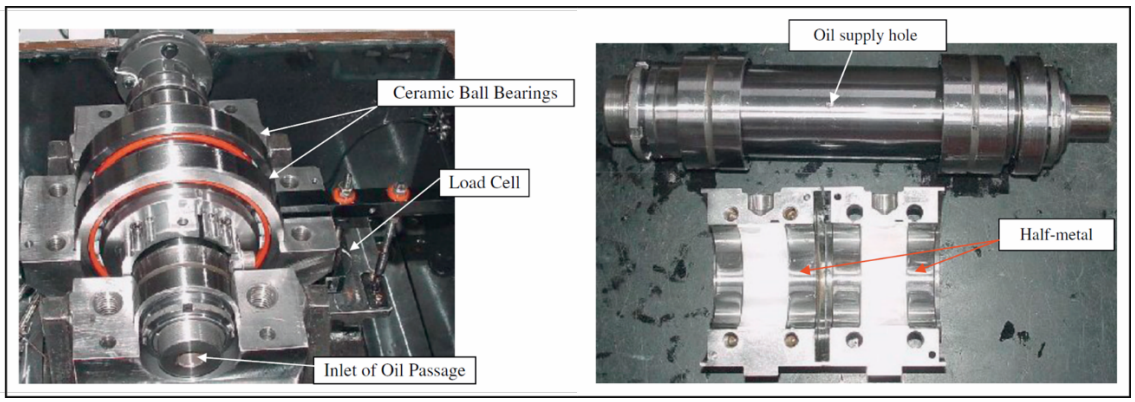


Figure 2.32 - Bearing test rig, Credits: Adapted from (Katafuchi e Kasai, 2009)

The manufacturer Federal Mogul also developed a test rig with similar configuration as MIBA and Idemitsu to analyze bearing wear in different load and lubrication conditions in order to develop bearings adapted to the recent severe engine operations, such as seen in engines with start-stop systems.

The seizure test developed by FM called “stress test” has a first phase with full lubrication (5h) and load and speed increasing stepwise to allow some initial surface adaption and a second phase (30h), in which the oil supply is almost completely shut

down, as shown in Figure 2.33. This test basically evaluates the seizure resistance by the time the bearing withstands such conditions.

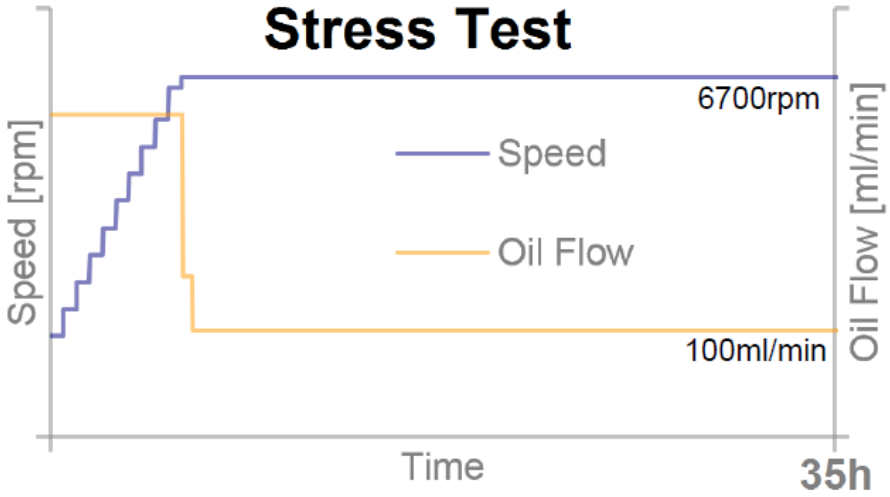


Figure 2.33 - FM Stress Test, Credits: (Häring, 2018).

This test can evaluate potential seizure and wear factors, such as shaft roughness, bearing cover layer thickness and material variation. However, despite its capability of comparing different materials in a certain engine operation, it does not simulate the start-stop condition, in which the lubricant fluid film between bearing and shaft is not built as the engine starts and high loads on the bearings are applied. To simulate this condition, FM developed the "Nautilus test", presented in Figure 2.34. Figure 2.35 presents the Nautilus test rig. In this test, a hydraulic main load is simulated, also considering the conrod side load of approximately 1.7 kN. The shaft radial roughness is 0.13 µm and the test cycle consists of a load increase of 60 MPa with 1200 rpm 5 times for 1 min, speed increase to 4200 rpm 5 times for 5 min and load increase of 127 MPa 6 times for 5 min. It is then believed that any bearing material that endures 30 mins of this test has excellent wear and seizure resistance (Häring, 2018).

All of this tests are standard tests from bearing and oil manufatures, that aim to evaluate bearing wear using different materials or lubricant compositions, respectively, in the same given condition. Theses tests, however, do not evaluate bearing wear in real engine conditions, not guaranteing that the wear mechanisms are the same in these tests and in real engine operations. (Nebelsiek, 2017) studied an engine with a start-stop system regarding the excessive bearing wear observed in this operation. To achieve a more realistic component test condition the load patterns in the core engine parts such as piston, conrods and crankshafts were calculated using engine design parameters and patterns of cylinder pressure by the engine start. Two HTHS oils (2.9 and 3.5) in two different working temperatures (90°C and 110°C) were used and, according to the oil viscosity and load the occurrence of mixed and hydrodynamic lubrication between shaft and bearing was determined. Better results were obtained with HTHS 3.5 at 90°C, when the viscosity is higher both due to the oil composition and operation temperature. As expected, the HTHS 2.9 oil presented much more occurrence of solid contact between parts in both temperatures. As a conclusion, it was appointed that the 2.6 HTHS oils should not be even tested, as severe wear was expected.

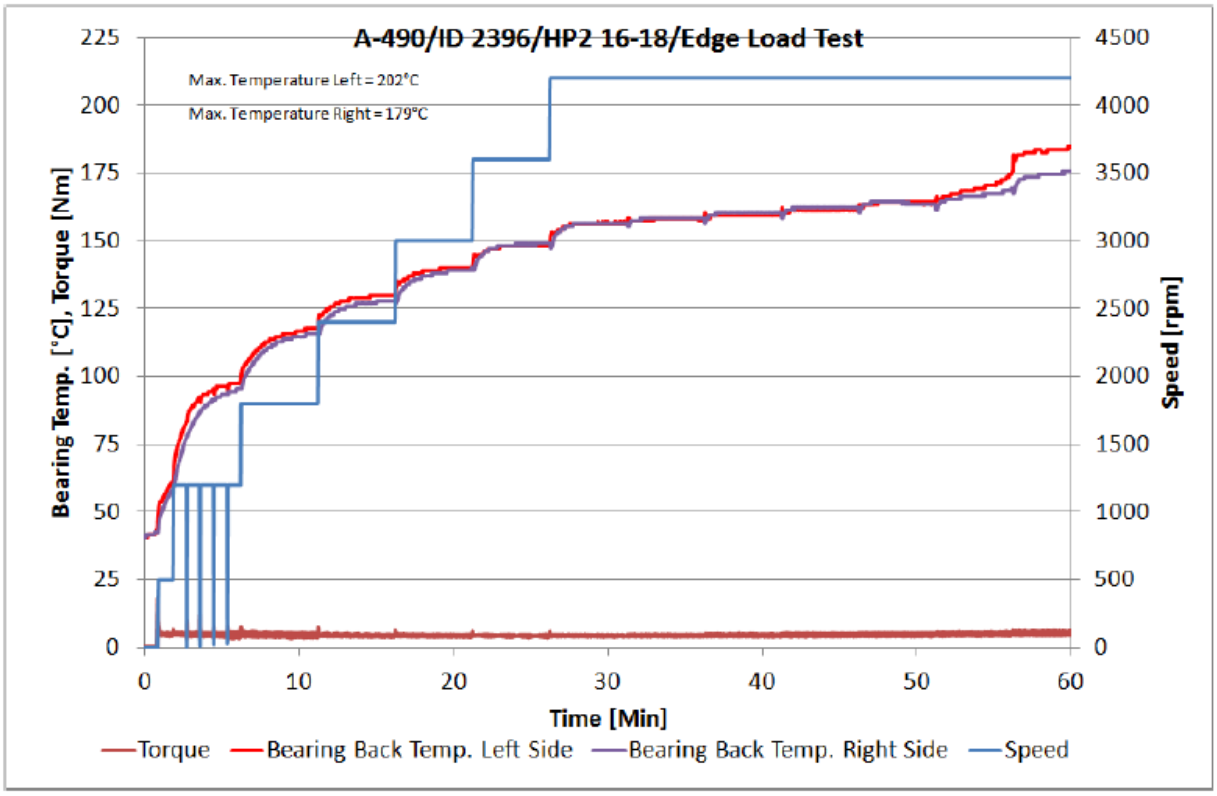


Figure 2.34 - FM Nautilus test, Credits: (Häring, 2018).

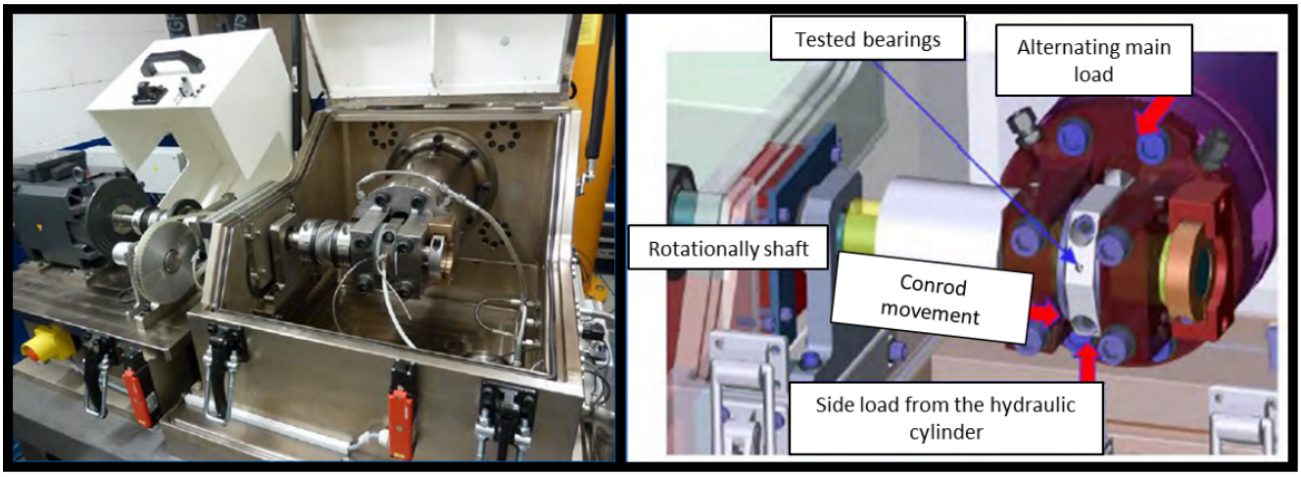


Figure 2.35 - FM Nautilus test rig, Credits: (Häring, 2018).

This research also appointed that, since the viscosity of an oil is dependent on its properties and additives (determined by the oil classification) and temperature and the viscosity of the oils tests were more influenced by the temperatures than by its composition, the temperature window in which the start- stop system could be activated should be between 90° C and 110° C.

According to the theory that the energy input during engine start was the main responsible for bearing wear, for further bearing wear studies at start-stop conditions a test bench simulating start-stop patterns should be used, in which it would be easier to alter just the engine start patterns, the bearing materials and oil used, diminishing the test time and costs. The component test bench proposed was the Engine Bearing Pulse Test Bench (TLPP - *Triebwerkslager Puls Prüfstand* in German), which should basically generate the connecting rod loads with hydraulic cylinders in the shortest possible time at different speeds, operating with identical oil pressure conditions as in the real engine

and capable of running more than 100.000 starts, which is necessary for the bearing release, in much less time than a normal durability test. The TLPP proposed in this work is studied in the present work, which aims to describe its first implementation steps. It is believed, that after the implementation phase, which comprehends the sensors installation and the determination of materials, operation parameters and program, that its durability results could be related to the obtained in normal durability tests. Hence, the best bearing material for a special operation condition could be determined with lower costs and time.

3 METHODOLOGY

3.1 Introduction

The present work aims to implement a component test bench suggested in a previous work by determining optimal operation program and conditions and evaluating its ability to simulate start-stop conditions and wear occurrence in several bearing materials. In this chapter, the research methodology is fully described, in order to guarantee the reliability of the results. First of all, the TLPP equipment is described, as well as the important systems and sensors for theirs duly operation. Then, the components used for the study are detailed and the research strategies for the program development are explored.

3.2 TLPP

Based on the premises that wear is the main source of increased bearing damage and that wear increase in start-stop operation is due to the severe load variations on the shaft (Nebelsiek, 2017), a new test bench simulating only the wear relevant parameters is suggested.

The combustion pressures determined in an ICE start are used to determine the load patterns in the core engine group parts such as piston and conrod. Considering that these load patterns were the only parameters that changed in the engine operation which could be responsible for the excessive bearing wear, this pattern is isolated and reproduced in an easier engine configuration, so that only factors impacting on the wear can be studied.

Analogously, the TLPP design took into consideration the design features of an ICE important to wear production. To simulate the wear in the core engine parts, the most important things to be reproduced are the load patterns in the parts and the lubrication conditions. In that case the load patterns could be simulated with a hydraulic cylinder, since they are already well known, and the oil and coolant supply and pressure conditioning could be done with the regular systems placed in the internal combustion engine. Thereby, the components need for the test are:

- 6-cylinder crankcase
- Oil pan of a horizontal MDEG engine
- Flywheel or control housing
- Cooling water module
- Oil spray nozzles
- Reduced gear drive for driving the oil pump

The engine configuration, in horizontal, facilitates maintenance and the exchange of core engine parts. The crankcase is attached with bolts to the test bench vertical plate without the cylinder head. Between the crankcase and the plate, a standard cylinder head gasket seals the engine. The open external oil channels are all connected to a closed oil circulation system. Even though various components responsible for the oil pressure build-up are not present in this test bench, a throttle valve is installed in the oil circuit, so the oil pressure level can be set to a constant real value.

A model of the test equipment is presented in Figure 3.1 the test bench is located in a base composed by a horizontal and a vertical steel plates to guarantee stability

and absorb the resulting bending stresses by attaching various components. The horizontal plate is located on four vibration-reducing machine feet, capable of intercepting and equalizing any vibration from the test room. In this test, the engine used is not a complete ICE and simulates only the force induced by the peak firing pressure, with hydraulic cylinders.

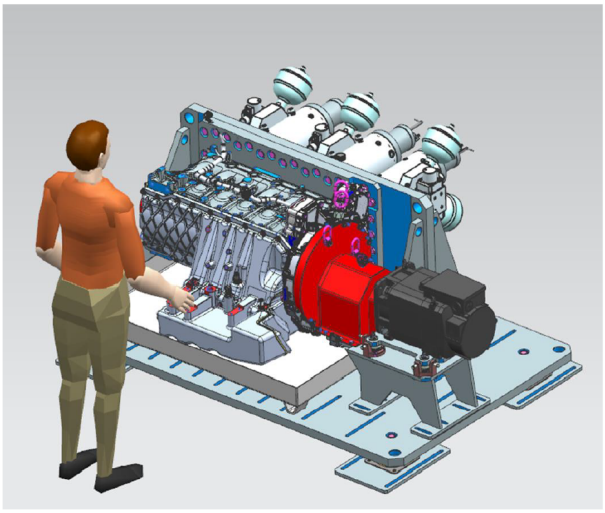


Figure 3.1 - TLPP Concept, Credits: (Nebelsiek, 2017)

3.2.1.1 Hydraulic cylinder

The combustion load in the test bench is reproduced by double acting hydraulic cylinders model 320 from Hänchen, whose dimensions are higher than a normal engine piston and the cylinder spacing. For that reason, only 3 hydraulic cylinders are used in the 6-cylinder crankcase, built in cylinder bores 1, 4 and 6. Due to its 2 servo valves, it has a very fast response time, being able to change position in 2 ms, enabling the representation of a load curve with up to 28 load values. The actual hydraulic cylinder, assembled in the test bench, is presented in Figure 3.2, which also shows the position of a movement sensor needed to measure and control the movements of the hydraulic cylinder. The sensor chosen for this task has a measurement taster and is the model ST3077 375 134-05, from Heidenhain.

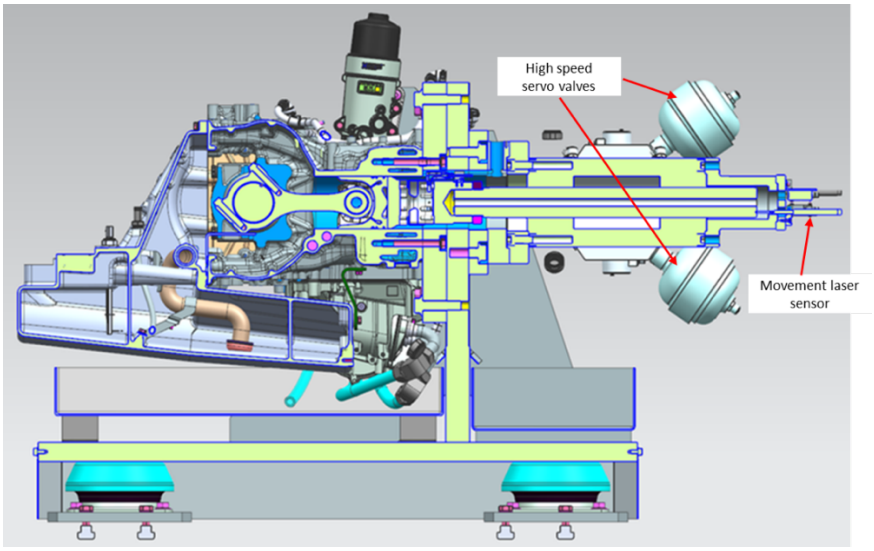


Figure 3.2 - Actual TLPP configuration with an overview of the hydraulic cylinder

A U3 load cell from HBM, which is a strain gauge-based load transducer capable of detecting loads from 0.5 to 100 kN, is located between the piston and the hydraulic cylinder to record and monitor the load generated by the cylinder, as presented in Figure 3.3. This ensures that the load pattern described by the cylinder in the piston is similar to the load in piston subjected to combustion.

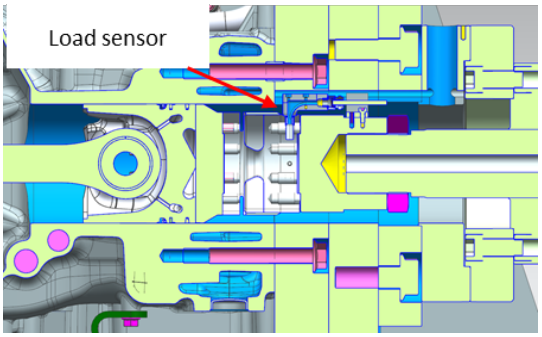


Figure 3.3 - Load measurement

3.2.1.2 Engine shaft

Since the load in TLPP acting in the connecting rods is generated by the hydraulic cylinders, piston and conrod movements are not necessary, and without then, less friction load is produced. However, with the lack of conrod movement, a new engine shaft is designed, as shown in Figure 3.4. In this crankshaft, the conrod bearing journals are placed in the same axis as the main bearing journals. The rigidity of this new shaft is maintained the same as in the series crankshaft and, in order to adapt the lubrication of the connecting rod bearing shells to the real conditions, the oil outlet holes for the new geometry have been adapted. The oil holes, however, besides having the same position as in the series crankshaft, do not have the same length, what could affect lubrication pressure and oil film build-up.

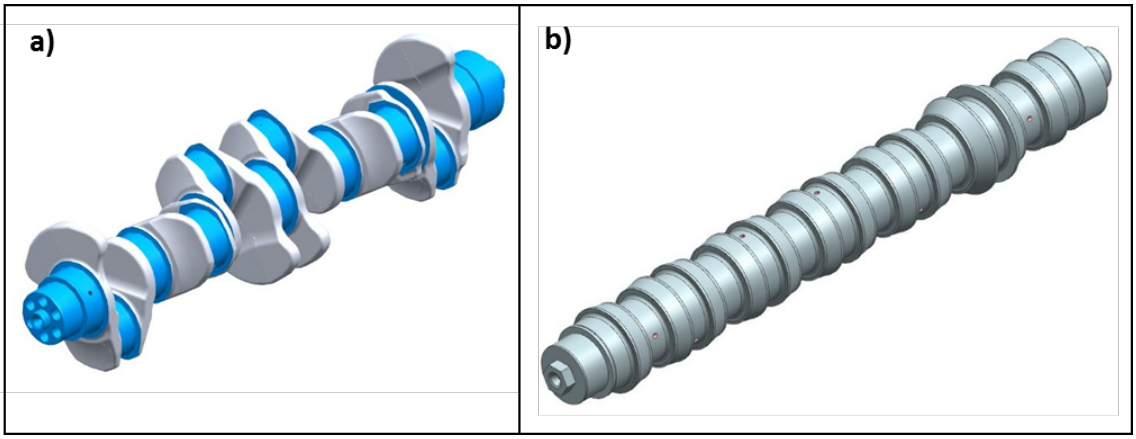


Figure 3.4 - Engine shafts a) cranked MDEG series 6-cylinder shaft and b) uncranked TLPP shaft

3.2.1.3 Electric Motor

While the hydraulic cylinders transmit the load produced into the piston, conrod, shaft and bearings, as the shaft is not cranked, no rotational movement is produced. To simulate the same rotational speed of a regular operational engine, and also accelerate the moments of inertia of all rotating elements of the test bench, an electric

motor is used. To determine the appropriate electric motor for this application, besides knowing the maximum rotational speed the test bench should achieve, the test bench moment of inertia must also be known. The moment of inertia of all the rotational elements of the test bench were then measured and the appropriated electrical engine is chosen.

For the electric motor assembly, a dummy flywheel was placed after the shaft to seal the engine, followed by an incremental encoder with a rotation measurement device attached, a clamping hub to compensate possible offsets between electric motor and crankshaft during assembly, a torsional stiff coupling, and another clamping hub between the coupling and the electric motor, as shown in Figure 3.5. The torque is measured by the current of the electric motor.

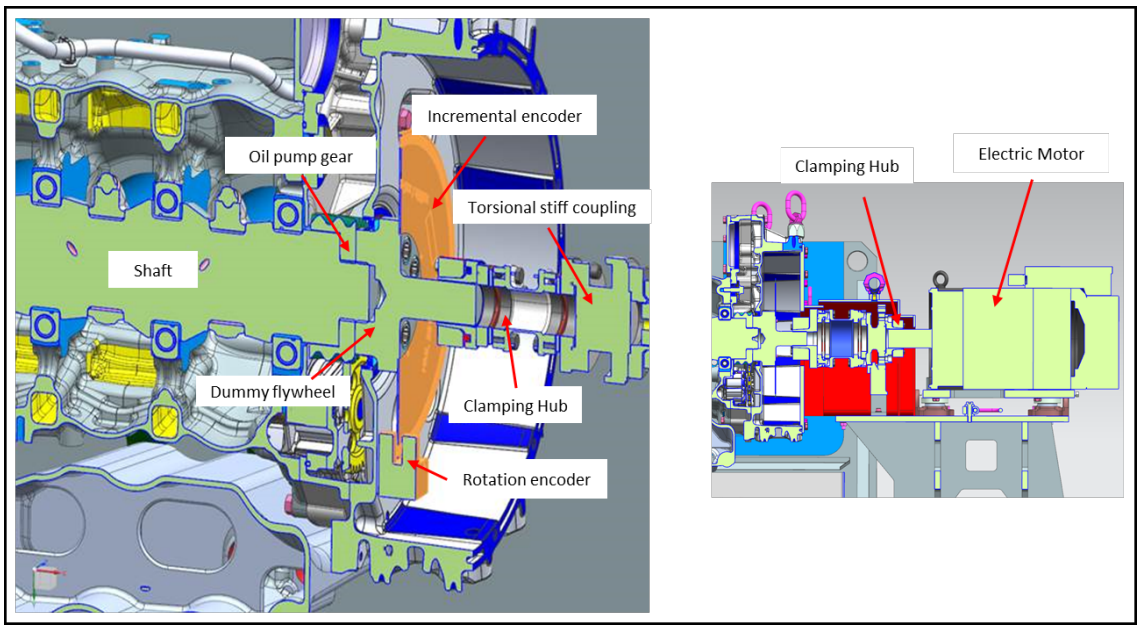


Figure 3.5 - Assembly of the Electric Motor in the Test Bench

The torque measuring hub is installed integrated to the speed measuring device to safeguard the correct execution of the given speeds and torques, serving as a protection against possible bearing fretting, which is wear caused by cyclic motion of small amplitude. If during the test fretting occurs, the resulting torque will increase significantly and the test run can end early, to avoid bearing failure and possible component damage.

The incremental encoder is a ring attached to the flywheel with 720 slots and 0.5° resolution that can be detected by a laser. In this ring, a small section with no slots is used to determine the correct crankshafts position. In that way it is possible to build pressure and rotational speed curves as a function of the crank angle. This device also ensures that, at each start, the shaft begins rotating at the same position. This is important to the lubricating system, as the engine is projected so that oil supply to the conrod bearings is not interrupted during cylinder load application, what can disrupt the fluid film build up in the bearings.

3.2.1.4 Oil Conditioning

Since this test bench only simulates the combustion pressures and no combustion actually occurs, the only temperature increase in the system is due to friction. Because of that, the oil temperature is also not increased, and since this contributes

significantly to the bearing wear, the oil temperature of the test bench is increased and controlled by an external oil conditioning system. It consists of a temperature control unit that processes oil from the sump and a pump, which transports the pre-tempered oil from the conditioning unit to the oil pan of the engine. The engine oil pump then sucks the oil out of the oil pan and supplies it to the core engine on the test bench. Actually, the conditioning system can increase the temperature up to 82% of the maximum possible temperature for MSS, and can keep the oil temperature for a long operational time at 78% of this maximum temperature. To ensure that the oil conditioning works the oil temperature is controlled with a temperature sensor in the oil pan.

3.2.1.5 Connecting rods

As only 3-cylinder bores are assembled with the hydraulic cylinder, only 3-cylinder bores need a piston, and consequently a conrod. In the other 3-cylinder bores pistons are not needed and 3 dummy conrods are placed just to guarantee proper shaft positioning, as shown in Figure 3.6, and therefore, have no temperature sensors.

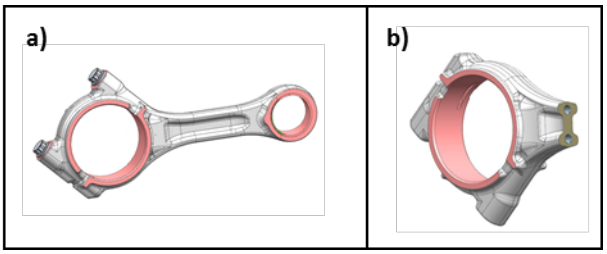


Figure 3.6 - Connecting rod types in TLPP: a) series con rod for cylinder 1, 4 and 6 and b) dummy con rod for cylinder 2, 3 and 5

In the 3 series connecting rods, placed in the same cylinder bores as the hydraulic cylinder, a thermocouple is assembled, as presented in Figure 3.7. Normally, the temperature sensors for this purpose are mounted directly on the back of the plain bearings, but since the bearings are replaced regularly for the experiments, this new location, 1 mm below the surface of the large con rod eye is found. This temperature measurements are useful for further data analysis.

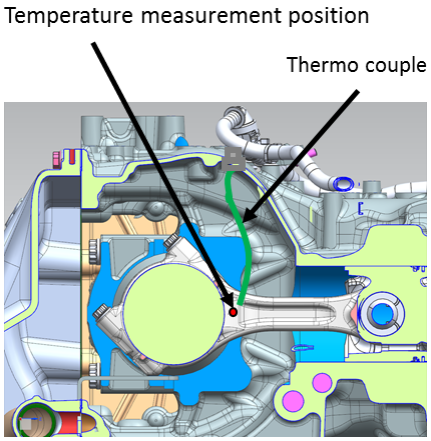


Figure 3.7 - Conrod temperature measurement

3.2.1.6 TLPP Automatization

A complex automation system controls TLPP and is basic composed of the following main units:

- **The central CPU (central processing unit)** stores the computer memory and because of that, is capable of executing instructions in a form of program coming from the operation or control unit. The central CPU is also connected to a block CPU, where the central CPU redirects the instructions for this specific test bench, to the central equipment control and the central oil supply line and to a connection to PMC (Process Management Calculator), to build a closed loop circuit. The central CPU has a manual stop switch in the control room in cases of emergencies.
- **The central equipment control** and the central oil supply line are connected to the oil supply central control for the hydraulic actuators and vegators, capable of detecting the oil levels in the line, and emergency switches for both the vegators and the whole central equipment and oil supply line control unit. This unit can also switch the equipment in case of emergency.
- **The block CPU** is connected to the PMC, to MR (Measurement Regulation) and send instructions to the equipment operating the test bench, such as the electric outlets, compressed air, cooling system and hydraulic valves. It also has a manual emergency stop switch.
- **The test bench** can also send a stop sign of a limit switch sign for the block CPU, for the CPU to actuate on the test bench. The measurements obtained during the test bench operation are collected by the measurement regulation system, which also controls the valves on the test bench and send signals to the block CPU and are capable of switching off the Block CPU in case the MR signs are not properly received by it.
- **The MR system** sends the measurements to the PMC system as it sends the MR system the set values and activate the measurements regulation system. This both units are connected by a watchdog.
- **The PMC system** is also connected to the block CPU by a watch dog and can send signals for the test bench to be activated. The PMC is capable of processing the data measured on the test bench obtained by MR system and records it in a software called jBeam, so that the data can be further analyzed and interpreted.

Basically, the operation unit gives instructions in a form of operation programs to the central and block CPU, where they are processed, activating the equipment that composes the test bench. The measurements obtained by the test bench operation are acquired by the MR system and interpreted in PMC system, which records the data in a data management software. All the units are connected by connecting channels such as Profibus, Profinet, Ethernet and EtherCAT. It is impornat to emphasize that all sensors used in the test bench were duly calibrated according to the procedures suggested by the manufacturers.

Regarding only the test bench sphere and its equipment, the electric outlet activates both the oil conditioning system of the test bench, developed by Pollux, and the Hausmann electrical enclosure, responsible for energy distribution to the Euchner incremental encoder assembled in the dummy flywheel and a frequency converter connected to the electric motor. The oil temperature in the oil sump is measured and interpreted by the oil conditioning system itself, which controls than, the oil warming process. The temperature of the oil measured in the conrods, the hydraulic cylinder movements, the load measurements between hydraulic cylinder and conrod and the dummy flywheel rotational speed are acquired by MR. PMC acquires the Haussmann signals, tracks the crank angle and interpret the measurements sent by MR. Figure 3.8 presents a scheme of the test bench automatization.

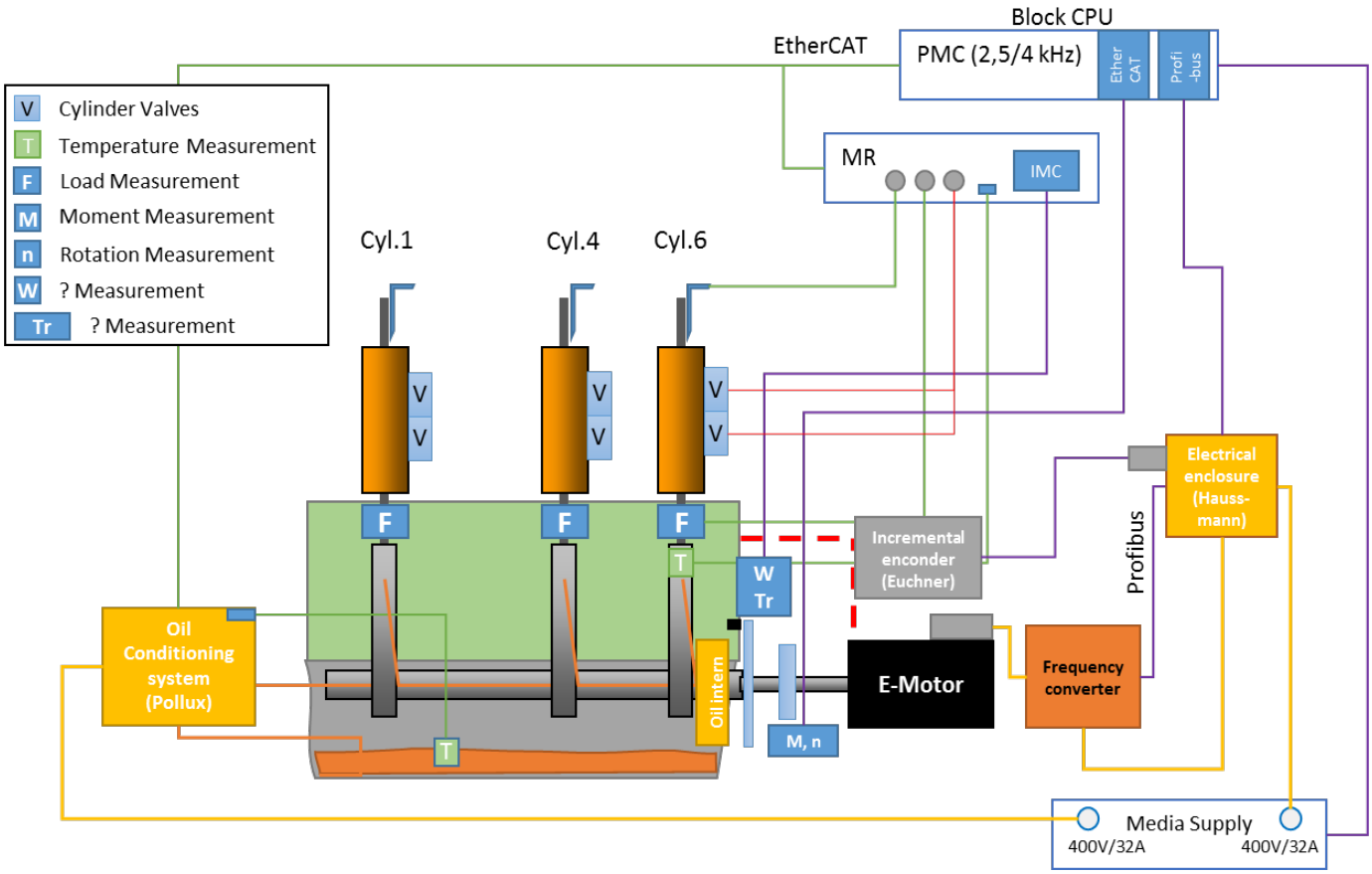


Figure 3.8 - Test bench equipment automatization scheme

3.2.1.7 TLPP Program

The pressure profiles an ICE as a function of the crank angle are shown in Figure 3.9. In the graphic, the cylinder pressure axis presents the percentages related to the highest load peak. Based on this graphic the TLPP programs is developed.

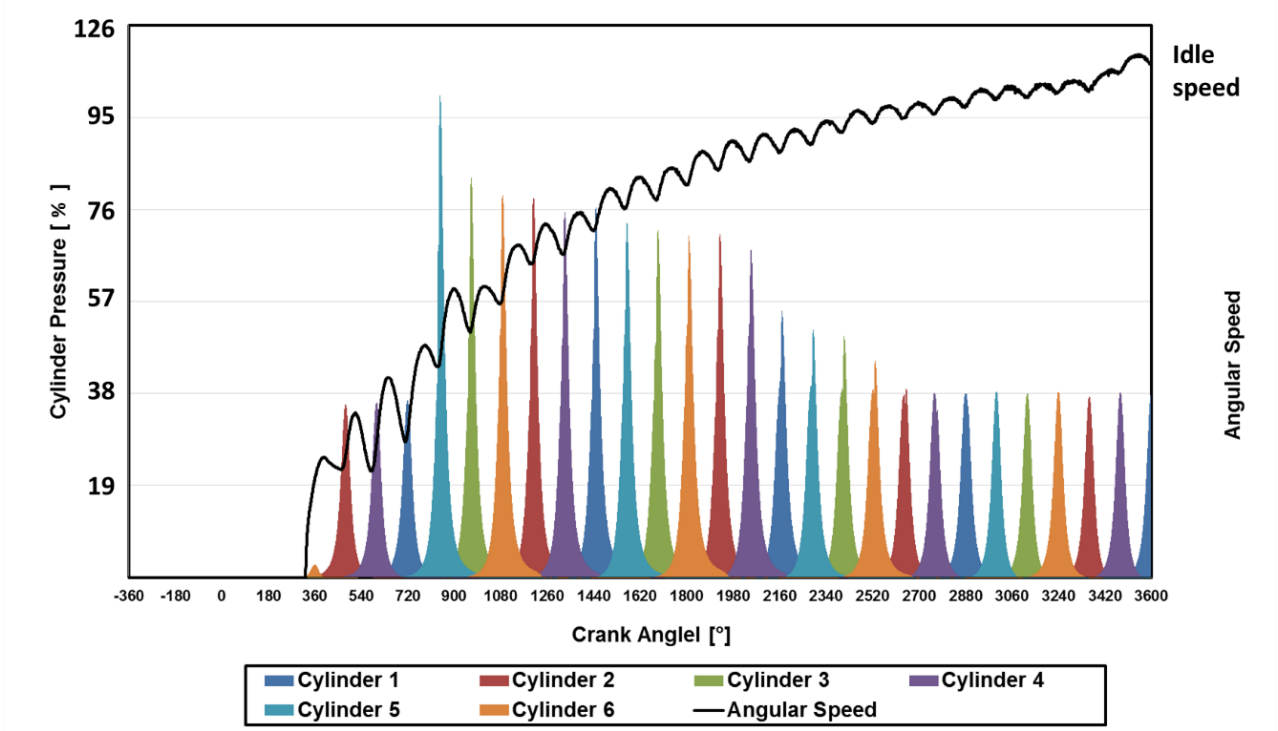


Figure 3.9 - Cylinder pressure and angular speed behavior during engine start, Credits: (Nebelsiek, 2017)

3.3 Test Materials

This phase comprehends all the methodology to develop test programs and acknowledge the bearing behavior during TLPP operation. All program versions in this phase are conducted with series bearings, already known not to withstand start-stop operation, and then, expected to present high wear rates, easier to measure and compare. Table 3.1 presents the bearing set configuration. The corresponding bearing materials specifications are listed in Annex 1.

Table 3.1 - Bearing set for validation tests

Bearing Type	Amount	Bearing Name
Upper main bearing	7	A370
Lower main bearing	7	G488
Upper conrod bearing	6	G488
Lower conrod bearing	6	A370
Thrust washer	2	A370

In all previous MDEG Daimler engine tests regarding ISS operation, the lubricant oil used was the Shell Rimula R6 LME 5W-30. According to the RNT research conducted, the worst wear results with this oil are obtained at the highest possible temperature for MSS. To test the most extreme conditions in TLPP for better comparison this test bench should also work with this temperature. However, due to limitations in the TLPP conditioning system engines, the oil temperature in this test bench can be stabilized in 78% of this temperature. Considering the other Shell oils available, with the same additive package as the HTHS 3.5, the Figure 3.10 shows that this oil viscosity at the highest temperature is similar to the HTHS 2.5 oil at 78% of this temperature, so, for the tests in TLPP, the oil used is the Shell Oil Blue, 0W-20, HTHS 2.6.

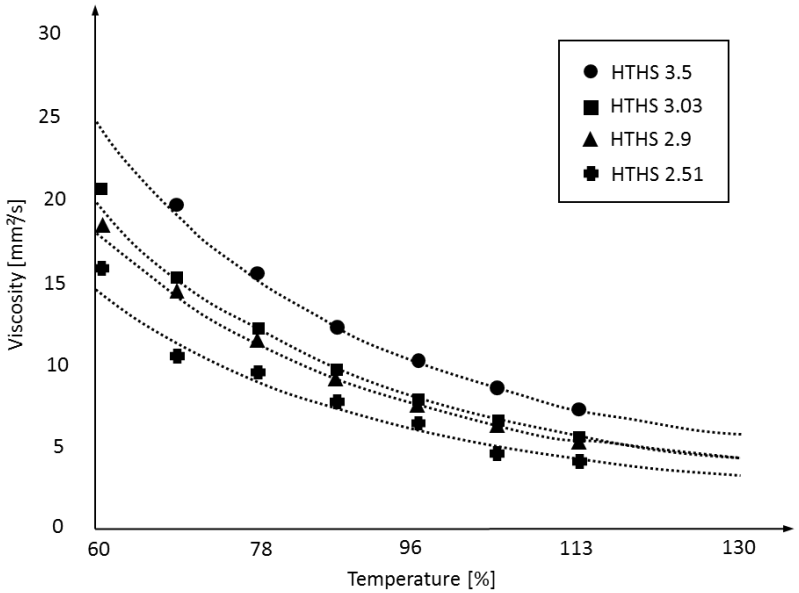


Figure 3.10 - Shell Oil Blue, 0W-20 oil viscosity dependence of temperature

3.4 Test Planning

Using the equipment presented in the previous sections, the research regarding the first TLPP program is tested, using the Shell Oil Blue, 0W-20, HTHS 2.6 at 78% of the maximum temperature in which the start-stop can be operated. Then, according to the ICE load patterns collected, a first TLPP program was developed. In the first test programs, the only parameters varing are the number of engine starts. Since the wear process occur primarily in surfaces, the dimension control of the parts before and after test is conducted. The preliminary measurements have the purpose of certifying that the bearing dimensions are within fabricant and designer tolerances and to be a reference for the geometric after measurements and calculate the final wear obtained during operation.

All main and conrod bearings are subjected to various dimensional checks in the precision measuring quality department, being the most important the wall thickness and bearing profile. Before all tests, the bearings are always cleaned and measured one time in each determined position. When they are measured before being tested and came directly from the supplier, they are only cleaned with alcohol, to clean eventual dirt particles. After the tests they are cleaned first with white spirit, a petroleum-derived organic solvent to clean the lubricant of the bearing surface. After that, to clean the oil coal in the back of the bearings a fine polishing paste model EMR fein from Ambassador is used. Then, another set of measuremnts is conduted, carring on one measurement in each position already measured before test.

To guarantee the good bearing positioning during wall thickness measurements, the bearings are positioned in a pallet module and separated by supports, as shown in Figure 3.11. The bearings must be positioned also according to the order shown in the figure, i.e., first the lower main bearing, followed by upper main bearings, lower conrod bearings and upper conrod bearings. Before measurement, all parts receive a code to indicate if they are lower or upper bearing shells, and also in which position they should be assembled. That is extremely important to guarantee proper comparison between measurements before and after engine operation.

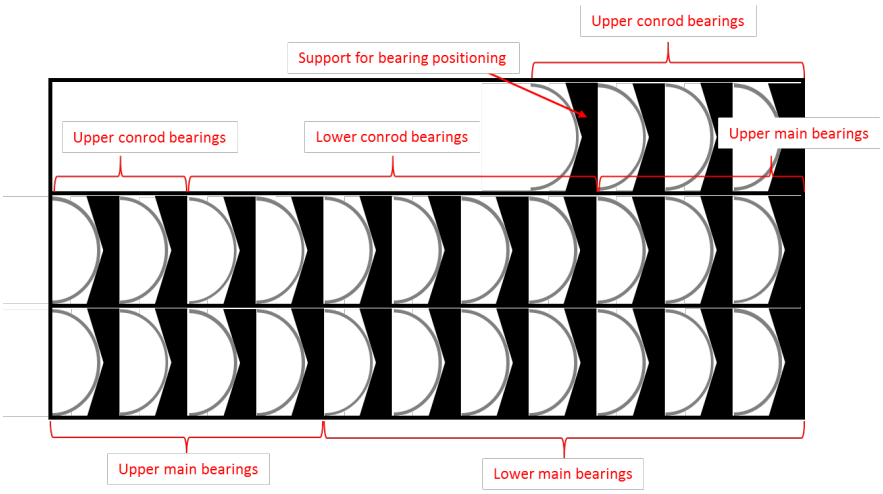


Figure 3.11 - Bearing position for measurements

The measurements are conducted by a coordinate measuring machine (CMM) model PMM-C 1000 from Leitz. The measurement developed for CMM to measure 6-cylinder MDEG bearings shell requires the bearing positioning explained previously. The measuring tool used had a 3.0 mm diamond tip to guarantee no damage to the bearing surface during measurement, similar to the one presented in Figure 3.12.



Figure 3.12 - CMM Measuring Tip, Credits: (Hexagon, 2018)

The measurement tool calibration is conducted every new bearing batch measurement by a probe test unit developed by Retter, as shown in Figure 3.13, according to the manufacturer suggestions. The device comprises a 30 mm ring gage and a 30 mm ceramic calibration sphere with holder and is used to guarantee the capability of the tool to measure inner and outer diameters. After calibration, the measurement accuracy of the equipment is 0.8 µm.



Figure 3.13 - Probe Testing Unit, Credits: (Retter, 2018)

The wall thickness is measured in 2 directions, as shown in Figure 3.14. According to Figure 3.14a the measurement tool walks a horizontal path in 5 different positions of the bearing in the angles 10°, 45°, 90° 135° and 170°, considering that the upper part of the bearing with the positioning nose down corresponds to 180° and the lower part is 0°. These measurements are done inside and outside. The difference between the outside and inside measurements give the wall thickness in these regions. Measurements are also done along the edges, as shown in Figure 3.14b. For bearings with oil grooves, measurements are made in 2 paths outlying by 6 mm the bearing edges. For bearings without oil grooves, measurements are also made in a path in the middle of the bearing. Once again, measurements are made inside and outside of the bearing and the difference between these two measurements give the wall thickness of these regions.

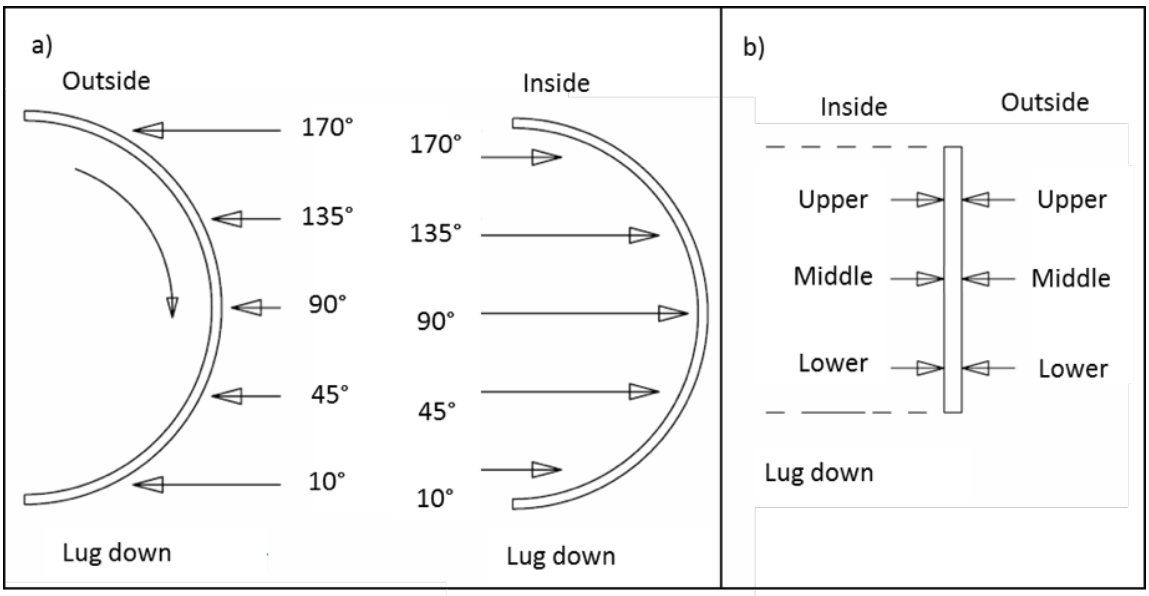


Figure 3.14 - Wall thickness bearing measurement positions

As explained previously, the critical region of MDEG bearings take place normally 45° of the bearing lugs. Because of that, the machine MarSurf VD 140 from Mahr, shown in Figure 3.15, is used to measure roughness of this region. The measuring tool used is the PCV 175-M/8 3045 with 1.0 µm accuracy.



Figure 3.15 - Machine MarSurf VD 140, Credits: (Mahr, 2019)

The measuring tool walks through the 25 mm at the 45° shell angle with 1.20 mm/s. It is then determined what is the biggest depth difference considering the edges as zero, as shown in Figure 3.16. In bearings with oil groove 2 results are obtained, one for the left and one for the right part of the bearing.

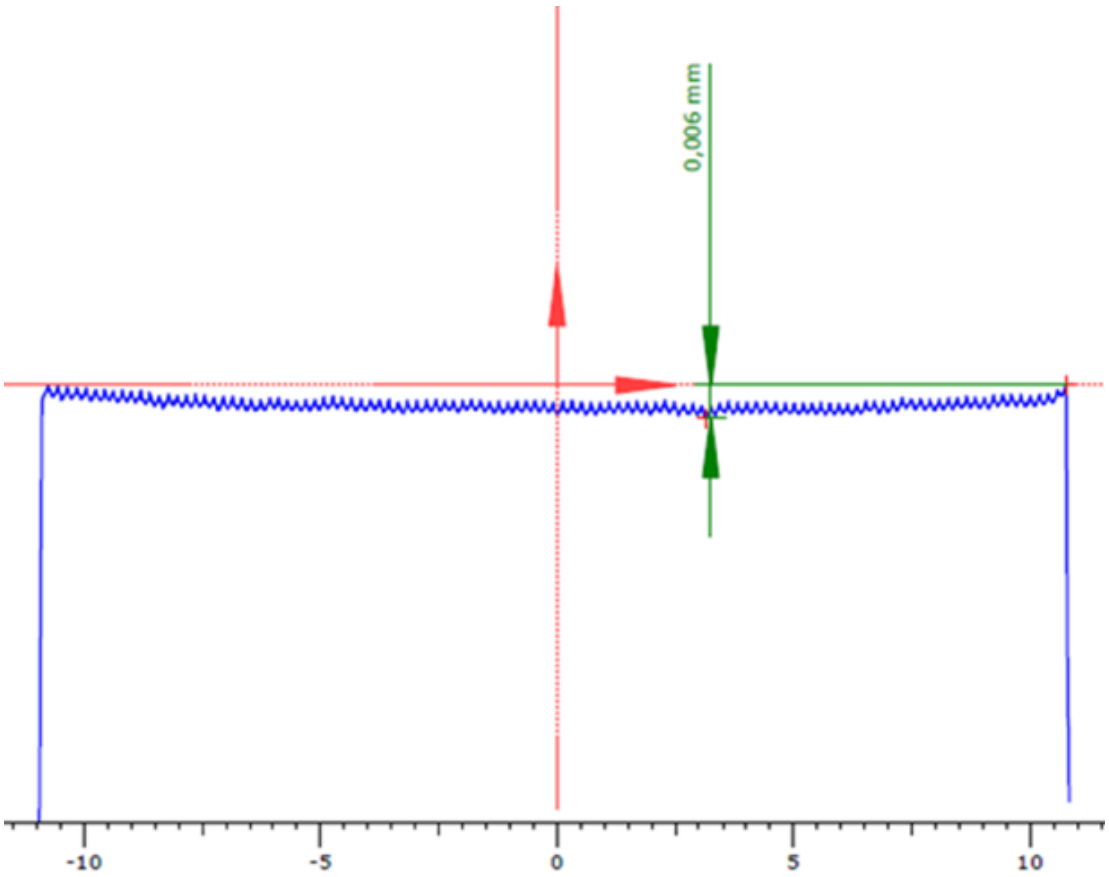


Figure 3.16 - Surface's biggest depth difference

The first TLPP program is then tested with some numbers of starts and the bearing thickness and profiles after test are collected and compared to the preliminary bearing measurements in order to evaluate wear. With the wear data acquired and the photograpy taken of the bearings, further investigations are conducted.

With the dimensional data collected and the data acquired from the TLPP automation program, jBeam, the lubrication regime was studied according tho the method suggested in section 2.2.2.4. In this method, the counterbody loads, i.e., the simulated combustion loads, the engine speeds in which the load application occurs, and the geometric and lubrication parameters are taken into consideration to determine the lubrication regime in each case, in order to justify the bearing wear profile observed after tests.

After that, using the method described in section 2.2.3, knowing the load applied between counterbodies and the sliding distance between the surfaces, the wear is calculated. Then, the calculated wear is compared to the actual wear observed in the tests and the results are discussed to evaluate if the method can be used in to predict wear in this kind of application.

With the analisis of the results obtained in the first tests, the challenges associated with the test bench implementation and program development are discussed, in order to solve them. Then, a knowing a little more about the functioning of the test bench, an optimization of the program is suggeted so that reliable results are obtained more efficiently and quickly.

4 RESULTS AND DISCUSSION

This chapter presents the results obtained according to the methods explained in the previous chapter, justifies the observed according to literature and explains the next steps of the research in a form of scientific discussion. It is divided in the subsections: Preliminary Bearing Measurements, which explains how the measurement data is obtained in interpreted; TLPP First Test program, which explained how the first test bench program is developed; First, Second and Third Test, which present the measurement and photographic data regarding these first tests; Lubrication Regime, which uses the methodology presented in section 2.2.2.4 to determine the lubrication regimes during operation; Wear Calculation, which uses the methodology presented in section 2.2.3 to determine wear with empirical methods; and New Test Program, which presents a new optimized test program after the test bench operation is better understood.

4.1 Preliminary Bearing Measurements

As explained previously, for the wall thickness two methods are used, the horizontal measurements in 5 bearing position (170°, 135°, 90°, 45° and 10°) inside and outside and the measurements along the bearing edges. Figures 4.1 and 4.2 present an example of the both measurements for general comments. The measurements presented are of a new G488 bearing, before being tested. Figure 4.1 presents the inside and outside measurement paths in the 5 positions determined. The horizontal axel scale is equivalent to 1mm, and the vertical axel scale to 2.5 mm. The higher measurement values presented in the middle of the inside paths especially in the angles 170° and 90° are related to the oil grove of this bearing. In bearings without oil groove more homogeneous measurements are expected. The heterogeneities presented outside in the same angles are related to bearings markings for identification.

Figure 4.2 presents the results obtained with measurements through the paths along the bearing edges. The images present exaggerated dimensions to illustrate the geometric pattern of the bearing. The angular scale corresponds to 30° and the axial scale 5µm. Thde Figure 4.2 shows the "ω form" of bearings before assembly, in which the diameter of the bearing in the bearing borders is slightly higher than its housing before assembly and higher than the bearing diameter in other positions. This feature can have geometric variations according to the manufacturer, but it is a strategy to facilitate the bearing assembly in its housing due to axial pressure and guarantee its positioning (Tambellini *et al.*, 2007).

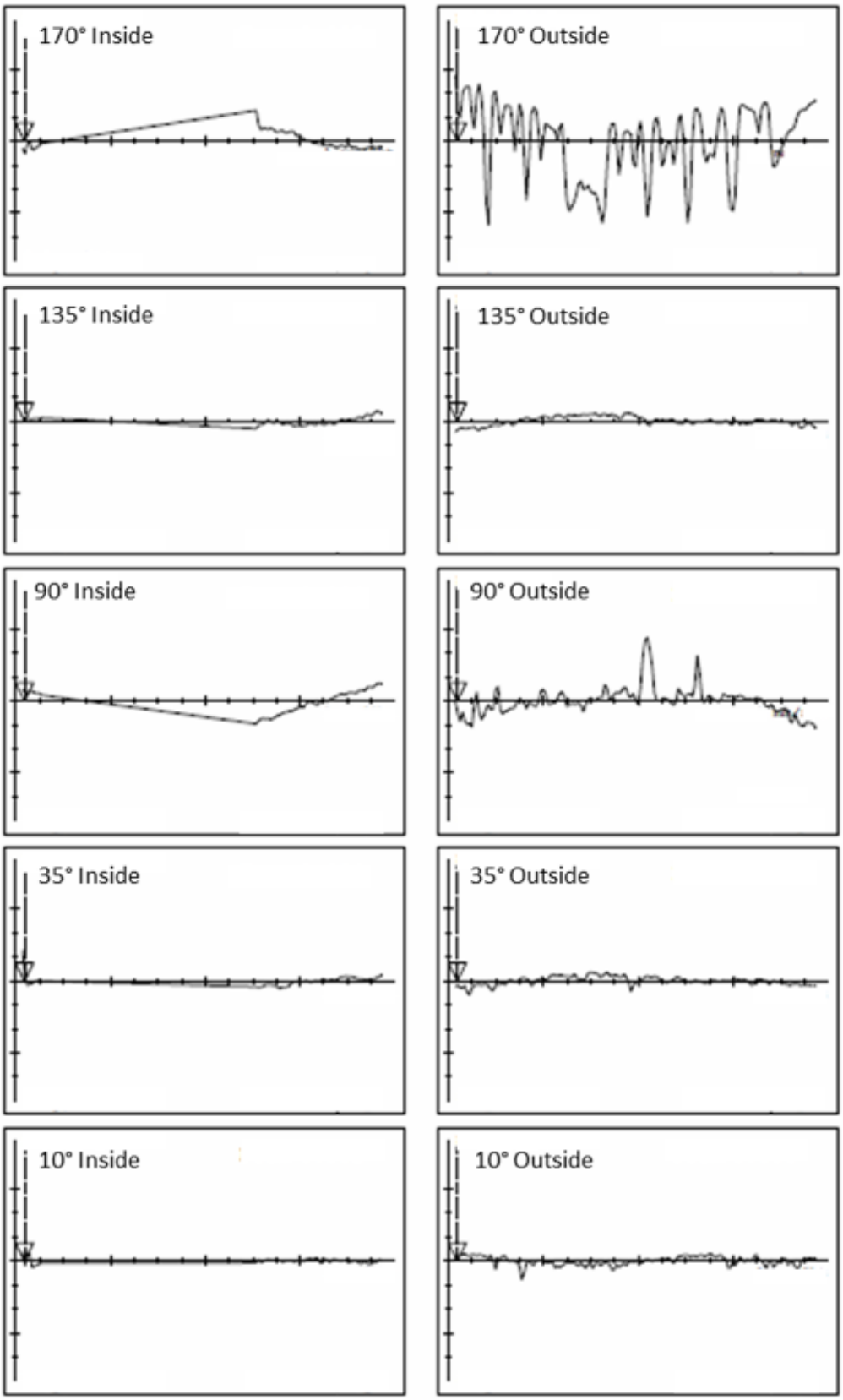


Figure 4.1 - Wall thickness with horizontal measurements

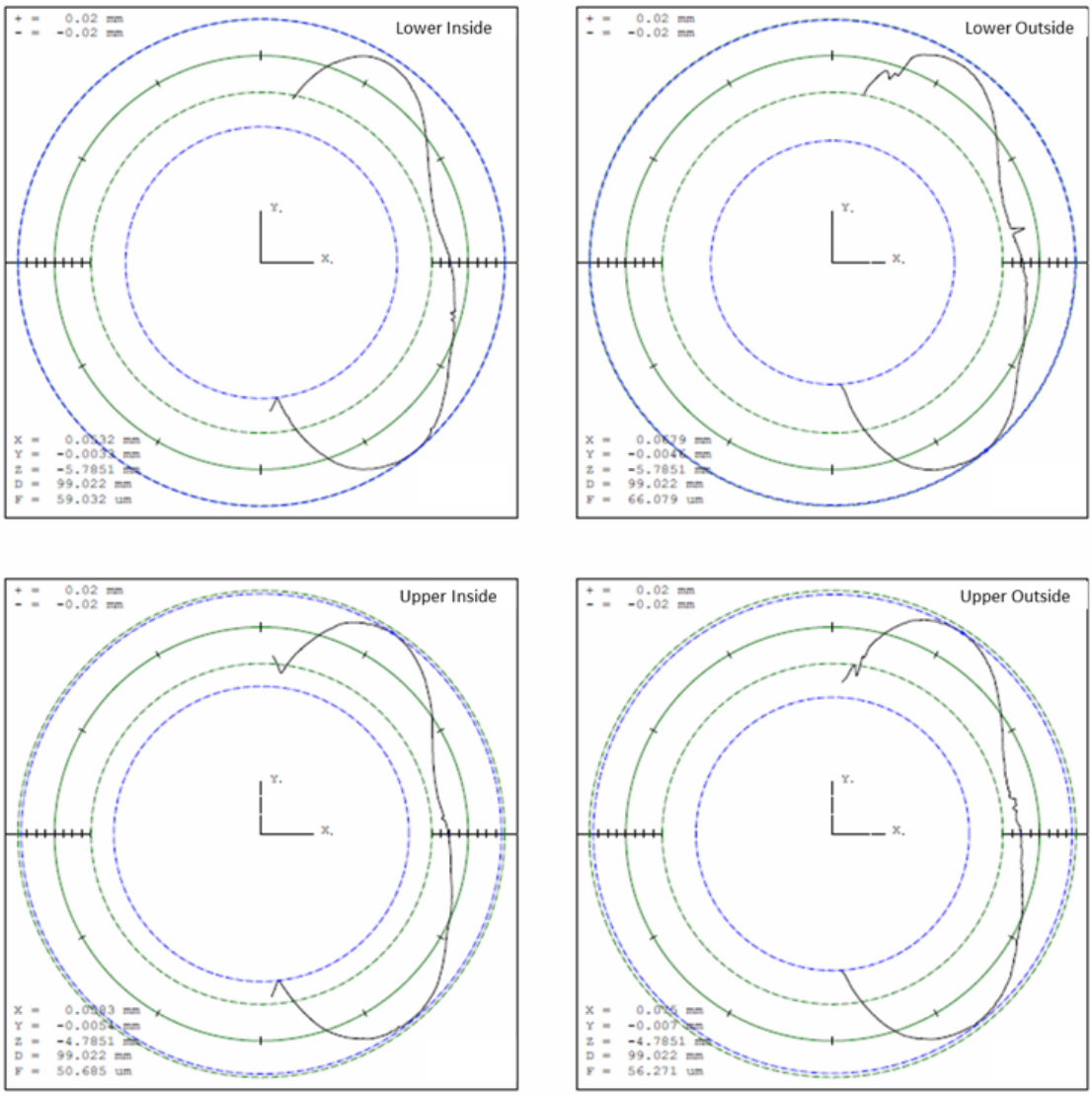


Figure 4.2 - Wall thickness with longitudinal measurements

As a result, from these measurements, it is determined the upper and lower measurement tracks. For the upper track, an average is estimated between the angles 21° and 28°; 85° and 94° and 151 and 159° and for the lower track between angles 20° and 27°; 87° and 94° and 153° and 160°.

4.2 TLPP First Program

The wear mechanism in a real engine is better represented when the real engine operating conditions are faithfully reproduced in TLPP. Hence, the main program tested tryies to reproduce same load curves obtained with an instrumented engine, as shown in Figure 4.3. Since the test bench was only 3 working cylinders, they will reproduce the load curves of two cylinders of the engine. Thus, load is applied in each con rod bearing shell every 360°, and not 720°, as in the real engine. Since each of the hydraulic cylinders simulates two different cylinders and thus different force profiles in each start, if at each start one different cylinder is started, a con rod bearing undergoes all possible load patterns after three engine starts on the test bench. The three starts are then called a cycle. To reproduce the rotational speed, the speed curve was smoothed, since

the electric motor cannot track the speed fluctuations. The load axis represents the percentages of the maximum load during start.

In Figure 4.3, the areas in which the speed is close to or zero are called hold times (H). This time is necessary after an engine stop, so that the shaft returns to its starting point and guarantees the load introduction at the same point on the crankshaft. If load is applied in the oil inlet bore region, the oil supply may be interrupted and harm the fluid film build up between bearing and shaft. The hold time is also important to guarantee that the following engine start begins from a standstill state, as it happens in a real engine, to let the oil circuit drain the oil through all leakages and to have the oil pump build up an oil volume flow while starting the engine as in a real engine use case, as well as time for the electric motor to cool down, guarantying its good performance and long lifetime.

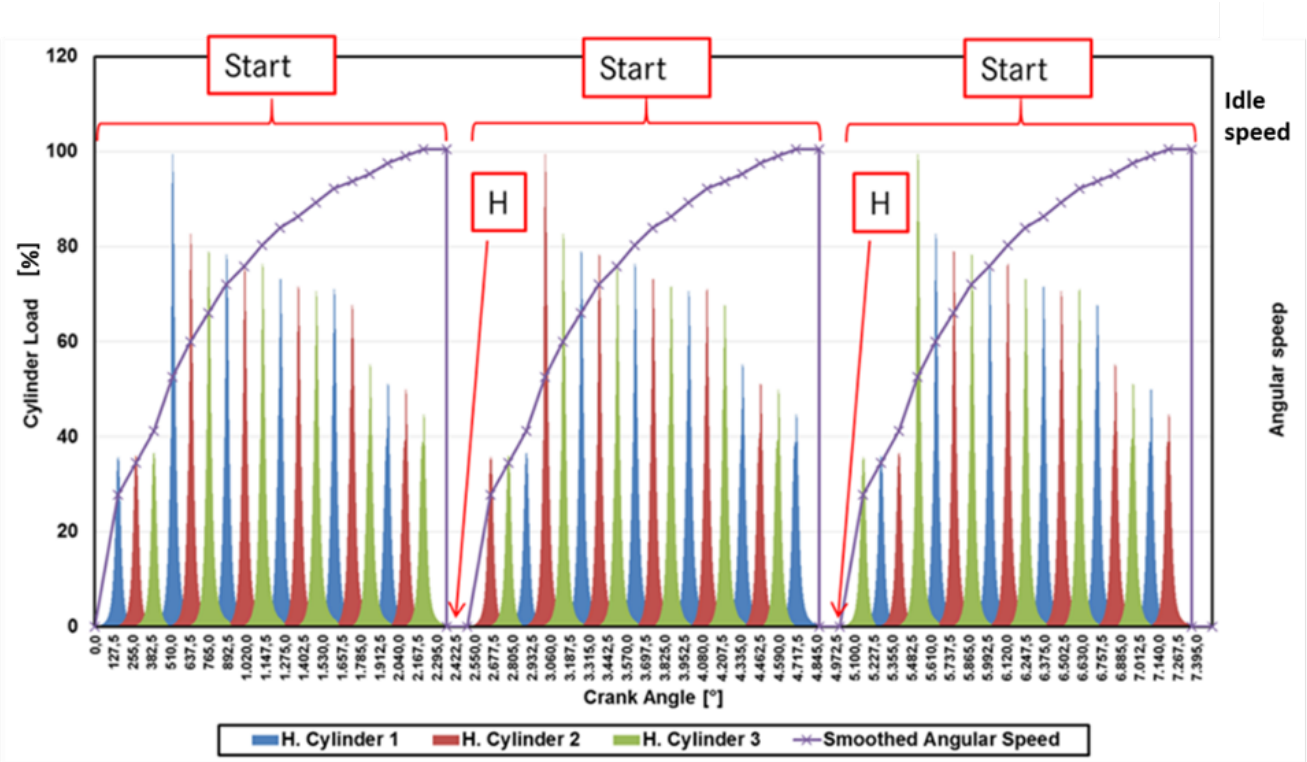


Figure 4.3 - TLPP program - Real engine start, Credits: Adapted from (Nebelsiek, 2017)

As a result of the test program suggested, after completion of a cycle, each connecting rod bearing is loaded as if it had experienced six real starts. The individual engine starts take about 1.1 seconds to reach their maximum speed.

Based on this suggested program, the first program developed for TLPP in the jBeam software platform is shown in Figure 4.4. This program follows the load pattern presented in a regular MDEG, simulating the load application in similar time and magnitude as in the regular combustion engine during a start and also the angular rotation speed, which raises while load is applied and reaches idle speed as the cylinders loads stabilize. Before the cycle star, all hydraulic cylinders are required to apply around 4% of the maximum load to test its proper functioning. After this test is completed, the electric motor starts rotating the shaft and after one second, the actual loads regarding an engine start are simulated. This process takes 1.07 s and, after that, the system takes 0.57 s to be totally switched off. As soon as the system is switched off, the load test in all the cylinders is once again conducted and a new start takes place.

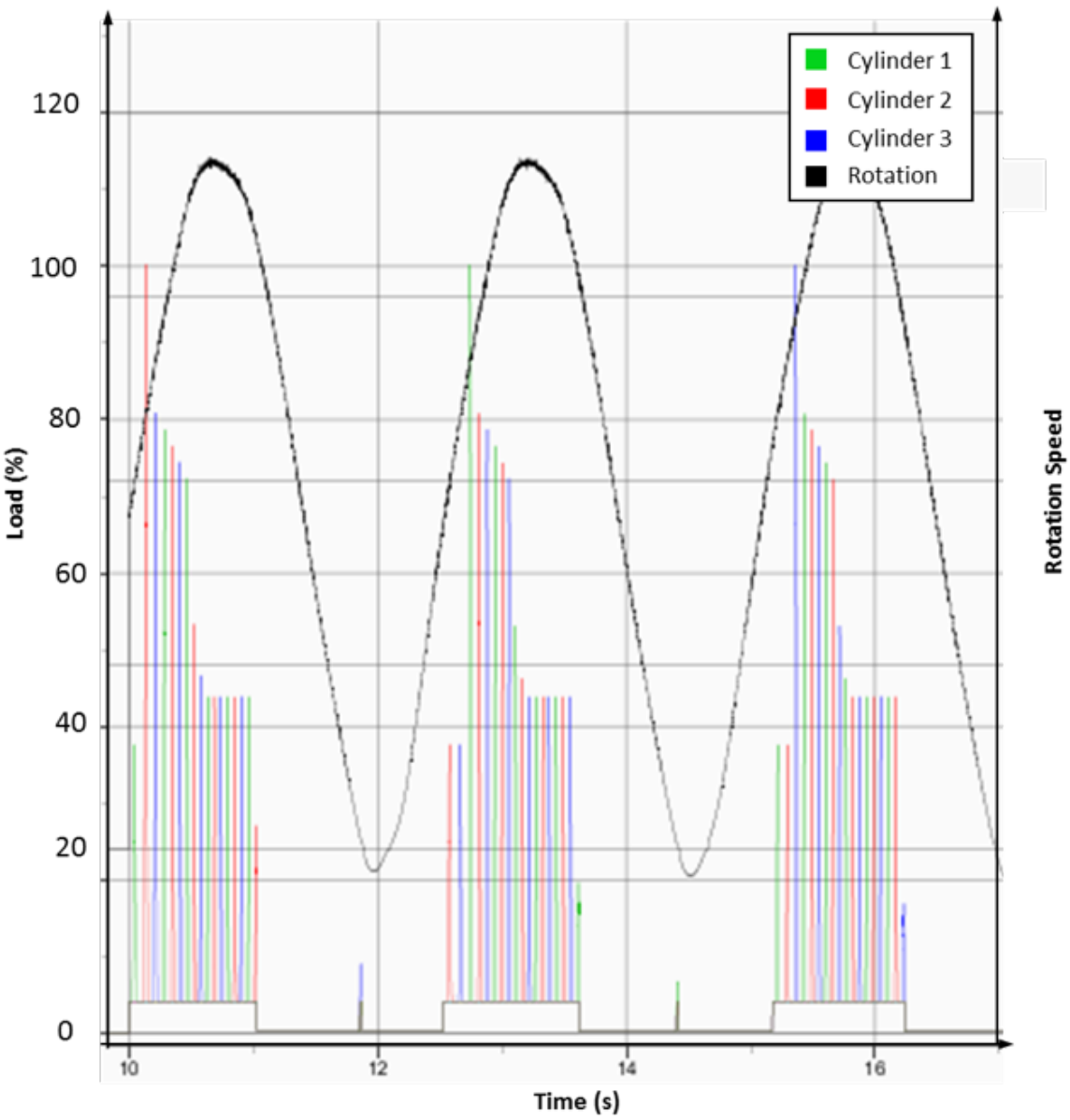


Figure 4.4 - First TLPP Program

To simulate the load application exactly when required, a wanted load curve is drawn on jBeam, the software that controls TLPP. However, for the load curve in TLPP to occur in the wanted moment, considering the delay between the signal and the actual load application, a signal curve based in the wanted curve is constructed by the software, considering the rotation in the moment and at each previous angle the signal must be done so that the real load curve is similar to the wanted curve, as seen in Figure 4.5. It is also important to point out that although the load curve in an ICE is continuous, the load curves applied in TLPP are built of discretized points.

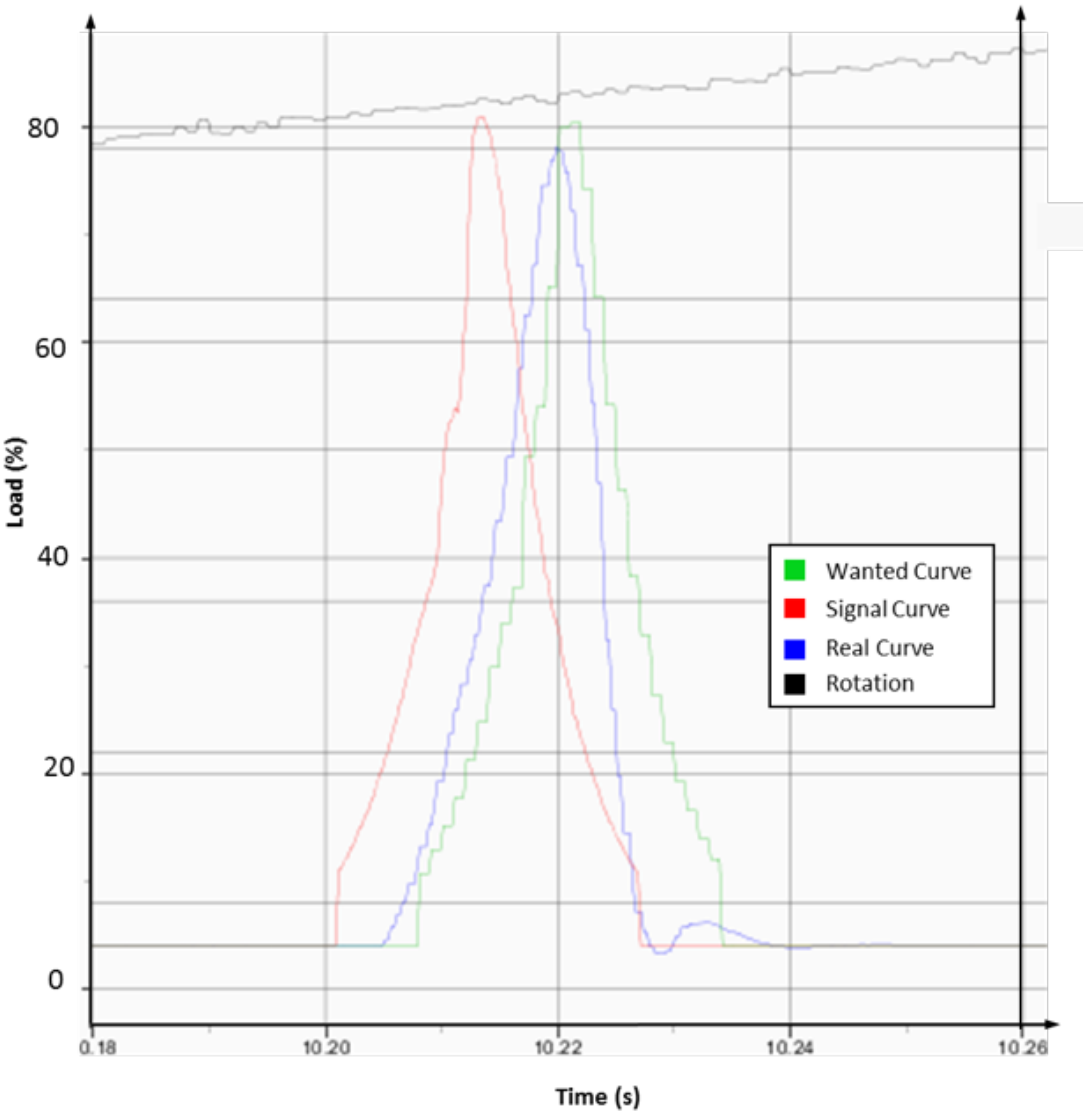


Figure 4.5 - Wanted, Signal and Real Load Curves

Using this first program, the measurement data aquired during tests, as well as the lubrication and wear analysis are conducted and discussed in the following sections.

4.3 First Test

According to the RNT research conducted previously in Daimler MDEG engines in start-stop cycles, the faster bearing wear occurs in the first 5,000 starts. With this premise, the first test conducted in TLPP was using the program shown in Figure 4.4 during 5,000 starts. Figure 4.6 shows the conrod and main beaings after test. In this figure the wear in clearly seen in the lower main bearings 1 and 7, which suggests the the shaft flexion of the axis, what is probably increased as the shaft is uncranked, and hence, with lower bending momentum. The upper conrod bearings 1, 4 and 7 presented also considerable wear when compared to the others, what is expected, as only in this positions the hydraulic cylinder load is applied. In the upper conrod bearings some trace of abrasive wear is also noted, which highlits the importance of oil filtration and the need to change engine oil frenquently not to damage engfine parts.

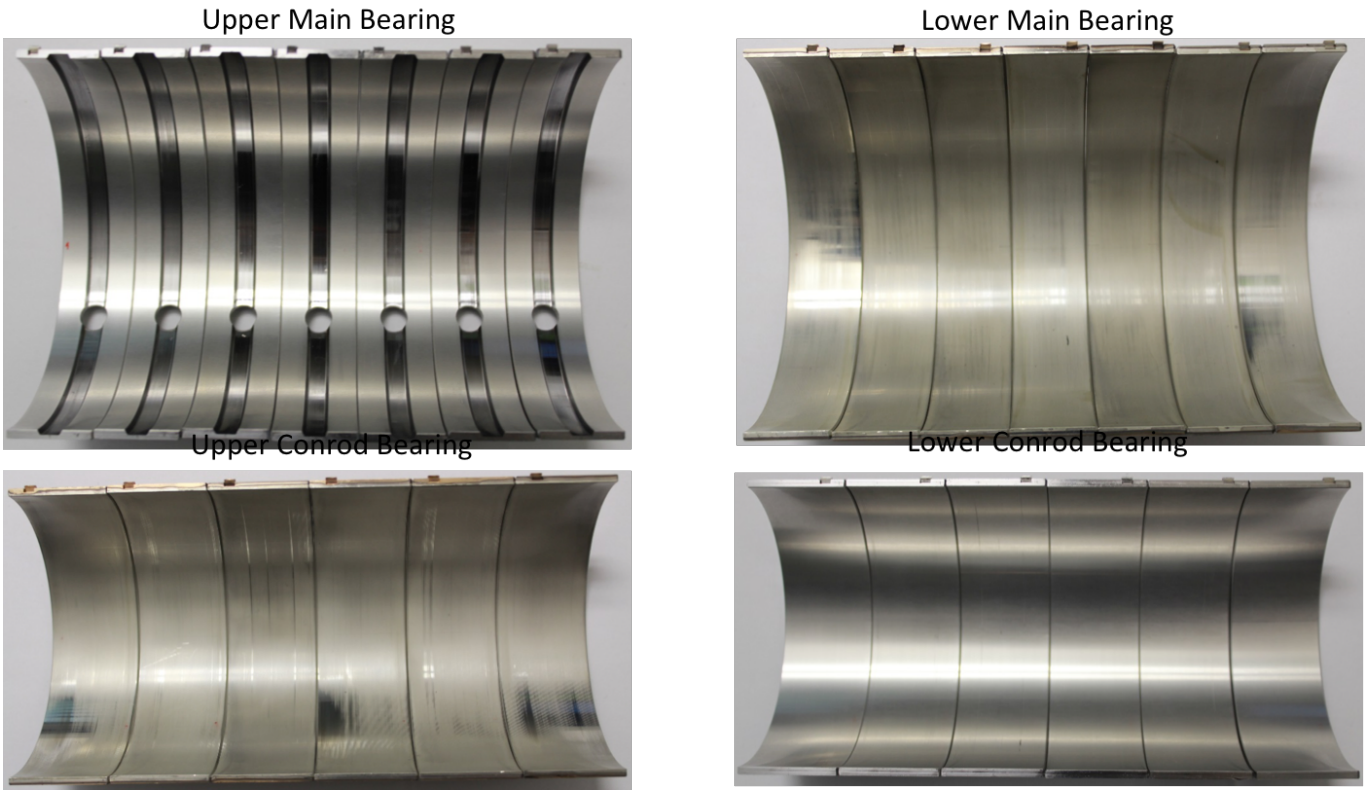


Figure 4.6 - Bearings after test 1

The geometric measurements made previous and after the test were recorded and subtracted to obtain the width worn out during the test bench operation in each bearing region. The wear results are shown in Table 4.1. The bearing set obtained a number, 14519493K1, as each bearing of the set. The upper main bearing had the 14567048K and the last number, from 1-7 is related to this positioning, the same happened for the lower main, upper conrod and lower conrod bearings, that received respectively the numbers 14567049K, 14567045K and 14567044K.

The wear variates slightly and randomly with the bearing measuring position in most of the cases and presented an average of 0.0012µm worn layer. Analysis made with worn layers are however not accurate as each bearing region withstands a different load charge and hence, should present a different wear pattern. For the conrod bearings, the ones expected to withstand higher loads, in some regions the wear width reaches 0.0028µm, as expected. However, the conrod bearings supposed to present more wear were the upper bearings in positions 1, 4 and 6, where the hydraulic cylinders are located. This difference is not clear by the results obtained and in addition, some results indicates negative wear, meaning the bearing width increased during operation. Even though this is possible due to particles deposit in the bearing shell, it is unlikely to occur in such early operation phase, especially the wear is observed in the bearing shells in general is not enough to produce this kind of deposit. All of these results, unfortunately cannot be further analyzed as they stand in a region of measuring inaccuracy of the measuring tool, which is 0.8 µm. This fact explains, however, the presence of negative wear, which means that the bearing width measured after the test is superior to the bearing width measured before.

Position	Position Average	14519493K1															
		Main bearings							Conrod bearings								
		Upper main bearing			Lower main bearing				Upper conrod bearing				Lower conrod bearing				
		Upper measuring track	Lower measuring Track	Average	Upper measuring track	Middle measuring track	Lower measuring Track	Average	Upper measuring track	Middle measuring track	Lower measuring Track	Average	Upper measuring track	Middle measuring track	Lower measuring Track	Average	
		(mm)	(mm)	(mm)	(mm)	(mm)	(mm)	(mm)	(mm)	(mm)	(mm)	(mm)	(mm)	(mm)	(mm)	(mm)	
	(°)	14567048K1			14567049K1				14567045K1				14567044K1				
Begin (20°-30°)	25	0,0015	0,0017	0,0016	0,0021	0,0017	0,0013	0,0017	0,0026	0,0016	0,0016	0,0019	0,0010	0,0023	0,0028	0,0020	
Middle (85°-95°)	90	0,0009	0,0016	0,0013	0,0027	0,0013	0,0014	0,0018	0,0000	0,0031	0,0028	0,0020	0,0017	0,0006	0,0020	0,0014	
End (150°-160°)	155	0,0009	0,0006	0,0007	0,0013	0,0013	0,0021	0,0016	0,0003	0,0013	0,0003	0,0006	-0,0004	0,0020	0,0015	0,0010	
Average		0,0011	0,0013	**0,0012**	0,0020	0,0014	0,0016	**0,0017**	0,0010	0,0020	0,0016	**0,0015**	0,0008	0,0016	0,0021	**0,0015**	
		14567048K2			14567049K2				14567045K2				14567044K2				
Begin (20°-30°)	25	0,0012	0,0015	0,0013	0,0015	0,0012	0,0018	0,0015	0,0007	0,0025	0,0009	0,0014	0,0007	0,0029	0,0022	0,0019	
Middle (85°-95°)	90	0,0011	0,0008	0,0010	0,0009	0,0011	0,0014	0,0011	0,0032	0,0009	0,0013	0,0018	0,0002	0,0020	0,0018	0,0013	
End (150°-160°)	155	0,0007	0,0008	0,0008	0,0010	0,0008	0,0007	0,0008	0,0011	0,0012	0,0018	0,0014	0,0006	0,0012	0,0018	0,0012	
Average		0,0010	0,0010	**0,0010**	0,0011	0,0010	0,0013	**0,0012**	0,0017	0,0015	0,0013	**0,0015**	0,0005	0,0020	0,0019	**0,0015**	
		14567048K3			14567049K3				14567045K3				14567044K3				
Begin (20°-30°)	25	0,0010	0,0013	0,0011	0,0017	0,0007	0,0016	0,0013	-0,0001	0,0029	0,0003	0,0010	0,0018	0,0004	0,0016	0,0013	
Middle (85°-95°)	90	0,0015	0,0011	0,0013	0,0025	0,0016	0,0019	0,0020	0,0029	-0,0004	0,0015	0,0013	0,0018	0,0009	0,0011	0,0013	
End (150°-160°)	155	0,0000	0,0014	0,0007	0,0002	0,0011	0,0010	0,0008	0,0021	0,0011	0,0020	0,0017	-0,0001	0,0002	0,0030	0,0010	
Average		0,0008	0,0013	**0,0011**	0,0015	0,0011	0,0015	**0,0014**	0,0016	0,0012	0,0013	**0,0014**	0,0012	0,0005	0,0019	**0,0012**	
		14567048K4			14567049K4				14567045K4				14567044K4				
Begin (20°-30°)	25	0,0016	0,0018	0,0017	0,0020	0,0015	0,0012	0,0016	0,0003	0,0023	0,0023	0,0016	0,0009	0,0027	0,0017	0,0018	
Middle (85°-95°)	90	0,0012	0,0009	0,0010	0,0012	0,0018	0,0001	0,0010	0,0022	0,0003	0,0001	0,0009	0,0004	0,0022	0,0017	0,0014	
End (150°-160°)	155	0,0010	0,0001	0,0005	0,0008	0,0007	0,0009	0,0008	0,0005	0,0007	0,0001	0,0004	-0,0004	0,0012	0,0005	0,0004	
Average		0,0013	0,0009	**0,0011**	0,0013	0,0013	0,0007	**0,0011**	0,0010	0,0011	0,0008	**0,0010**	0,0003	0,0020	0,0013	**0,0012**	
		14567048K5			14567049K5				14567045K5				14567044K5				
Begin (20°-30°)	25	0,0015	0,0017	0,0016	0,0015	0,0013	0,0014	0,0014	0,0008	0,0025	0,0018	0,0017	0,0021	0,0003	0,0004	0,0009	
Middle (85°-95°)	90	0,0021	0,0006	0,0013	0,0017	0,0014	0,0022	0,0018	0,0012	0,0009	0,0019	0,0013	0,0007	0,0020	0,0004	0,0010	
End (150°-160°)	155	-0,0001	0,0017	0,0008	0,0012	0,0017	0,0007	0,0012	0,0016	-0,0005	-0,0006	0,0002	0,0011	-0,0007	0,0003	0,0002	
Average		0,0012	0,0013	**0,0012**	0,0015	0,0015	0,0014	**0,0015**	0,0012	0,0010	0,0010	**0,0011**	0,0013	0,0005	0,0004	**0,0007**	
		14567048K6			14567049K6				14567045K6				14567044K6				
Begin (20°-30°)	25	0,0019	0,0008	0,0013	0,0016	0,0011	0,0013	0,0013	0,0017	0,0012	0,0024	0,0018	0,0012	0,0004	0,0027	0,0014	
Middle (85°-95°)	90	-0,0005	0,0016	0,0006	0,0014	0,0015	0,0003	0,0011	0,0013	0,0018	0,0015	0,0015	0,0008	0,0014	0,0018	0,0013	
End (150°-160°)	155	0,0013	0,0000	0,0007	0,0016	0,0005	0,0010	0,0010	-0,0005	0,0001	-0,0004	-0,0003	0,0018	-0,0009	0,0035	0,0015	
Average		0,0009	0,0008	**0,0009**	0,0015	0,0010	0,0009	**0,0011**	0,0008	0,0010	0,0012	**0,0010**	0,0013	0,0003	0,0027	**0,0014**	
		14567048K7			14567049K7												
Begin (20°-30°)	25	0,0009	0,0020	0,0014	0,0019	0,0022	0,0014	0,0018									
Middle (85°-95°)	90	0,0024	0,0000	0,0012	0,0008	0,0023	0,0009	0,0013									
End (150°-160°)	155	0,0016	0,0009	0,0012	0,0011	0,0017	0,0003	0,0010									
Average		0,0016	0,0010	**0,0013**	0,0013	0,0021	0,0009	**0,0014**									

Table 4.1 - Wear measurement of the first test

The analysis of the bearing profile at shell angle of 45° for conrod bearings and 90° for main bearings, where the most load is applied, is shown from Figures 4.7 to 4.12. All these figures show in the bearing profiles previous to the test bench operation a pattern of fine protrusions averaging 1µm between a peak and a valley, most probably from the fabrication process. After testing, however, the bearing profiles are different according to the position they were placed. The upper main bearings presented minor alterations, what can be explained by the low load impact in this bearing shell. The lower main bearing shells, being the loaded bearings, presented, after being tested, a smoother and more homogeneous profile, as shown in Figure 4.6, pointing out the surface polishing process as the first step of the bearing wear process. As all lower and upper main bearings presented a similar profile, only the profile of the first bearing is shown in Figures 4.7 and 4.8.

In the conrod bearings, even in the unloaded lower conrod bearing shells, the polishing process, can be noted in Figure 4.9, as it shows the decrease of asperities width, as well as a flatter surface. However, the most difference, as it was expected, is seen in Figure 4.10, that presents the profiles of the first upper conrod bearing before and after operation, in which in some parts of the bearing shell all the asperities are worn out, giving place to a smooth surface. It is important to remember that just the cylinders 1, 4 and 6 have a hydraulic cylinder and, hence, just the bearings 1, 4 and 6 are loaded. The upper conrod bearings 1, 4 and 6 presented the same profile after tested as shown in Figure 4.10. The other upper conrod bearings presented, as expected, no distinguished change before operation, as shown by the profile of the second upper conrod bearing in Figure 4.11. Figure 4.12 shows the profile of the second lower conrod bearing, which presented a profile similar to the other lower conrod bearings.

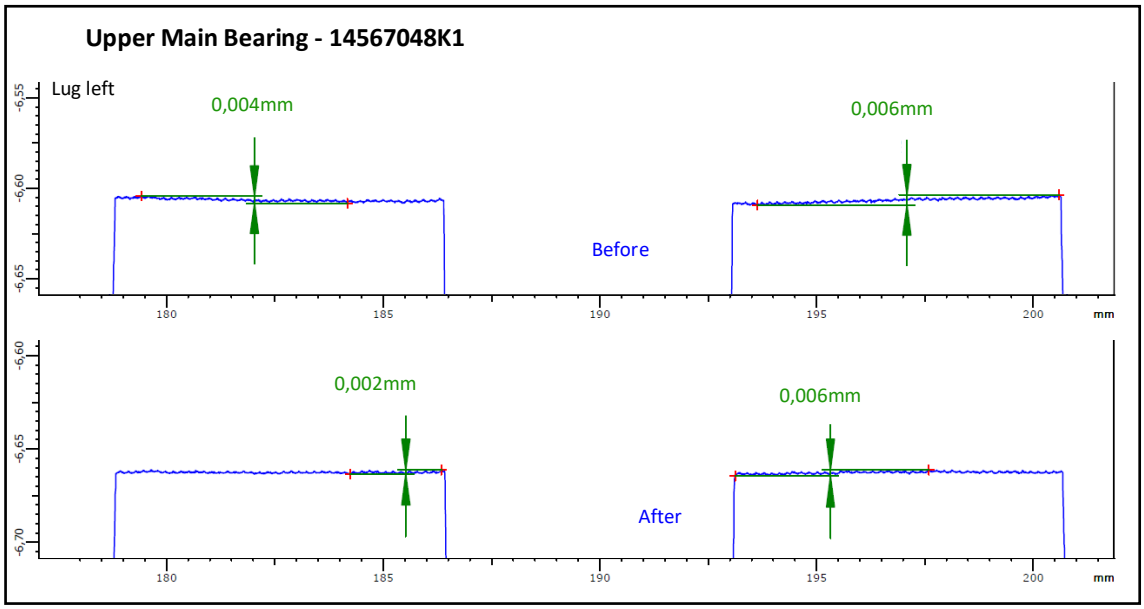


Figure 4.7 - Profile of Upper Main Bearing 1 – Test 1

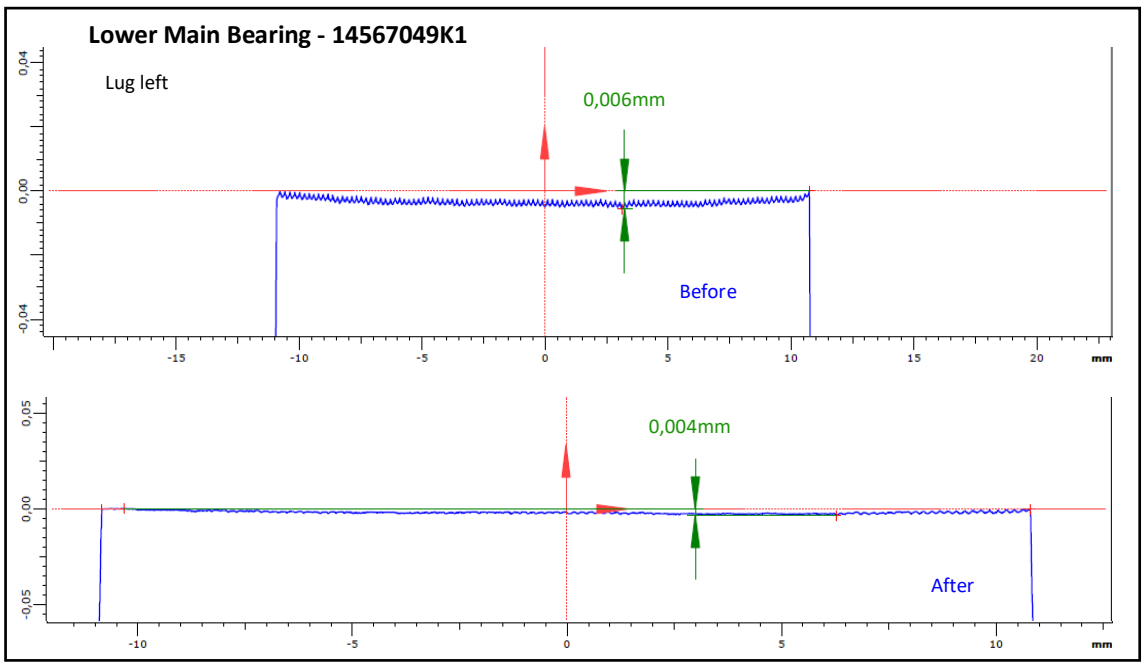


Figure 4.8 - Profile of Lower Main Bearing 1 – Test 1

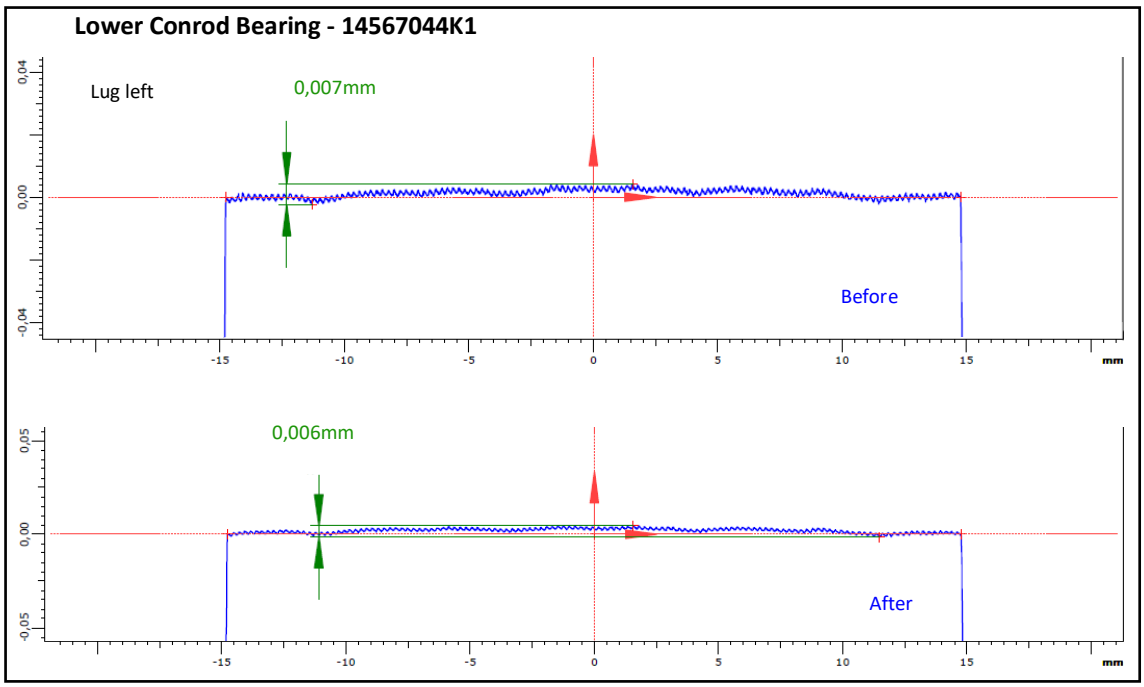


Figure 4.9 - Profile of Lower Conrod Bearing 1 – Test 1

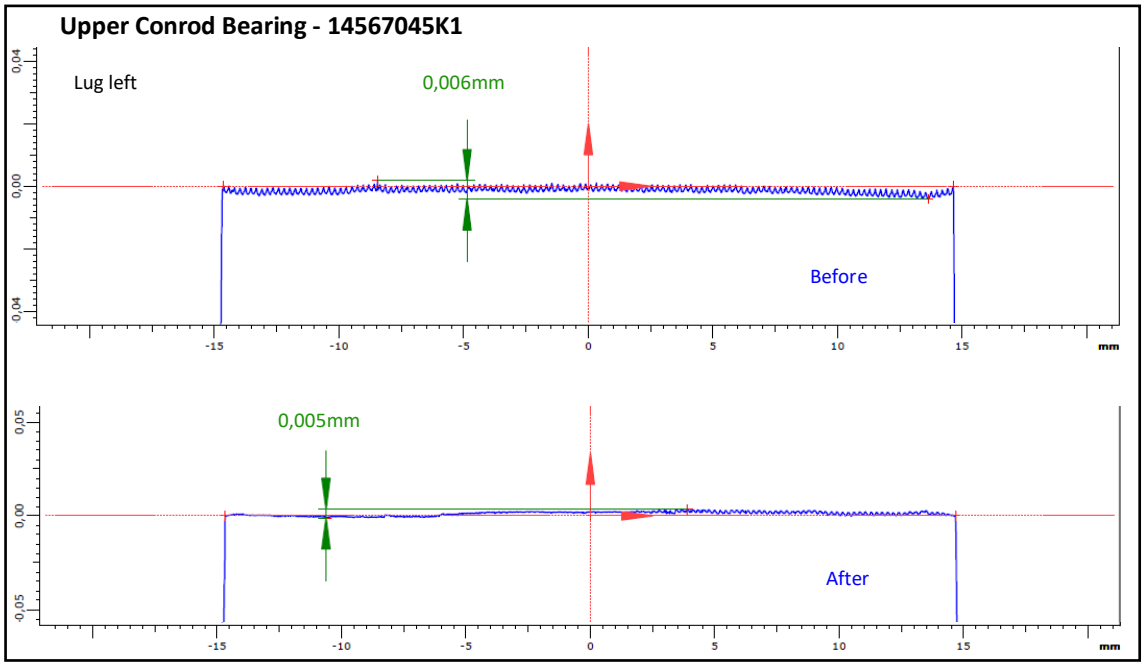


Figure 4.10 - Profile of Upper Conrod Bearing 1 – Test 1

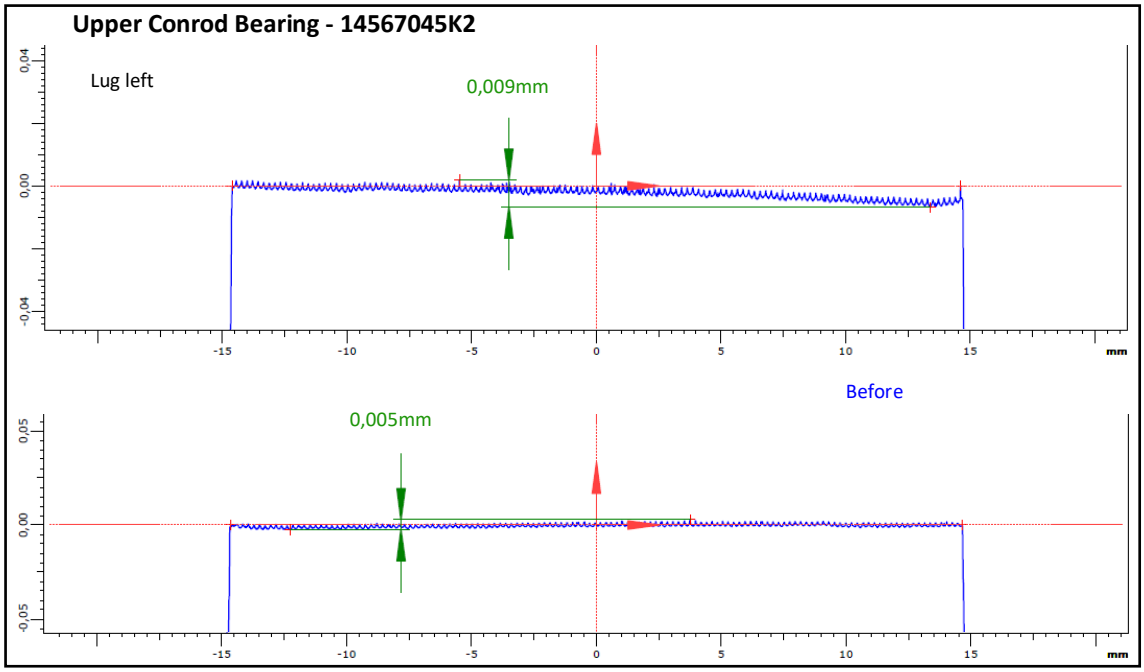


Figure 4.11 - Profile of Upper Main Bearing 2 – Test 1

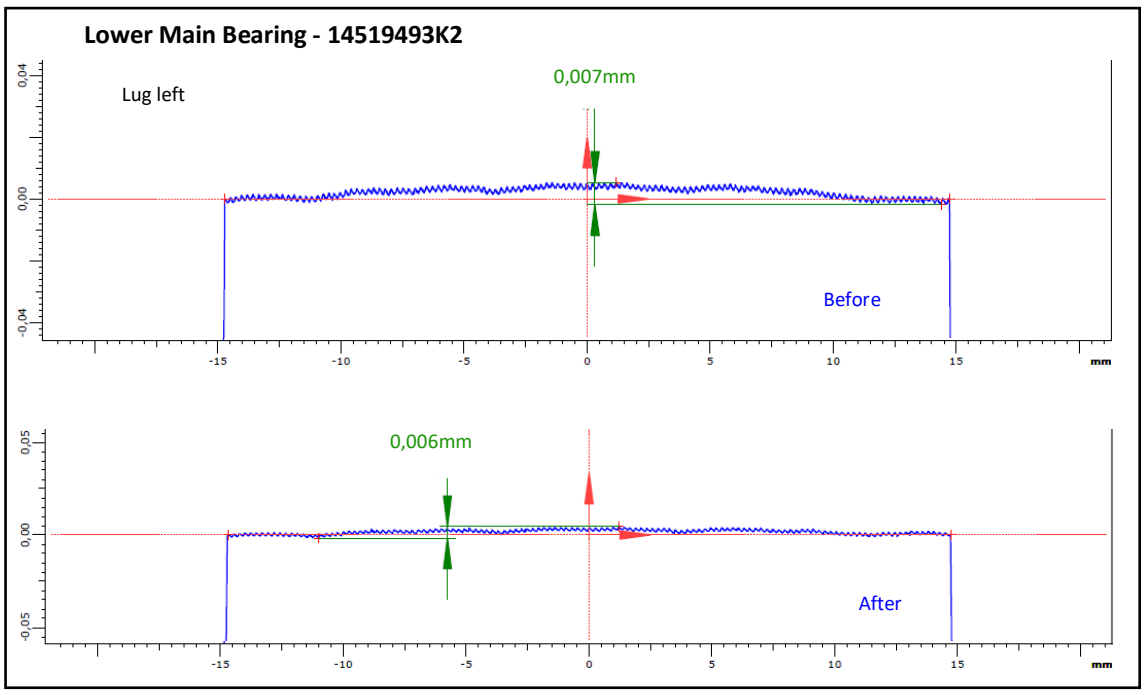


Figure 4.12 - Profile of Lower Main Bearing 2 – Test 1

4.4 Second Test

In order to obtain more representative results to the wear analysis, a second test was conducted with the same program, but with 30,000 starts, aiming deeper worn layers, capable of being analyzed by the measuring system available. Figure 4.13 shows the conrod and main beaings after the second test. In this figure the wear seen in the lower main bearings 1 and 7 increased when compared to the bearings of the first test, as well as the wear in the upper conrod bearings 1, 4 and 7. This was expected, as the operation time increased. However, the bearing sprofiles already shown that the bearing wear presented only a mild increase, instead of increase of 6x, as it was expeted, since the operation time increased 6x.In this figure, more traces of abrasive wear are also evidenced.

The wear results are presented in Table 4.2 in the same way they were presented for the first tests. In this test the bearing set is called 14519493K2 and the upper main, lower main, upper conrod and lower conrod bearings are respectively named 14565812K, 14565835K, 14565782K and 14565756K, followed by the number corresponded to their positioning.

The analysis of the bearing profile where the most load is applied for this second test is shown from Figures 4.14 to 4.17. The figures show a very similar pattern seen in the bearing profiles of the first test. Figures 4.14 and 4.15 show respectively the upper main and lower conrod bearings, and as seen for the first test, slight to no wear is seen in these bearings, in the first positions and in the others as well. Figures 4.16 and 4.17 present respectively the lower main and upper conrod bearings in position 1. They present it surface almost entirely polished by sliding wear, and this happens also for all lower main bearings and all loaded conrod bearings (1, 4 and 6). A particularity can be seen in Figure 4.16, that shows the left bearing surface completely worn out and the left surface almost untouched. That indicates misalignment, most probably by improper bearing position.

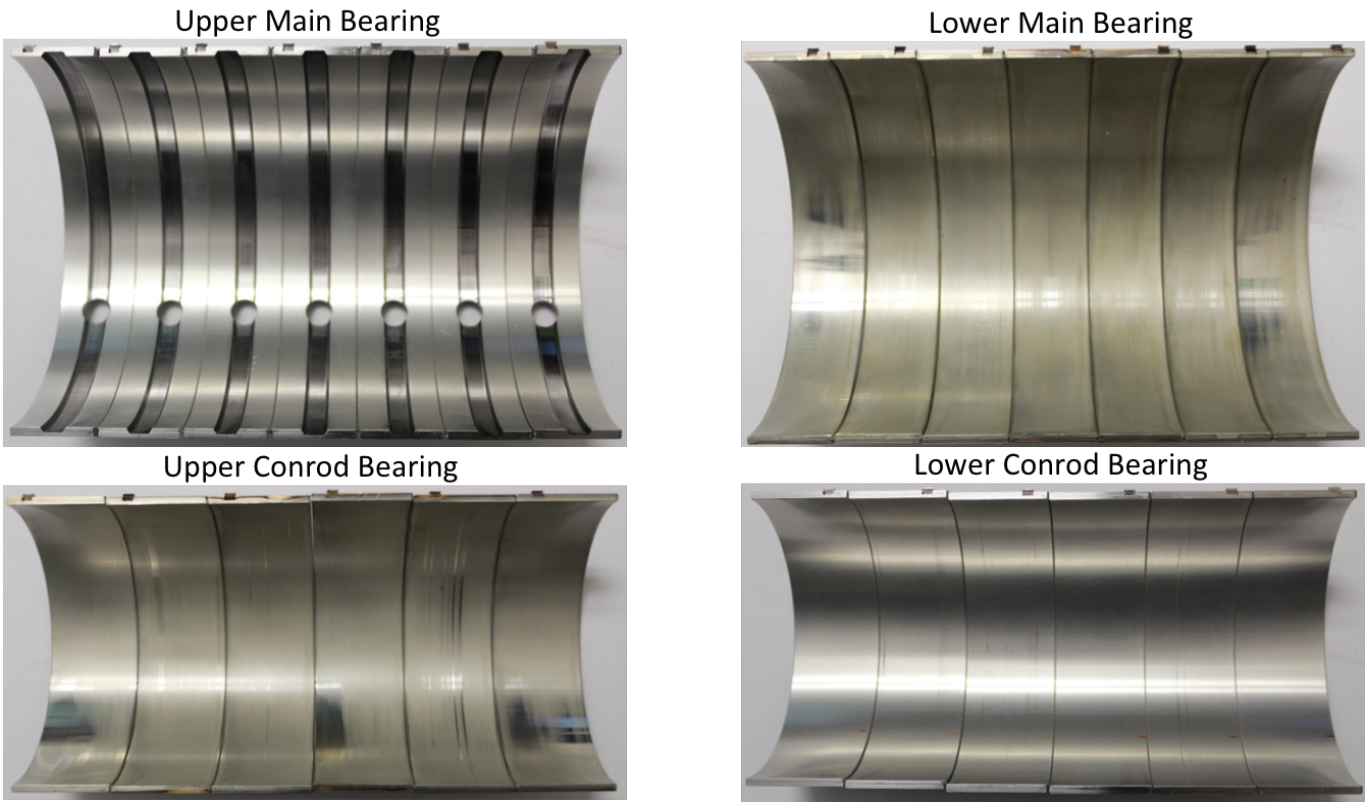


Figure 4.13 - Bearings after test 2

Curiously, the upper and lower conrod bearings in position 5, despite presenting almost no sign of sliding in their entire surface, deep material removal is seen in two regions of the bearing shells, what is cohoborated by the analisis of Figure 4.13. This kind of wear is typical of wear by abrasive particles. As in this position, specifically, no load is applied, the lack of sliding wear is justified. The abrasive particles reach these bearings through the oil distribution system and originates most probably from wear in loaded bearing in its vicinity or dirty particles originated from the manufacturing of engine components that detached after some time of test run. This second possibility is the most likely to have occurred, because not much bearing wear was seen after this test and the particles worn out of the bearings probably had their dimensions smaller than the fluid film thickness and for abrasive wear to occur, the abrasive particles have to be greater than the fluid film. Also, important to emphasize, wear by abrasive particles occur in both bearings, as the abrasive particles rotate in the fluid film.

With this analysis it is seen that the effect of lubrication on abrasive wear contrasts strongly with that on sliding wear. Proper lubrication during sliding movement tends to reduce sliding wear by lowering the tangential stresses on the surface and by decreasing the incidence and severity of asperity contact. Abrasive wear, however, can even be increased by the use of lubrication as abrasive particles are easily disseminated through lubricating oils and are normally larger than the Hydrodynamic or Elastohydrodynamic film thickness, which, therefore, cannot prevent contact between the particle and the counter face. Thus, methods to remove these contaminant parts from a tribological system such as filtration or centrifugal methods are extremely important (Hutchings e Shipway, 2017).

Position	Position Average	14519493K2															
		Main bearings							Conrod bearings								
		Upper main bearing			Lower main bearing				Upper conrod bearing				Lower conrod bearing				
		Upper measuring track	Lower measuring Track	Average	Upper measuring track	Middle measuring track	Lower measuring Track	Average	Upper measuring track	Middle measuring track	Lower measuring Track	Average	Upper measuring track	Middle measuring track	Lower measuring Track	Average	
		(mm)	(mm)	(mm)	(mm)	(mm)	(mm)	(mm)	(mm)	(mm)	(mm)	(mm)	(mm)	(mm)	(mm)	(mm)	
	(°)	14565812K1			14565835K1				14565782K1				14565756K1				
Begin (20°-30°)	25	0,0014	0,0015	0,0014	0,00155	0,00155	0,00145	0,0015	0,0023	0,003	0,0033	0,0029	0,00155	0,0009	0,00205	0,0015	
Middle (85°-95°)	90	0,00065	0,0002	0,0004	0,00185	0,0012	0,00105	0,0014	0,0005	0,0007	0,0008	0,0007	0,0003	0,0003	0,0003	0,0003	
End (150°-160°)	155	0	0,0006	0,0003	0,00065	0,0009	0,0009	0,0008	-0,0003	0,0003	0,0007	0,0002	0,0008	-5E-05	0,0018	0,0009	
Average		0,0007	0,0008	**0,0007**	0,0013	0,0012	0,0011	**0,0012**	0,0008	0,0013	0,0016	**0,0013**	0,0009	0,0004	0,0014	**0,0009**	
		14565812K2			14565835K2				14565782K2				14565756K2				
Begin (20°-30°)	25	0,00115	0,001	0,0011	0,00145	0,00155	0,0019	0,0016	0,0019	-0,0001	0,00045	0,0008	0,00165	0,00045	0,0014	0,0012	
Middle (85°-95°)	90	0,00045	0,00035	0,0004	0,0006	0,00065	0,0006	0,0006	0,00135	0,00035	0,0003	0,0007	0,0003	0,00035	0,00025	0,0003	
End (150°-160°)	155	0,00055	0,0003	0,0004	0,0006	0,0019	0,00085	0,0011	0,0007	0,00055	0,00055	0,0006	0,00095	-0,00015	0,00125	0,0007	
Average		0,0007	0,0005	**0,0006**	0,0009	0,0014	0,0011	**0,0011**	0,0013	0,0003	0,0004	**0,0007**	0,0010	0,0002	0,0010	**0,0007**	
		14565812K3			14565835K3				14565782K3				14565756K3				
Begin (20°-30°)	25	0,00165	0,00155	0,0016	0,0014	0,001	0,0015	0,0013	0,00105	0,00155	0,0011	0,0012	0,00115	0,00055	0,00165	0,0011	
Middle (85°-95°)	90	0,0006	5E-05	0,0003	0,00075	0,0009	0,00105	0,0009	0,00085	0,00065	0,00095	0,0008	0,0006	0,00065	0,00035	0,0005	
End (150°-160°)	155	0,00145	0,00025	0,0009	0,00095	0,00105	0,0014	0,0011	0,00045	0,0007	0,00125	0,0008	0,00075	-5E-05	0,00215	0,0009	
Average		0,0012	0,0006	**0,0009**	0,0010	0,0010	0,0013	**0,0011**	0,0008	0,0010	0,0011	**0,0010**	0,0008	0,0004	0,0014	**0,0009**	
		14565812K4			14565835K4				14565782K4				14565756K4				
Begin (20°-30°)	25	0,00155	0,0015	0,0015	0,0015	0,0011	0,0022	0,0016	0,00165	0,00155	0,0015	0,0016	0,0019	0,0009	0,0014	0,0014	
Middle (85°-95°)	90	0,00015	0,0005	0,0003	0,0012	0,00045	-0,0002	0,0005	-0,00015	0,00065	0,00135	0,0006	0,00045	0,0004	0,00015	0,0003	
End (150°-160°)	155	0,0005	0,00065	0,0006	0,00165	0,00085	0,00085	0,0011	-0,00045	0,00115	0,00125	0,0006	0,0011	5E-05	0,0027	0,0013	
Average		0,0007	0,0009	**0,0008**	0,0015	0,0008	0,0009	**0,0011**	0,0004	0,0011	0,0014	**0,0009**	0,0011	0,0004	0,0014	**0,0010**	
		14565812K5			14565835K5				14565782K5				14565756K5				
Begin (20°-30°)	25	0,0014	0,00135	0,0014	0,00215	0,00135	0,0011	0,0015	0,0009	0,00235	0,0021	0,0018	0,00125	0,0009	0,00175	0,0013	
Middle (85°-95°)	90	0,00025	0,0002	0,0002	0,0001	0,00115	0,00105	0,0008	0,00165	0,00045	0,00015	0,0007	0,0003	0,00125	0	0,0005	
End (150°-160°)	155	0,00055	0,0002	0,0004	0,0008	0,0009	0,0011	0,0009	-0,0002	-0,0001	0,00025	0,0000	0,0004	0	0,0017	0,0007	
Average		0,0007	0,0006	**0,0007**	0,0010	0,0011	0,0011	**0,0011**	0,0008	0,0009	0,0008	**0,0008**	0,0006	0,0007	0,0011	**0,0008**	
		14565812K6			14565835K6				14565782K6				14565756K6				
Begin (20°-30°)	25	0,0004	0,00115	0,0008	0,00155	0,00165	0,0013	0,0015	0,0016	0,00165	0,0017	0,0017	0,0023	0,00095	0,0014	0,0016	
Middle (85°-95°)	90	0,00055	0,0006	0,0006	0,0006	0,006	0,0002	0,0023	0,00075	0,00075	0,00115	0,0009	0,001	0,00095	0,0002	0,0007	
End (150°-160°)	155	0,00105	0,00105	0,0010	0,0011	0,00085	0,00085	0,0009	-1E-04	0,00095	0,00075	0,0005	0,00145	0,0003	0,0015	0,0011	
Average		0,0007	0,0009	**0,0008**	0,0011	0,0028	0,0008	**0,0016**	0,0008	0,0011	0,0012	**0,0010**	0,0016	0,0007	0,0010	**0,0011**	
		14565812K7			14565835K7												
Begin (20°-30°)	25	0,00155	0,0014	0,0015	0,0017	0,00125	0,0018	0,0016									
Middle (85°-95°)	90	0,00075	0,0005	0,0006	0,0009	0,0009	0,00045	0,0008									
End (150°-160°)	155	0,0007	0,0007	0,0007	0,0003	0,00085	0,0008	0,0007									
Average		0,0010	0,0009	**0,0009**	0,0010	0,0010	0,0010	**0,0010**									

Table 4.2 - Wear measurement on the second test

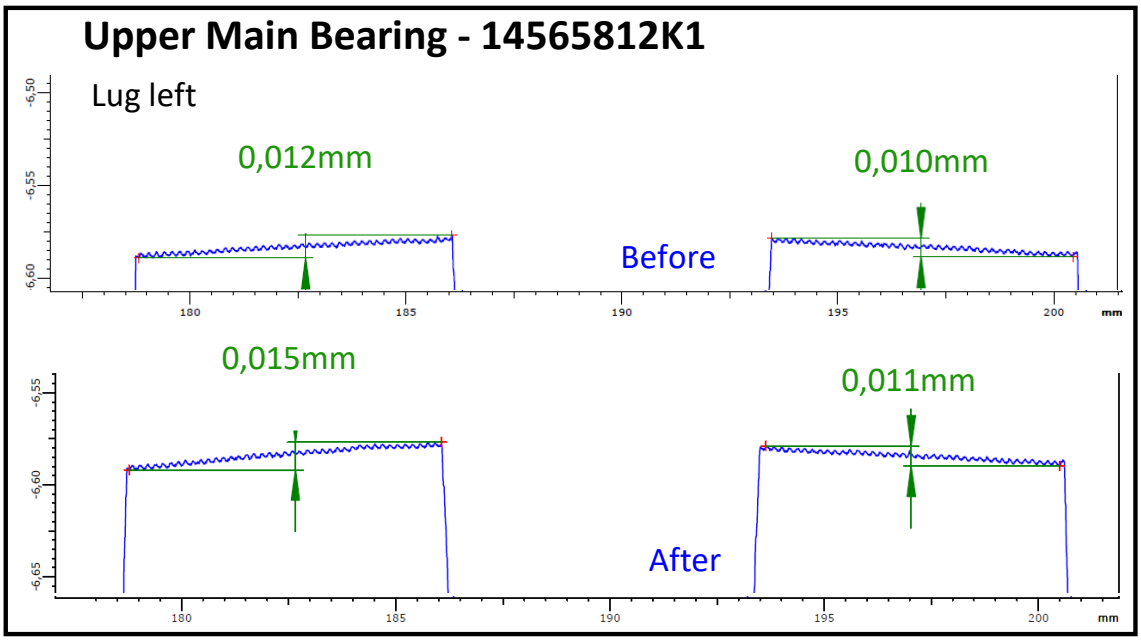


Figure 4.14 - Profile of Upper Main Bearing 1 – Test 2

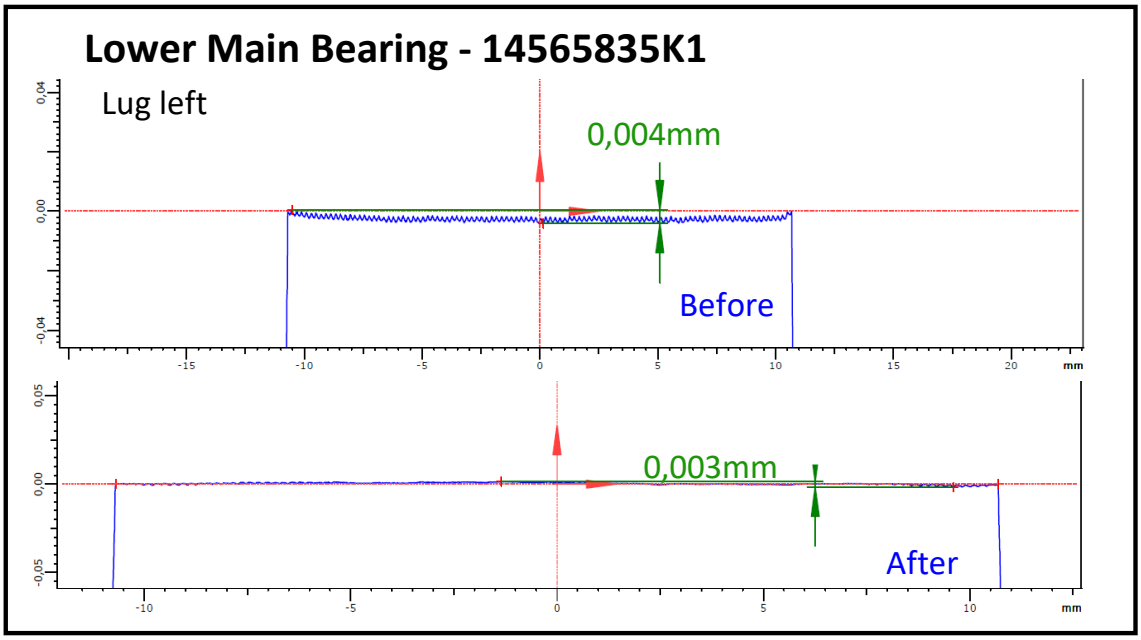


Figure 4.15 - Profile of Lower Main Bearing 1 – Test 2

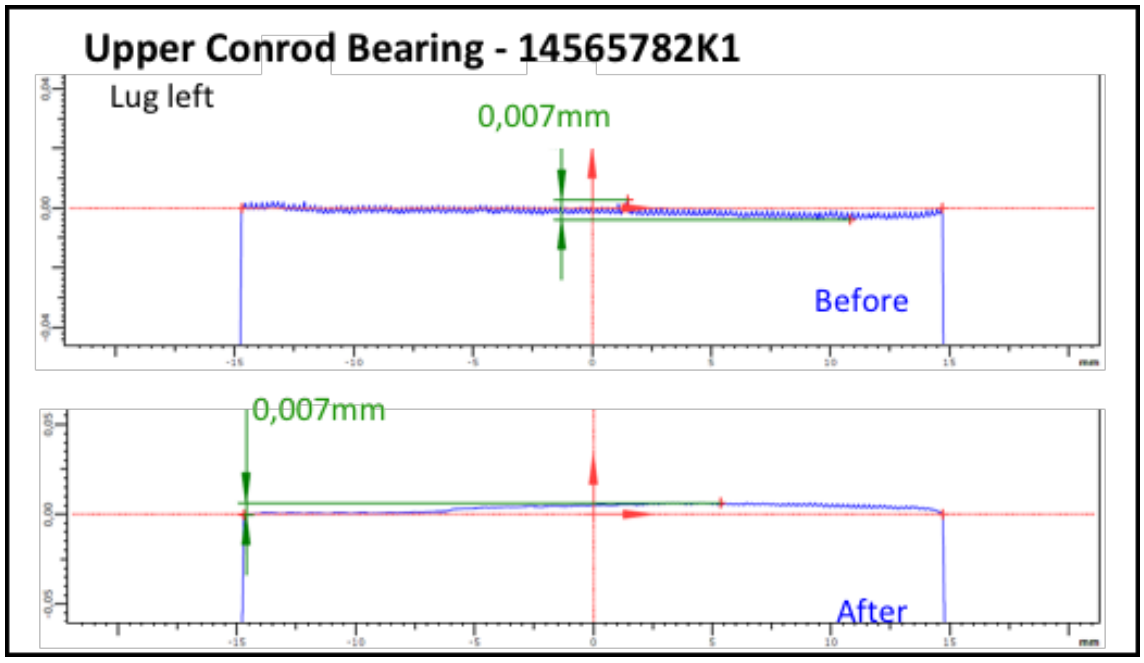


Figure 4.16 - Profile of Upper Conrod Bearing 1 – Test 2

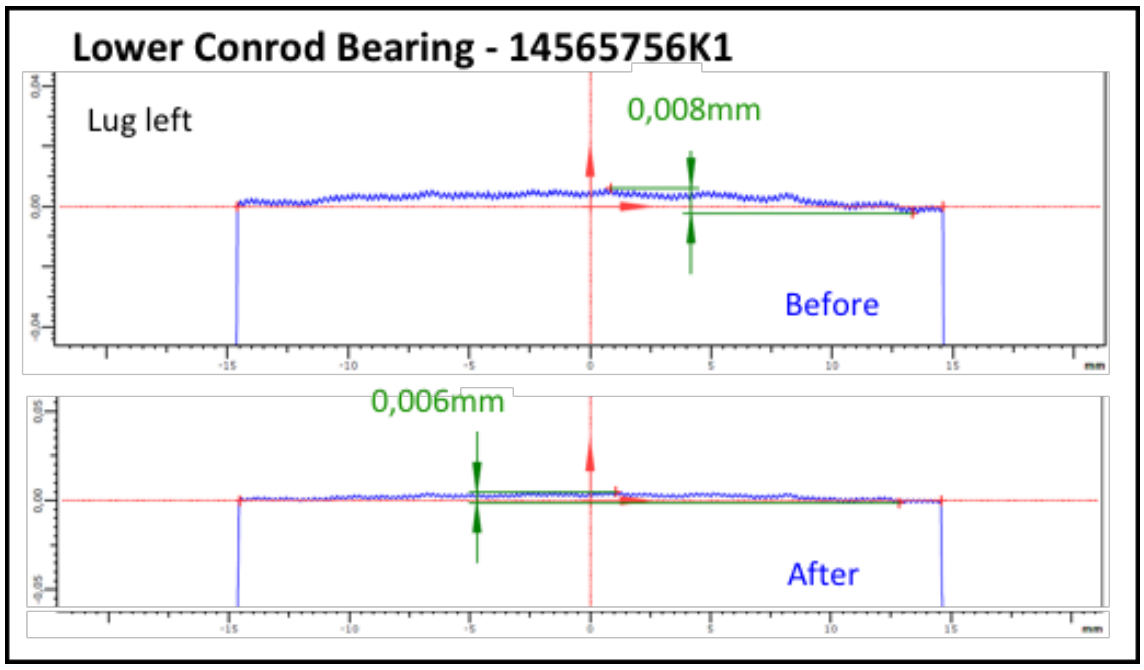


Figure 4.17 - Profile of Lower Conrod Bearing 1 – Test 2

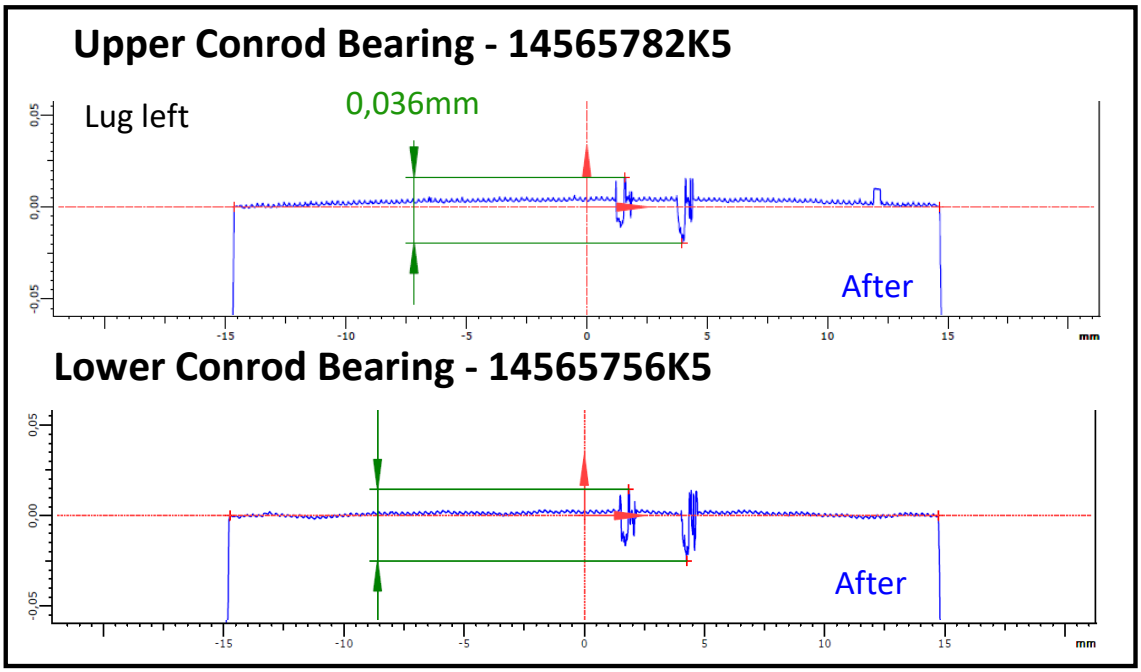


Figure 4.18 - Profile of Upper Conrod Bearing 5 – Test 2

The wear seen after the second test is very similar to the wear seen in the first test, despite the expected, mainly according to the measurements conducted. It is believed it was due to the test program that presented no stop time between starts. Thus, during the first 5.000 starts, the oil film was built up between the engine component, and due to the lack of stop time, the oil did not flow back to the oil pan. In this case, the bearing had significant contact with the shaft only during the film built up, and then, it the contact occurred momentary just at individual load peaks during start. This situation does not portray the reality, in which the bearing-shaft contact is in much frequent and deeper, as the oil has time to be drained back between starts and during a start there is not enough time to build a proper fluid film.

4.5 Lubrication Regime

Nebelsiek (Nebelsiek, 2017), in the previous work, suggested that the energy application during a power stroke should be considered to estimate the lubrication regime between bearings and shaft. In this previous work, EST engine was studied, and with the same program used in the present work, the load application in all cylinders during a start was recorded, as shown in Figure 4.3. Using the theory of the energy application during a stroke, calculated as the sum of the product of the resultant load application in a cylinder, its bore and the start duration, the energy application for the 6 cylinders during a start, considering the first 3 power strokes for each cylinder, was calculated. In this study, two tests were conducted with Shell Rimula R6 LME 5W-30, 3.5 one at 78% of the maximum possible temperature for MSS and one at the highest temperature. Table 4.3 presents the percentages power considering the maximum power peak calculated for each cylinder and it was determined, for both tests, the lubrication regime for each power stroke.

In this work, after determining the limiting engine rotation, that was compared to the minimum and maximum rotations during the stroke, and if ω_b was superior to both values, it was considered that Elastohydrodynamic regime took place, represented in red. If ω_b was superior just to one value, it was considered that a mix of

Elastohydrodynamic and Hydrodynamic regime took place, represented in yellow. If ω_b was inferior to both values, it was considered that only Hydrodynamic regime took place, represented in green.

Table 4.3 - Energy Application in EST Bearings during Start, Credits: (Nebelsiek, 2017)

		Cylinder 1	Cylinder 2	Cylinder 3	Cylinder 4	Cylinder 5	Cylinder 6
HTHS 3,5 90°C	Power [%]	28	19	61	23	60	66
	Power [%]	80	76	92	77	89	88
	Power [%]	82	100	95	96	88	78
HTHS 3,5 110°C	Power [%]	28	19	61	23	60	66
	Power [%]	80	76	92	77	89	88
	Power [%]	82	100	95	96	88	78

However, analyzing the section 2.2.2.4, and mainly Equation 2.19, it is clear that the limit rotation, ω_b, is determined at the moment of a load application, and should be compared than with the rotation in the moment of load application. To use the average energy application and the average engine rotation can lead to errors, as the load distribution and rotation variate intensely during in a power stroke, as shown in Figure 4.19. The determination of average energy can lead one to believe the bearing-shaft pair is under Hydrodynamic lubrication regime instead of momentarily in Elastohydrodynamic or even Boundary lubrication during higher load peaks.

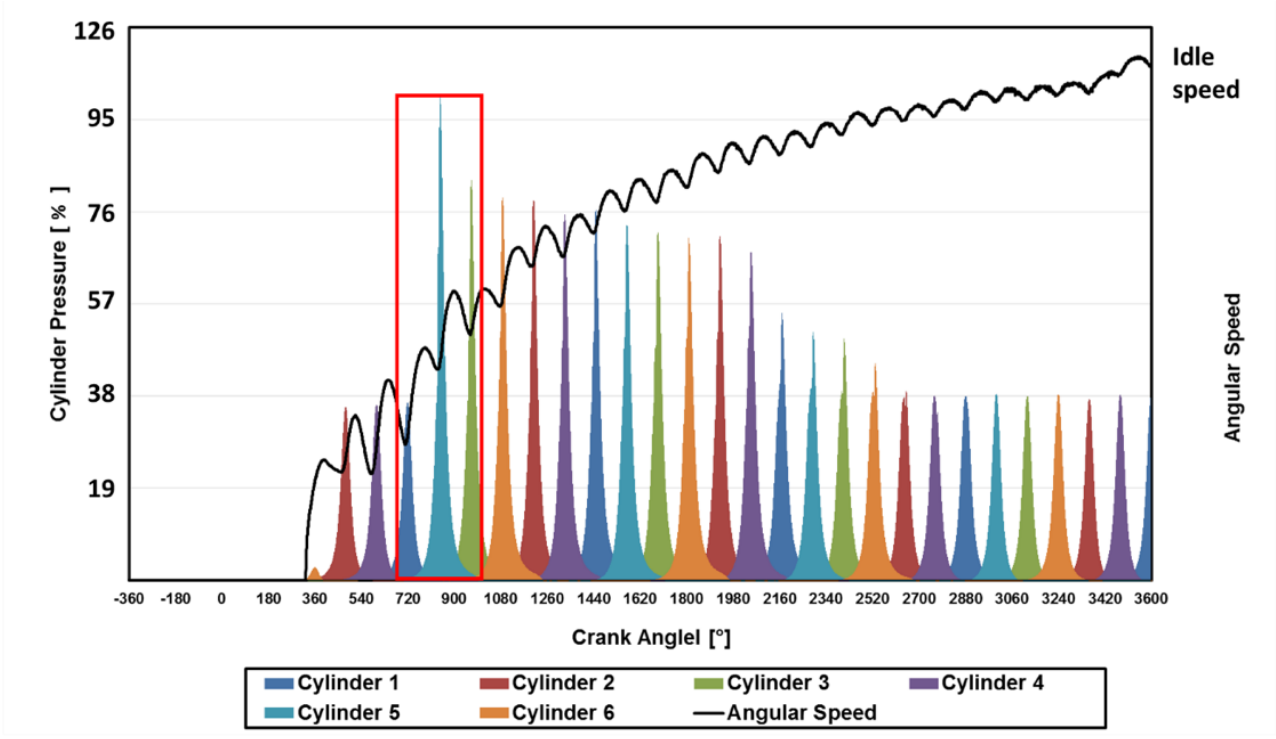


Figure 4.19 - Load and Rotation Variation during a power stroke, Credits: Adapted from (Nebelsiek, 2017)

Hence, it is believed, that the ω_b should be determined just with the load peaks of each power stroke, the only moment when it is really possible that the lubrication regime is altered. Then, in this work, the load peaks of each stroke in all tests were recorded and the method presented in section 2.2.2.4 was used to define the lubrication

regime variation during the tests course, using bearing and shaft geometric parameters and properties of the lubricant used.

Considering that it is composed of a much more wear resistant material then the bearings, and much little wear will be observed after the tests, the same shaft was used for all TLPP tests. According to the bearing technical drawings the external diameter of the MB has to be 99 mm with tolerance H6, the inner diameter has to be 94 mm, with a tolerance from 0 to -0.020 and the bearing width 22.7 mm with tolerance from 0 to -0.3. Analogously, according technical drawings, the external diameter of the CB have to be 87 mm with tolerance H6, the inner diameter have to be 82 mm, with a tolerance from 0 to -0.020, and the bearing width 30.3 mm with tolerance from 0 to -0.3. As the inner diameter depends on the bearing fabrication and coating placement, the inner diameter will be considered the external diameter of the bearing subtracted from the average bearing width obtained during measurements. For the lubrication oils chosen that the minimum film thickness, h_o, is 0.0005mm, meaning that that is the minimum thickness that the oil can maintain its molecules bounded, and at a minimum attempt to reduce this thickness by load application, the film will be broken. With all the data collected, the Sommerfeld number, S, the relative bearing clearance, ψ, the dynamic viscosity for the HTHS oil at 78% of the maximum possible temperature for MSS and the bearing area, A, were calculated.

The maximum load peaks for the TLPP program were collected, as well as the shaft rotation in the exact moment, as shown in Figure 4.20. According to section 2.2, the friction losses in this work will be disregarded, so the load applied by the hydraulic cylinder will be considered the load applied in the conrod bearing. Also considering no friction losses, the load applied by the hydraulic cylinder in the shaft should, can also be calculated by the strategy suggested in section 2.2. However, as for each conrod load application, 7 MB suffer an opposite force and the only parameters known are the load application and shaft geometry, 2 relations can be built: the balance of shear stresses and bending moments. Hence, an equation system can be built with 7 incognitos and 2 equations, meaning no exact solution can be found. An estimation of the load distribution in the lower main bearings can be seen in Figure 4.21. Note that the arrows representing the load application are merely a draft, and their scale do not represent the exact load magnitude and also, that because of the positioning of the hydraulic cylinder, the bearings closer to the position 7 receive more load than the bearings closer to the position 1.

However, exact results for the exact load application in the main bearings, and even in the conrod bearings, considering even energy losses, can only be obtained through computational methods. As in this work, several approximations are used in order to focus in the tribological analysis, it will be also considered that for each load application in a conrod bearing, 1/6 of the load will be applied in each main bearing. Note that for the load applied in one conrod bearing, 1/6 of the load is made in all bearings, and while 1 conrod bearing has its load application interleaved with other 2, the main bearings suffer the impact of the load application of all cylinders.

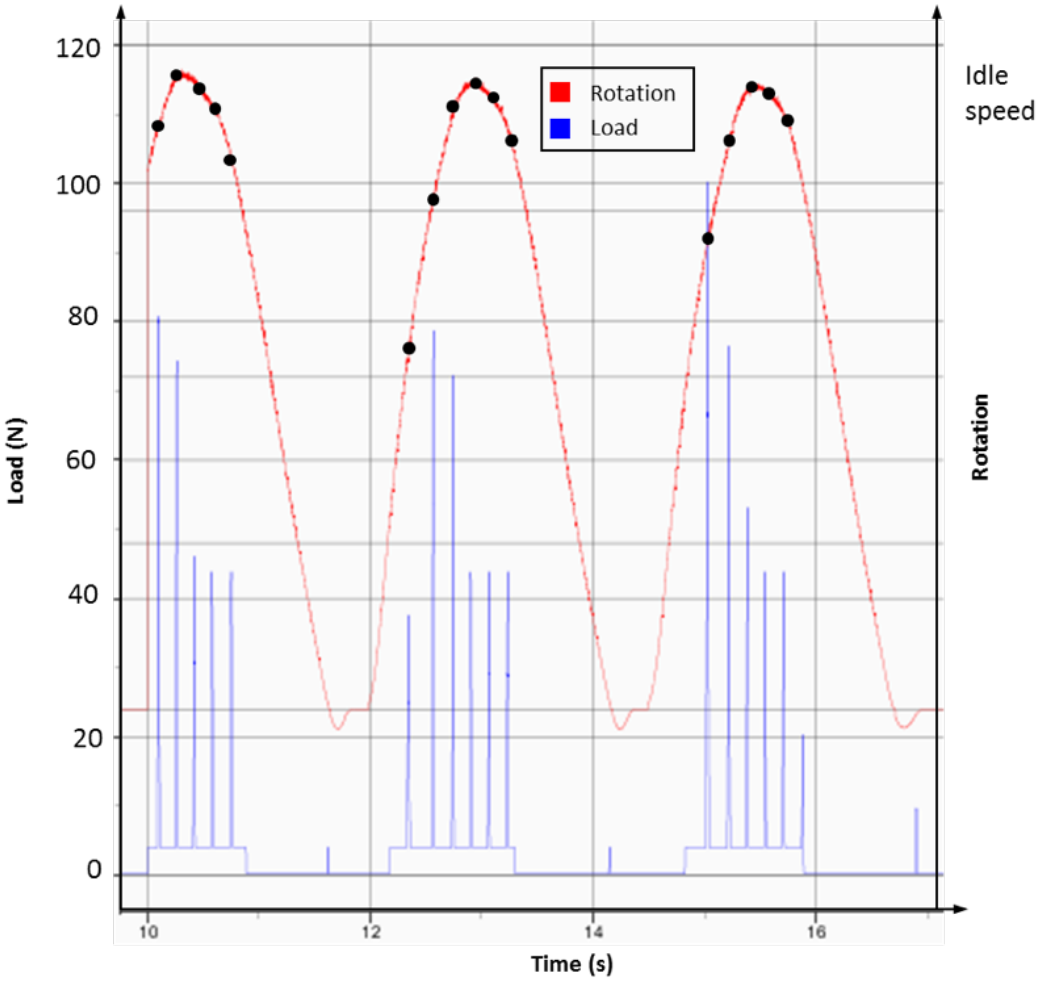


Figure 4.20 - Rotation and Load recordings

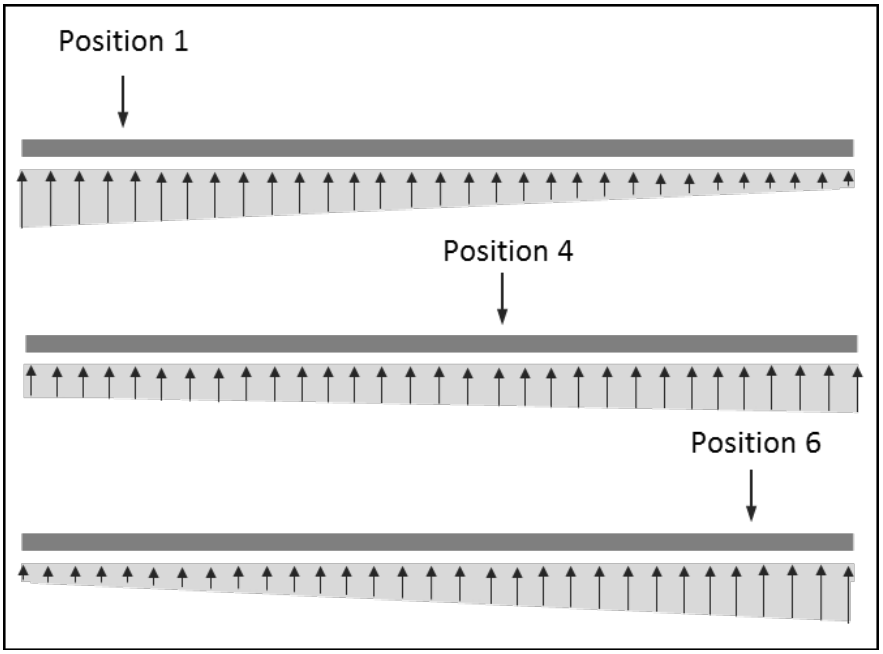


Figure 4.21 - Estimation of Load Distribution in the Lower Main Bearings

Knowing the load, rotation and the Sommerfeld number, relative bearing clearance, dynamic viscosity of the oil and bearing area, for each load and rotation pair,

the limit rotation could be calculated. Table 4.4 and 4.5 show the comparison of the actual and limiting rotation for the test 1, when it started, that is, with the bearing measurements conducted before the test, for conrod and main bearings respectively.

The Tables 4.4 and 4.5 show in green the limit rotation when it is below the actual rotation, which means hydrodynamic lubrication regime and in red the limit rotation when it is above the actual rotation, meaning Elastohydrodynamic lubrication regime. For the conrod bearings the only situation in which the Elastohydrodynamic regime occurs is during the highest load peak after the third start, as shown in Figure 4.19. Although all the load application is equal in all three conrods, the limit rotation differs slightly due to the bearing geometry. More specifically, the higher the bearing clearance, the higher the limit rotation. That occurs because, as the bearing clearance increases, the fluid film between bearing and shaft weakens, needing more pressure to be kept bonded, possible only with higher engine rotation or alteration of further parameters, such as oil viscosity. As, according to calculation, the loads in the main bearings are much lower than for the conrod bearings, it is estimated that in all situations just the hydrodynamic lubrication occur.

However, this estimation is not accurate because the dimensional measurements, and specially the bearing profiles show wear occurrence during the 5,000 starts, what would not be possible in a hydrodynamic regime. This inaccuracy occurs for mainly 2 reasons. First of all, at the beginning of the tests, the oil channels were not filled by oil, and neither the surface between bearings and shafts, as the oil pump starts to work with the shaft rotation. So, until the fluid film is completely built up, what can take from 3-4 seconds in MDEG engines, according to Figure 2.25, direct contact between counter bodies and sliding wear occur. Considering that a start in TLPP lasts less than a second, the fluid film can take longer to be built, as the rotation decreases, and also the work of the oil pump. The second reason for the incongruences on the results are due to the load estimations for the main bearings, as it is known that the load distribution is not homogeneous for all the bearings. The main bearings that withstand more load would present a higher rotation limit, so that the fluid film would not break.

Table 4.4 - Rotation Comparison in the Conrod Bearings – Before Test 1

14567045K1		14567045K4		14567045K6	
Actual Rotation	Limit Rotation	Actual Rotation	Limit Rotation	Actual Rotation	Limit Rotation
1/s	1/s	1/s	1/s	1/s	1/s
72.9	62.2	72.9	62.3	72.9	64.9
79.2	57.8	79.2	57.9	79.2	60.3
79.4	35.7	79.4	35.8	79.4	37.3
76.3	33.8	76.3	33.9	76.3	35.3
69.6	33.8	69.6	33.9	69.6	35.3
44.3	29.1	44.3	29.1	44.3	30.3
63.7	60.9	63.7	61.0	63.7	63.6
74.8	55.9	74.8	56.0	74.8	58.3
78.8	33.8	78.8	33.9	78.8	35.3
77.3	33.8	77.3	33.9	77.3	35.3
73.9	33.8	73.9	33.9	73.9	35.3
58.5	77.1	58.5	77.3	58.5	80.5
70.4	59.0	70.4	59.2	70.4	61.6
77.6	40.9	77.6	41.0	77.6	42.7
78.5	33.8	78.5	33.9	78.5	35.3
75.5	33.8	75.5	33.9	75.5	35.3

Table 4.5 - Rotation Comparison in the Conrod Bearings – Before Test 1

14567049K1		14567049K2		14567049K3		14567049K4		14567049K5		14567049K6		14567049K7	
Actual Rotation	Limit Rotation	Actual Rotation	Limit Rotation	Actual Rotation	Limit Rotation	Actual Rotation	Limit Rotation	Actual Rotation	Limit Rotation	Actual Rotation	Limit Rotation	Actual Rotation	Limit Rotation
1/s	1/s	1/s	1/s	1/s	1/s	1/s	1/s	1/s	1/s	1/s	1/s	1/s	1/s
72.9	10.3	72.9	10.1	72.9	10.4	72.9	10.4	72.9	10.9	72.9	10.6	72.9	9.9
79.2	9.6	79.2	9.4	79.2	9.7	79.2	9.7	79.2	10.1	79.2	9.9	79.2	9.2
79.4	5.9	79.4	5.8	79.4	6.0	79.4	6.0	79.4	6.3	79.4	6.1	79.4	5.7
76.3	5.6	76.3	5.5	76.3	5.7	76.3	5.7	76.3	5.9	76.3	5.8	76.3	5.4
69.6	5.6	69.6	5.5	69.6	5.7	69.6	5.7	69.6	5.9	69.6	5.8	69.6	5.4
44.3	4.8	44.3	4.7	44.3	4.9	44.3	4.9	44.3	5.1	44.3	5.0	44.3	4.6
63.7	10.1	63.7	9.9	63.7	10.2	63.7	10.2	63.7	10.7	63.7	10.4	63.7	9.7
74.8	9.3	74.8	9.1	74.8	9.3	74.8	9.3	74.8	9.8	74.8	9.5	74.8	8.9
78.8	5.6	78.8	5.5	78.8	5.7	78.8	5.7	78.8	5.9	78.8	5.8	78.8	5.4
77.3	5.6	77.3	5.5	77.3	5.7	77.3	5.7	77.3	5.9	77.3	5.8	77.3	5.4
73.9	5.6	73.9	5.5	73.9	5.7	73.9	5.7	73.9	5.9	73.9	5.8	73.9	5.4
58.5	12.8	58.5	12.6	58.5	12.9	58.5	12.9	58.5	13.5	58.5	13.2	58.5	12.2
70.4	9.8	70.4	9.6	70.4	9.9	70.4	9.9	70.4	10.4	70.4	10.1	70.4	9.4
77.6	6.8	77.6	6.7	77.6	6.8	77.6	6.8	77.6	7.2	77.6	7.0	77.6	6.5
78.5	5.6	78.5	5.5	78.5	5.7	78.5	5.7	78.5	5.9	78.5	5.8	78.5	5.4
75.5	5.6	75.5	5.5	75.5	5.7	75.5	5.7	75.5	5.9	75.5	5.8	75.5	5.4

Considering the same load application, the same rotation limits were calculated for the main bearings after the 5,000 starts, that is, using the bearings dimensions obtained after the test. Table 4.6 and 4.7 show the comparison of the actual and limiting rotation for conrod and main bearings respectively.

The results shown by tables 4.6 and 4.7 are very similar to the results shown by tables 4.4 and 4.5, as the oil viscosity and load application in the bearings continues the same, the only changes are dimensional, due to the wear occurrence in this first 5,000 starts. However, with the worn surfaces of the bearings, the bearing clearances increase, and as previously explained, the rotation limit tends to increase and one more load application occurred in a higher rotation than the limit, increasing regions of Elastohydrodynamic lubrication.

With this analysis, it is proven that, to estimate the actual lubrication regime of a bearing-shaft system, the actual dimensions of the bearing and shaft should be known. This situation is already explored in studies that explain the difficulties to determine tribological conditions of a system in simulation models, as they have to be constantly updated with experimental data (Allmaier *et al.*, 2011; Allmaier *et al.*, 2012; Priestner *et al.*, 2012).

Table 4.6 - Rotation Comparison in the Conrod Bearings – After Test 1

14567045K1		14567045K4		14567045K6	
Rotation	Limit Rotation	Rotation	Limit Rotation	Rotation	Limit Rotation
1/s	1/s	1/s	1/s	1/s	1/s
72,9	64,0	72,9	63,7	72,9	66,4
79,2	59,5	79,2	59,1	79,2	61,7
79,4	36,8	79,4	36,6	79,4	38,1
76,3	34,9	76,3	34,7	76,3	36,1
69,6	34,9	69,6	34,7	69,6	36,1
44,3	29,9	44,3	29,7	44,3	31,0
63,7	62,7	63,7	62,4	63,7	65,0
74,8	57,6	74,8	57,2	74,8	59,7
78,8	34,9	78,8	34,7	78,8	36,1
77,3	34,9	77,3	34,7	77,3	36,1
73,9	34,9	73,9	34,7	73,9	36,1
58,5	79,4	58,5	79,0	58,5	82,4
70,4	60,8	70,4	60,4	70,4	63,0
77,6	42,1	77,6	41,9	77,6	43,7
78,5	34,9	78,5	34,7	78,5	36,1
75,5	34,9	75,5	34,7	75,5	36,1

Table 4.7 - Rotation Comparison in the Main Bearings – After Test 1

14567049K1		14567049K2		14567049K3		14567049K4		14567049K5		14567049K6		14567049K7	
Actual Rotation	Limit Rotation	Actual Rotation	Limit Rotation	Actual Rotation	Limit Rotation	Actual Rotation	Limit Rotation	Actual Rotation	Limit Rotation	Actual Rotation	Limit Rotation	Actual Rotation	Limit Rotation
1/s	1/s	1/s	1/s	1/s	1/s	1/s	1/s	1/s	1/s	1/s	1/s	1/s	1/s
72,9	10,3	72,9	10,1	72,9	9,8	72,9	10,4	72,9	10,9	72,9	10,6	72,9	9,9
79,2	9,6	79,2	9,4	79,2	9,1	79,2	9,7	79,2	10,1	79,2	9,9	79,2	9,2
79,4	5,9	79,4	5,8	79,4	5,6	79,4	6,0	79,4	6,3	79,4	6,1	79,4	5,7
76,3	5,6	76,3	5,5	76,3	5,3	76,3	5,7	76,3	5,9	76,3	5,8	76,3	5,4
69,6	5,6	69,6	5,5	69,6	5,3	69,6	5,7	69,6	5,9	69,6	5,8	69,6	5,4
44,3	4,8	44,3	4,7	44,3	4,6	44,3	4,9	44,3	5,1	44,3	5,0	44,3	4,6
63,7	10,1	63,7	9,9	63,7	9,6	63,7	10,2	63,7	10,7	63,7	10,4	63,7	9,7
74,8	9,3	74,8	9,1	74,8	8,8	74,8	9,3	74,8	9,8	74,8	9,5	74,8	8,9
78,8	5,6	78,8	5,5	78,8	5,3	78,8	5,7	78,8	5,9	78,8	5,8	78,8	5,4
77,3	5,6	77,3	5,5	77,3	5,3	77,3	5,7	77,3	5,9	77,3	5,8	77,3	5,4
73,9	5,6	73,9	5,5	73,9	5,3	73,9	5,7	73,9	5,9	73,9	5,8	73,9	5,4
58,5	12,8	58,5	12,6	58,5	12,2	58,5	12,9	58,5	13,5	58,5	13,2	58,5	12,2
70,4	9,8	70,4	9,6	70,4	9,3	70,4	9,9	70,4	10,4	70,4	10,1	70,4	9,4
77,6	6,8	77,6	6,7	77,6	6,5	77,6	6,8	77,6	7,2	77,6	7,0	77,6	6,5
78,5	5,6	78,5	5,5	78,5	5,3	78,5	5,7	78,5	5,9	78,5	5,8	78,5	5,4
75,5	5,6	75,5	5,5	75,5	5,3	75,5	5,7	75,5	5,9	75,5	5,8	75,5	5,4

Considering the analysis done for the first test and that the load application and oil viscosity remains the same, the same analysis was conducted for the second test and Tables 4.8 and 4.9 show the comparison of the actual and limiting rotation for conrod and main bearings respectively before the testes and Tables 4.10 and 4.11, after 30,000 starts.

These four tables show very similar results to the ones obtained by the first test. Before being tested, the conrod bearing-shaft pairs were supposed to be in the Elastohydrodynamic regime just in the highest load peak in the 3 start-cycle for the main bearings-shaft pairs were estimated to be only in the hydrodynamic regime. The rotation limits also increased after the bearing surfaces were worn out after 30,000 starts. However, the bearing clearances were expected to be slightly higher in the second test, because the shaft used in the first and second tests was the same and it was also expected to suffer wear in some level. The wear of the shaft is considered negligible in this work as it is significantly harder when compared to the bearing materials and this wear would not be noticeable in the measurement equipment used in the research.

The rotation limit increased 2.4% for the conrod and 1.95% for the main bearings after 5,000 starts in test 1 and 1.98% and 1.57% after 30,000 starts in test 2. The higher increase in conrods is justified by the higher wear calculated for conrod bearings in comparison to the main bearings. The increase was supposed to be higher for 30,000 starts than for 5,000 starts, as deeper bearing wear was expected. However, as already discussed in section 4.2, it is believed that almost no further wear occurred after 5,000 starts because no stop time between starts was foreseen in the program, leaving no time for the oil to flow back to the oil pan and disrupt the fluid film. In this case, when the fluid film is already built up, the analysis of load application to disrupt the fluid film can be perfectly applied. Then, the contact between bearing and shaft could have occurred when the limit rotation was reached, in very seldom occasions, as seen in tables from 4.7 to 4.14. Even when the limit rotation is reached, there is no guarantee that direct contact occurs, because in the elastohydrodynamic regime, the load can influence more on a future contact, but the counter faces not necessarily touch. Furthermore, the calculation of rotation limit increase is based on the bearing dimensional measurements, associated with high uncertainties.

Table 4.8 - Rotation Comparison in the Conrod Bearings – Before Test 2

14565782K1		14565782K4		14565782K6	
Rotation	Limit Rotation	Rotation	Limit Rotation	Rotation	Limit Rotation
1/s	1/s	1/s	1/s	1/s	1/s
72,9	61,7	72,9	62,5	72,9	64,6
79,2	57,3	79,2	58,1	79,2	60,0
79,4	35,4	79,4	35,9	79,4	37,1
76,3	33,6	76,3	34,0	76,3	35,2
69,6	33,6	69,6	34,0	69,6	35,2
44,3	28,8	44,3	29,2	44,3	30,2
63,7	60,4	63,7	61,2	63,7	63,3
74,8	55,4	74,8	56,2	74,8	58,1
78,8	33,6	78,8	34,0	78,8	35,2
77,3	33,6	77,3	34,0	77,3	35,2
73,9	33,6	73,9	34,0	73,9	35,2
58,5	76,5	58,5	77,5	58,5	80,2
70,4	58,6	70,4	59,3	70,4	61,4
77,6	40,6	77,6	41,1	77,6	42,5
78,5	33,6	78,5	34,0	78,5	35,2
75,5	33,6	75,5	34,0	75,5	35,2

Table 4.9 - Rotation Comparison in the Main Bearings – Before Test 2

14565835K1		14565835K2		14565835K3		14565835K4		14565835K5		14565835K6		14565835K7	
Rotation	Limit Rotation	Rotation	Limit Rotation	Rotation	Limit Rotation	Rotation	Limit Rotation	Rotation	Limit Rotation	Rotation	Limit Rotation	Rotation	Limit Rotation
1/s	1/s	1/s	1/s	1/s	1/s	1/s	1/s	1/s	1/s	1/s	1/s	1/s	1/s
72,9	10,4	72,9	10,6	72,9	10,5	72,9	10,6	72,9	10,6	72,9	10,5	72,9	10,0
79,2	9,7	79,2	9,9	79,2	9,8	79,2	9,8	79,2	9,8	79,2	9,8	79,2	9,3
79,4	6,0	79,4	6,1	79,4	6,0	79,4	6,1	79,4	6,1	79,4	6,1	79,4	5,7
76,3	5,7	76,3	5,8	76,3	5,7	76,3	5,7	76,3	5,8	76,3	5,7	76,3	5,4
69,6	5,7	69,6	5,8	69,6	5,7	69,6	5,7	69,6	5,8	69,6	5,7	69,6	5,4
44,3	4,9	44,3	5,0	44,3	4,9	44,3	4,9	44,3	4,9	44,3	4,9	44,3	4,7
63,7	10,2	63,7	10,4	63,7	10,3	63,7	10,3	63,7	10,4	63,7	10,3	63,7	9,8
74,8	9,3	74,8	9,6	74,8	9,5	74,8	9,5	74,8	9,5	74,8	9,5	74,8	9,0
78,8	5,7	78,8	5,8	78,8	5,7	78,8	5,7	78,8	5,8	78,8	5,7	78,8	5,4
77,3	5,7	77,3	5,8	77,3	5,7	77,3	5,7	77,3	5,8	77,3	5,7	77,3	5,4
73,9	5,7	73,9	5,8	73,9	5,7	73,9	5,7	73,9	5,8	73,9	5,7	73,9	5,4
58,5	12,9	58,5	13,2	58,5	13,1	58,5	13,1	58,5	13,1	58,5	13,1	58,5	12,4
70,4	9,9	70,4	10,1	70,4	10,0	70,4	10,0	70,4	10,0	70,4	10,0	70,4	9,5
77,6	6,8	77,6	7,0	77,6	6,9	77,6	7,0	77,6	7,0	77,6	6,9	77,6	6,6
78,5	5,7	78,5	5,8	78,5	5,7	78,5	5,7	78,5	5,8	78,5	5,7	78,5	5,4
75,5	5,7	75,5	5,8	75,5	5,7	75,5	5,7	75,5	5,8	75,5	5,7	75,5	5,4

The calculation presented in this section is helpful to understand how the load application and rotation can influence on the lubrication regime of the bearings, and hence, the probability of wear occurrence. However, as seen by the measurement uncertainties calculation, the bearing measurements were not accurate enough, leading to several uncertainties in the lubrication regime determination. Also, the calculations just determine if the bearings are under hydrodynamic lubrication or not, there is no clarification if they are in Elastohydrodynamic or boundary lubrication, what can make extreme difference in the wear behavior.

The determination of the load application in all bearings presented many simplifications. The disregard of friction forces is not accurate, as a significate amount of the energy produced in the combustion is lost because of friction losses in the engine. In TLPP, although the functioning differs from a regular combustion engine, the friction factor must be considered for more accurate results. Moreover, the load distribution for the main bearings can only be really estimated with the use of computational aid.

Several instrumentations can be used in the bearings to determine during all the operation time the fluid film thickness in real time. With this kind of instrumentation, more accurate results on wear speed, alteration of wear speed when new bearing layers are reached, fluid thickness variation, and determination of lubrication regime during the whole operation time can be determined.

However, even with all possible instrumentation, it is believed that, due to the complexity of the problem, faster developments would be obtained associating the experimental studies to computational simulation, as conducted by the bearing manufacturer MIBA (Priestner *et al.*, 2012; Allmaier *et al.*, 2013). It is important to emphasize that all previous research was conducted with just one hydraulic cylinder applying load in a bearing pair, and never before the whole engine structure was used to simulate wear in real engine conditions.

Table 4.10 - Rotation Comparison in the Conrod Bearings – After Test 2

14567913K1		14567913K4		14567913K6	
Rotation	Limit Rotation	Rotation	Limit Rotation	Rotation	Limit Rotation
1/s	1/s	1/s	1/s	1/s	1/s
72,9	63,0	72,9	63,7	72,9	66,0
79,2	58,5	79,2	59,2	79,2	61,2
79,4	36,2	79,4	36,6	79,4	37,9
76,3	34,3	76,3	34,7	76,3	35,9
69,6	34,3	69,6	34,7	69,6	35,9
44,3	29,4	44,3	29,8	44,3	30,8
63,7	61,7	63,7	62,4	63,7	64,6
74,8	56,6	74,8	57,3	74,8	59,3
78,8	34,3	78,8	34,7	78,8	35,9
77,3	34,3	77,3	34,7	77,3	35,9
73,9	34,3	73,9	34,7	73,9	35,9
58,5	78,1	58,5	79,0	58,5	81,8
70,4	59,8	70,4	60,5	70,4	62,6
77,6	41,5	77,6	41,9	77,6	43,4
78,5	34,3	78,5	34,7	78,5	35,9
75,5	34,3	75,5	34,7	75,5	35,9

Table 4.11 - Rotation Comparison in the Main Bearings – After Test 2

14565835K1		14565835K2		14565835K3		14565835K4		14565835K5		14565835K6		14565835K7	
Rotation	Limit Rotation	Rotation	Limit Rotation	Rotation	Limit Rotation	Rotation	Limit Rotation	Rotation	Limit Rotation	Rotation	Limit Rotation	Rotation	Limit Rotation
1/s	1/s	1/s	1/s	1/s	1/s	1/s	1/s	1/s	1/s	1/s	1/s	1/s	1/s
72,9	10,6	72,9	10,8	72,9	10,7	72,9	10,7	72,9	10,7	72,9	10,8	72,9	10,2
79,2	9,8	79,2	10,0	79,2	9,9	79,2	10,0	79,2	10,0	79,2	10,0	79,2	9,4
79,4	6,1	79,4	6,2	79,4	6,1	79,4	6,2	79,4	6,2	79,4	6,2	79,4	5,8
76,3	5,8	76,3	5,9	76,3	5,8	76,3	5,8	76,3	5,8	76,3	5,9	76,3	5,5
69,6	5,8	69,6	5,9	69,6	5,8	69,6	5,8	69,6	5,8	69,6	5,9	69,6	5,5
44,3	4,9	44,3	5,0	44,3	5,0	44,3	5,0	44,3	5,0	44,3	5,0	44,3	4,7
63,7	10,4	63,7	10,6	63,7	10,5	63,7	10,5	63,7	10,5	63,7	10,5	63,7	10,0
74,8	9,5	74,8	9,7	74,8	9,6	74,8	9,6	74,8	9,6	74,8	9,7	74,8	9,1
78,8	5,8	78,8	5,9	78,8	5,8	78,8	5,8	78,8	5,8	78,8	5,9	78,8	5,5
77,3	5,8	77,3	5,9	77,3	5,8	77,3	5,8	77,3	5,8	77,3	5,9	77,3	5,5
73,9	5,8	73,9	5,9	73,9	5,8	73,9	5,8	73,9	5,8	73,9	5,9	73,9	5,5
58,5	13,1	58,5	13,4	58,5	13,3	58,5	13,3	58,5	13,3	58,5	13,3	58,5	12,6
70,4	10,0	70,4	10,3	70,4	10,2	70,4	10,2	70,4	10,2	70,4	10,2	70,4	9,7
77,6	7,0	77,6	7,1	77,6	7,0	77,6	7,1	77,6	7,1	77,6	7,1	77,6	6,7
78,5	5,8	78,5	5,9	78,5	5,8	78,5	5,8	78,5	5,8	78,5	5,9	78,5	5,5
75,5	5,8	75,5	5,9	75,5	5,8	75,5	5,8	75,5	5,8	75,5	5,9	75,5	5,5

4.6 Wear Calculation

The Archard equation, presented in section 2.2.3, is a rough wear estimation, correlating the wear rate, the normal load, the hardness of the softer surface and the dimensionless wear coefficient. As also explained in this section, a useful parameter obtained by this equation is the dimensional wear coefficient *k*, correspondent to the ratio between the dimensionless wear coefficient and the surface hardness. This coefficient represents the volume of material removed by wear (mm3) per unit of normal load (N) per distance slid (m), can be used to compare wear rates in different materials and is determined by Equation 4.1

$$k = \frac{Q}{W} \tag{4.1}$$

Considering the average wear thickness in the loaded bearings (upper CB and lower MB) and the geometry parameters of the bearings, the worn volume during operation was calculated. Considering the diameter of the bearing and the average of 6 revolutions per start, the sliding distance was also calculated. According to the graphics of load application in the TLPP program, the average load in each cylinder during the whole operation was 0,35% of the maximum load peak during a start. Knowing all these parameters, the dimensional wear coefficient was calculated for the bearings of the first and second test and the results are shown in Table 4.12.

Table 4.12 - Dimensional Wear Coefficient for Loaded bearing in the first and second test

Shaft Position	**14519493K1**		**14519493K2**	
	Main bearing	**Conrod bearing**	**Main bearing**	**Conrod bearing**
	k	***k***	***k***	***k***
	(mm³/Nm)	(mm³/Nm)	(mm³/Nm)	(mm³/Nm)
1	31,9	5,5	3,9	0,8
2	21,9	5,5	3,5	0,4
3	25,9	4,9	3,5	0,6
4	21,4	3,5	3,4	0,6
5	27,5	3,8	3,4	0,5
6	21,6	3,6	4,9	0,6
7	26,5	0,0	3,1	0,0

The dimensional wear coefficients calculated in the table prove that the use of Archard application in this kind of operation is not recommended, as it is normally used for wear estimation when counter bodies are fully in contact, and not sometimes divided by a fluid film. This explains the difference of values among the coefficients, there were supposed to be the same, as the same material was used for the loaded bearings in both tests.

These results, however, are important for 2 analysis: the difference between values found for the main and conrod bearing coefficient and the difference between the results of the first and second test. The difference between the coefficient of the main and conrod bearings lies just on the load application difference that for the main bearing is

1/7 of the conrod bearing. These results prove that this load distribution is not correct and emphasize the need of computational tools to obtain the exact load application.

The difference between the coefficients obtained in the first and second test lies on the lubrication. Although the second test had 6 times the sliding distance when compared to the first test, as already said, it is believed that after a certain operation time, the fluid film between bearings and shaft was completely built up, avoiding the contact between surfaces and wear.

The determination of the fluid film thickness and consequently the lubrication regime during the whole test operation, as suggested in the previous subsection, can be also helpful to determine the dimensional wear coefficient of bearing materials. With the determination of the exact moments when contact between counter bodies occur, the load and sliding distance can be determined just for these moments, and the volume worn out could be related to these dimensions to determine the real dimensional wear thickens and evaluate the best bearing material in a test.

4.7 Third Test

After analyzing the problems presented in the first program, mainly related to the lack of time for the fluid film between bearing and shaft to be dissipated, a new test program was built with the exact load pattern, but with a stop time between starts of 5s, as in the EST program, as shown in Figure 4.22. Figure 4.23 shows the conrod and main beaings after the third test. In this figure the wear seen in the lower main bearings 1 and 7 increased when compared to the bearings of the first two test, as well as the wear in the upper conrod bearings 1, 4 and 7. Furthermore, wear in other main bearings can be seen, This was expected, as the operation time increased and the lubrication decreased with the standstill time between starts.

The wear results are presented in Table 4.13 in the same way they were presented for the first tests. In this test the bearing set is called 14519493K3 and the upper main, lower main, upper conrod and lower conrod bearings are respectively called 14565812K, 14565835K, 14565782K and 14565756K, followed by the number corresponded to their positioning.

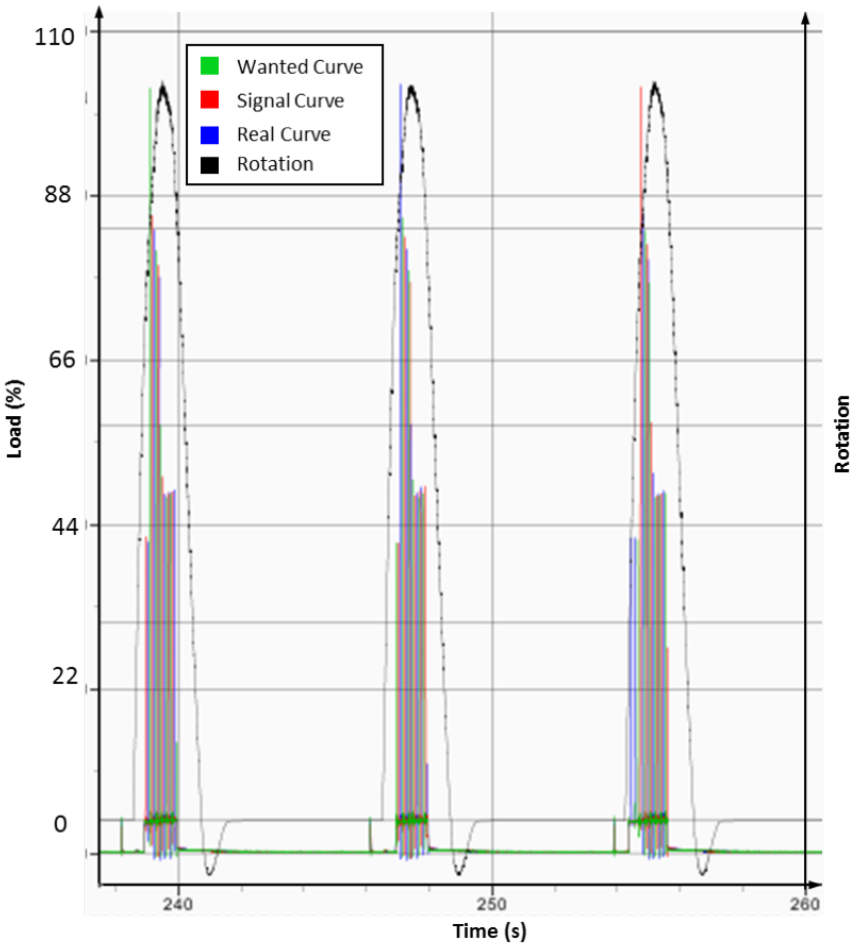


Figure 4.22 - Second TLPP Program

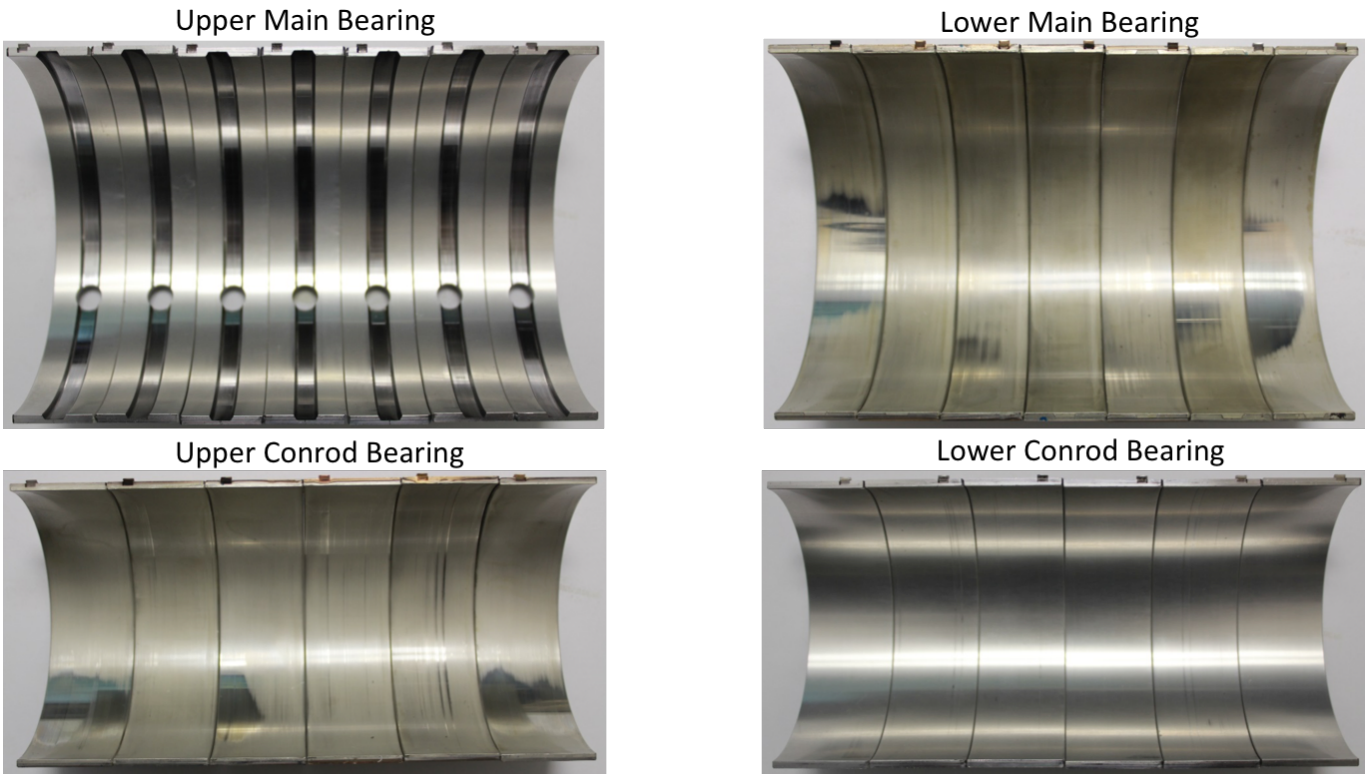


Figure 4.23 - Bearings after test 3

Table 4.13 - Wear results of the third test

14519493K3														
Main bearings							Conrod bearings							
Upper main bearing			Lower main bearing				Upper conrod bearing				Lower conrod bearing			
Upper measuring track	Lower measuring Track	Average	Upper measuring track	Middle measuring track	Lower measuring Track	Average	Upper measuring track	Middle measuring track	Lower measuring Track	Average	Upper measuring track	Middle measuring track	Lower measuring Track	Average
(mm)	(mm)	(mm)	(mm)	(mm)	(mm)	(mm)	(mm)	(mm)	(mm)	(mm)	(mm)	(mm)	(mm)	(mm)
14567916K1			14567917K1				14567913K1				14567912K1			
0,0007	0,0005	0,0006	0,0007	0,0006	0,0006	0,0006	0,0016	0,0015	0,0026	0,0019	0,0009	0,0006	0,0003	0,0006
0,0004	0,0005	0,0004	0,0032	0,0022	0,0011	0,0021	0,0011	0,0006	0,0006	0,0008	0,0004	0,0004	-0,0003	0,0002
-0,0004	0,0005	0,0001	0,0006	0,0008	0,0006	0,0007	0,0005	0,0001	0,0006	0,0004	0,0004	0,0005	0,0006	0,0005
0,0002	0,0005	**0,0004**	0,0015	0,0012	0,0007	**0,0011**	0,0011	0,0007	0,0013	**0,0010**	0,0005	0,0005	0,0002	**0,0004**
14567916K2			14567917K2				14567913K2				14567912K2			
0,0006	0,0010	0,0008	0,0009	0,0004	0,0006	0,0007	0,0001	0,0011	0,0012	0,0008	0,0008	0,0004	0,0002	0,0005
0,0004	0,0004	0,0004	0,0003	0,0054	0,0004	0,0020	0,0014	-0,0004	0,0000	0,0004	0,0003	0,0003	0,0003	0,0003
0,0003	0,0004	0,0003	0,0005	0,0005	0,0005	0,0005	0,0010	0,0009	-0,0005	0,0005	0,0000	0,0006	0,0010	0,0005
0,0004	0,0006	**0,0005**	0,0005	0,0021	0,0005	**0,0011**	0,0008	0,0006	0,0003	**0,0006**	0,0004	0,0004	0,0005	**0,0004**
14567916K3			14567917K3				14567913K3				14567912K3			
0,0008	0,0006	0,0007	0,0009	0,0010	0,0009	0,0009	0,0008	0,0002	0,0004	0,0005	0,0010	0,0006	0,0010	0,0008
0,0008	0,0003	0,0005	0,0007	0,0006	0,0004	0,0006	0,0007	0,0009	0,0009	0,0008	0,0004	0,0005	0,0005	0,0004
0,0001	0,0003	0,0002	0,0008	0,0006	0,0002	0,0005	0,0000	0,0008	0,0008	0,0005	0,0003	0,0003	0,0004	0,0003
0,0006	0,0004	**0,0005**	0,0008	0,0007	0,0005	**0,0007**	0,0005	0,0006	0,0007	**0,0006**	0,0005	0,0005	0,0006	**0,0005**
14567916K4			14567917K4				14567913K4				14567912K4			
0,0010	0,0010	0,0010	0,0011	0,0009	0,0008	0,0009	0,0005	0,0014	0,0021	0,0013	0,0007	0,0008	0,0008	0,0008
0,0010	0,0001	0,0005	0,0002	-0,0041	0,0004	-0,0012	0,0000	-0,0004	0,0000	-0,0002	0,0003	0,0005	0,0002	0,0004
0,0001	0,0000	0,0000	0,0006	0,0005	0,0006	0,0006	0,0005	-0,0008	0,0004	0,0000	-0,0002	-0,0003	0,0012	0,0003
0,0007	0,0004	**0,0005**	0,0006	-0,0009	0,0006	**0,0001**	0,0003	0,0001	0,0008	**0,0004**	0,0003	0,0003	0,0008	**0,0005**
14567916K5			14567917K5				14567913K5				14567912K5			
0,0013	0,0011	0,0012	0,0011	0,0019	0,0023	0,0018	-0,0005	0,0001	-0,0008	-0,0004	0,0011	0,0022	0,0012	0,0015
0,0010	0,0006	0,0008	0,0013	0,0006	0,0015	0,0011	0,0005	-0,0003	0,0004	0,0002	0,0007	0,0004	-0,0002	0,0003
0,0012	0,0008	0,0010	0,0029	0,0029	0,0029	0,0029	-0,0024	-0,0005	0,0001	-0,0009	-0,0018	-0,0012	-0,0005	-0,0012
0,0012	0,0009	**0,0010**	0,0018	0,0018	0,0022	**0,0019**	-0,0008	-0,0002	-0,0001	**-0,0004**	0,0000	0,0004	0,0001	**0,0002**
14567916K6			14567917K6				14567913K6				14567912K6			
0,0007	0,0007	0,0007	0,0008	0,0009	0,0006	0,0008	0,0009	0,0010	0,0020	0,0013	0,0006	0,0006	0,0010	0,0007
-0,0002	0,0008	0,0003	0,0002	0,0003	0,0002	0,0002	0,0001	0,0010	0,0000	0,0004	0,0001	0,0004	-0,0003	0,0001
0,0002	0,0007	0,0004	0,0003	0,0002	0,0008	0,0004	0,0010	-0,0004	-0,0003	0,0001	0,0004	0,0004	0,0009	0,0005
0,0002	0,0007	**0,0005**	0,0004	0,0005	0,0005	**0,0005**	0,0006	0,0005	0,0006	**0,0006**	0,0004	0,0005	0,0005	**0,0004**
14567916K7			14567917K7											
0,0003	0,0008	0,0005	0,0007	0,0008	0,0009	0,0008								
0,0006	-0,0003	0,0001	0,0015	0,0013	0,0004	0,0011								
0,0006	0,0001	0,0003	0,0002	0,0009	0,0004	0,0005								
0,0005	0,0002	**0,0003**	0,0008	0,0010	0,0006	**0,0008**								

This test, however, presented very similar wear when compared to the first two tests, which lead to the deeper analysis of the wear profiles obtained before and after tests in the most loaded region of the bearings. For this analysis the upper conrod bearing 1 was considered, as it is one of the 3 bearings which receive the higher loads, and hence, are expected to be most severely worn out. Figure 4.24 presents a conrod bearing profile before testing, and it is seem that the component comes from the manufactures presenting a regular roughness, with peaks and valleys of coating measuring approximately 2 µm. The Figures 4.25 to 4.27 presented the conrod bearings after the tests 1, 2 and 3 respectively. It is clearly seem by this profiles that the surface presents more wear from test one to two and even more wear from test two to three, in which the coating is completely worn out and the surface is homogeneously flat.

It is them believed that, the measuring tip during bearing thickness measurements can fall even in a peak of in a valley of the bearing coating, leading to a 2µm inaccuracy of the bearing thickness. Hence, to obtain valid results, the coatings should be completely worn out so that the initial 2 µm measurement inaccuracy would not be a problem.

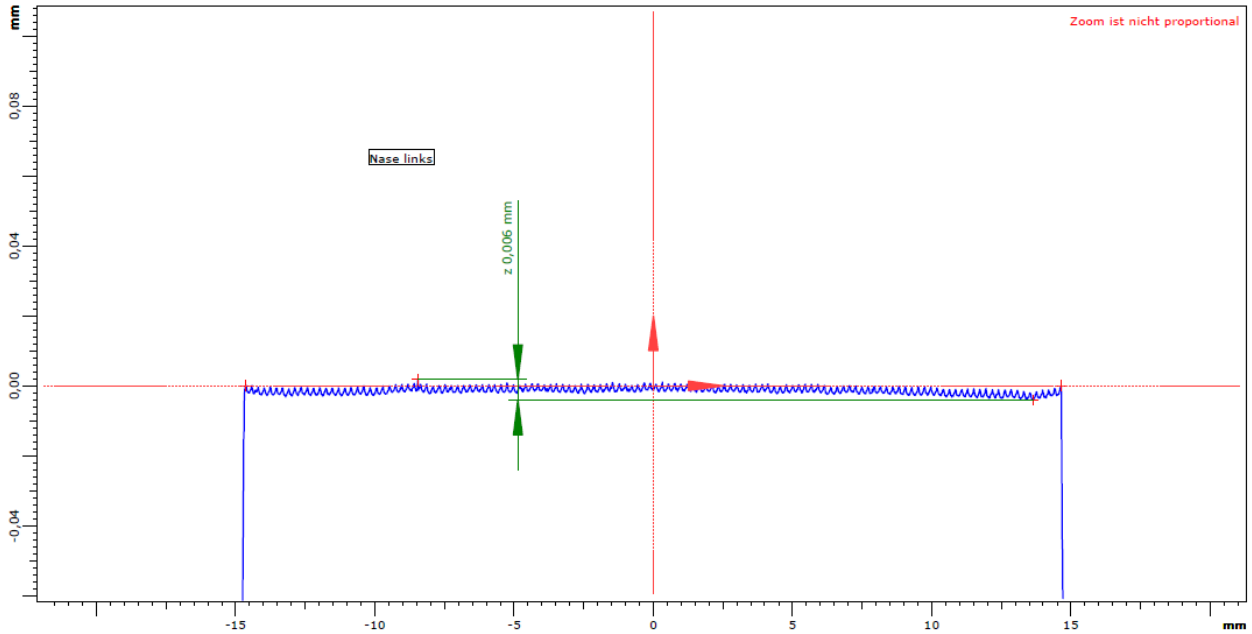


Figure 4.24 - Conrod bearing profile before test

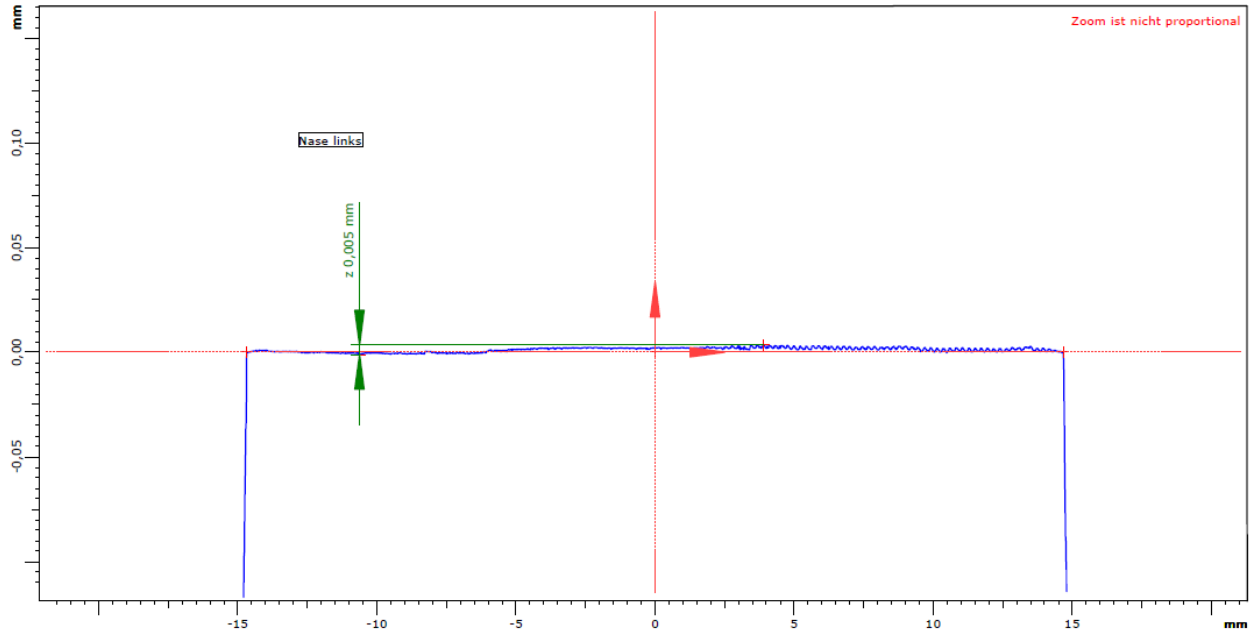


Figure 4.25 - Conrod bearing profile after test 1

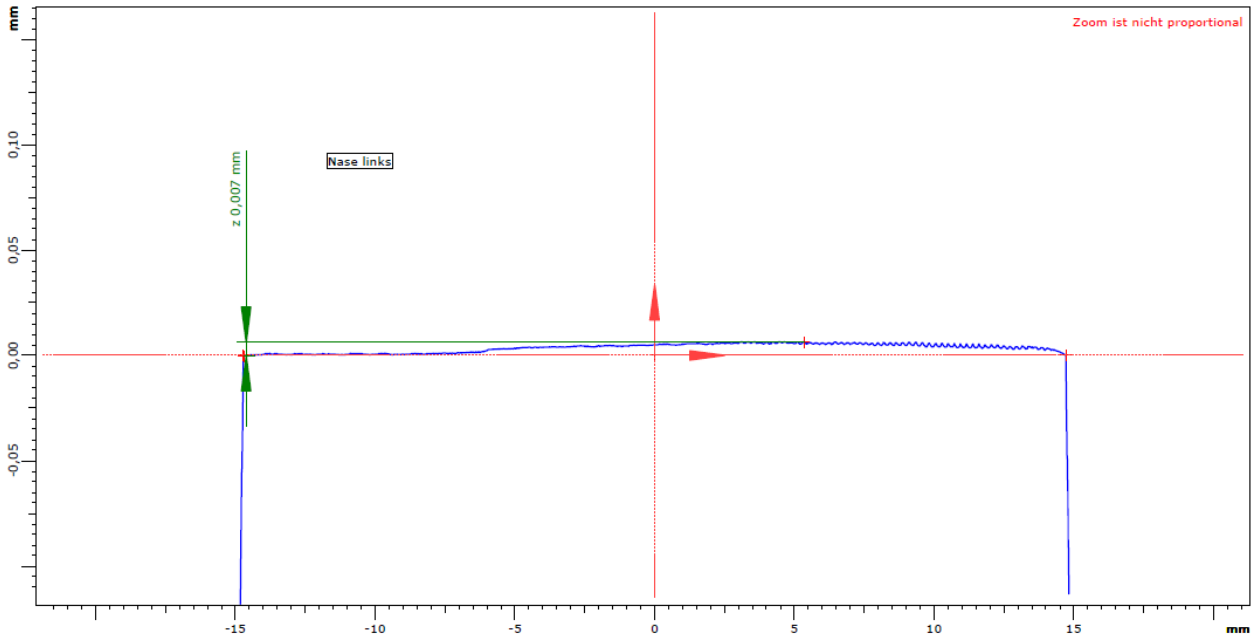


Figure 4.26 - Conrd bearing profile after test 2

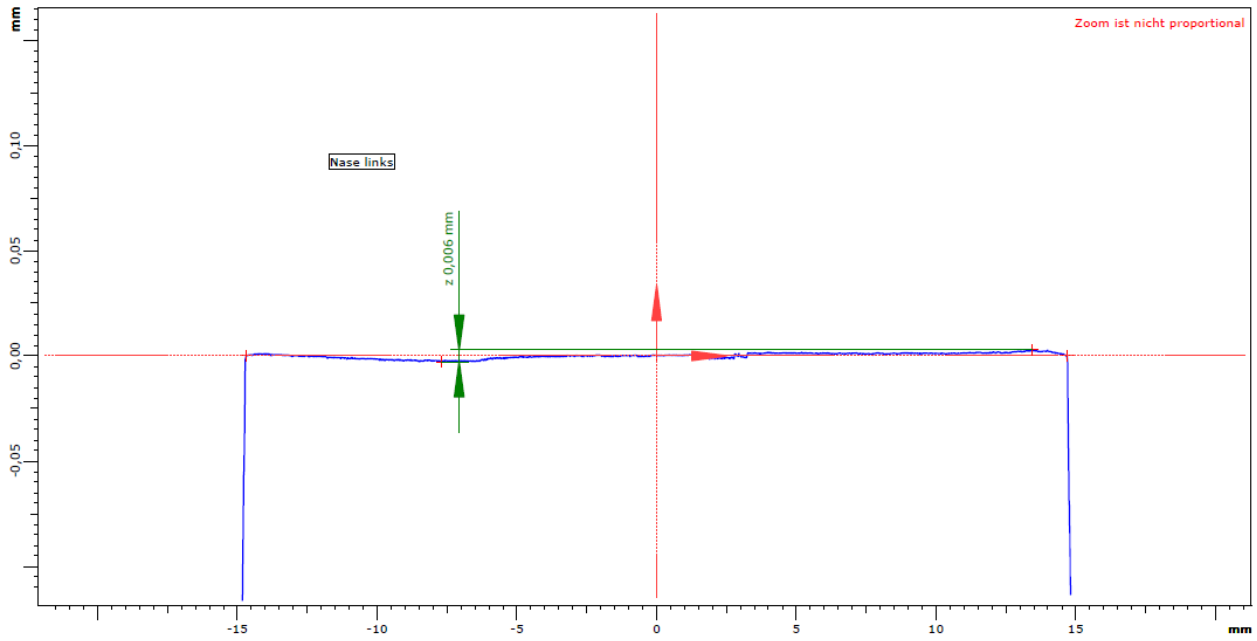


Figure 4.27 - Conrod bearing profile after test 3

4.8 New Test Program

During the course of TLPP implementation several problems have presented themselves. After the design and production of special components, the test bench was assembled and automatized by external companies. A new project like this is both challenging for the automation companies and for the intern Daimler personal, which take some time to adapt to the new concept and computational tools. Moreover, during the quest to find an appropriate operation program for TLPP, the second test proposed presented various obstacles due to lack of data acquisition capacity.

With the need to increase the number of starts performed in the least possible time, together with the need to develop simpler programs for the system to have the capacity to acquire the test data, a simplified program was developed. In a previous work also regarding this theme (Nebelsiek, 2017), it was considered that energy input of a cylinder in an engine starting, calculated through the integral the cylinder pressure curve, was responsible for the break or inhibition of a proper fluid film, and hence, was the main cause of wear. In this work, TLPP could be used not only to reproduce individually the combustion loads though an engine start, but to use the theory of the energy input. Under this assumption, the program cycle presented in Figure 4.28 was developed.

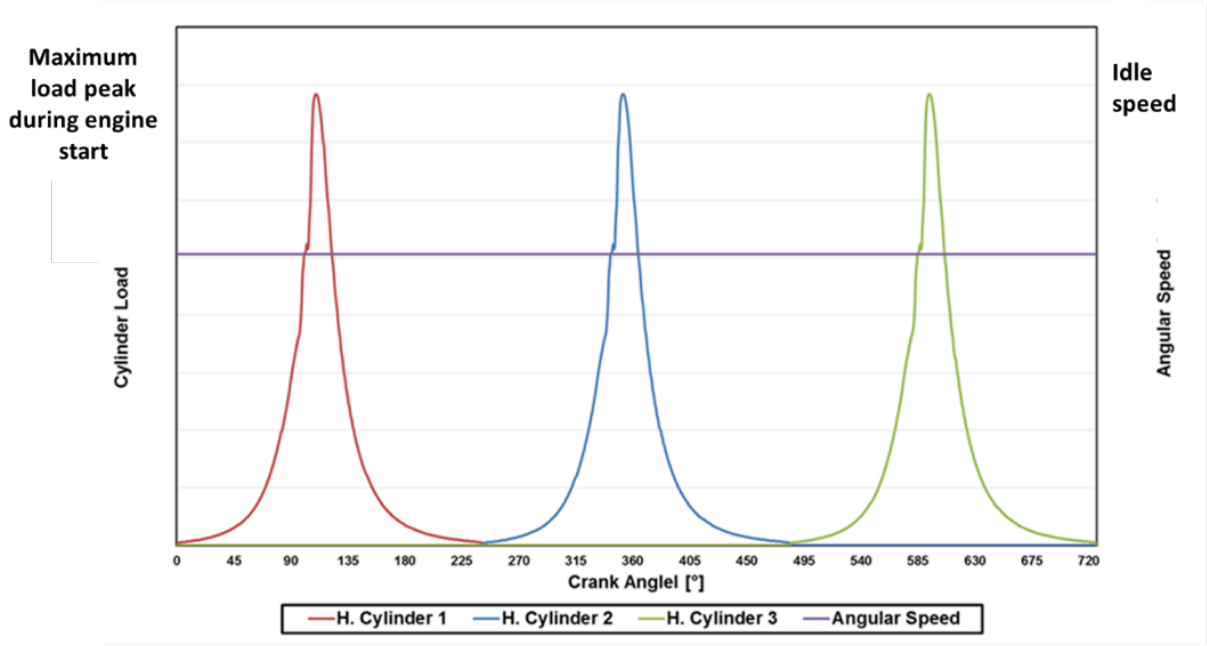


Figure 4.28 - TLPP program - Simplified engine start, Credits: Adapted from (Nebelsiek, 2017)

To obtain a better approximation of this program to a real operational engine, 5 rotational plateaus were considered, and after a cycle, a ramp of 1 second is applied to reach the other rotational speed. After reaching the 5th plateau, the individual plateaus are run again in reverse order, as shown in Figure 4.29.

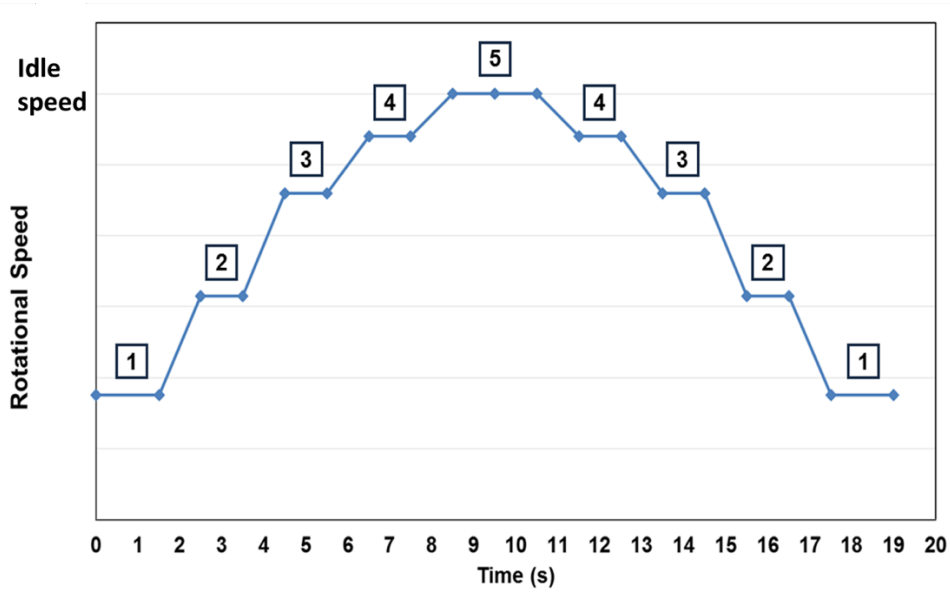


Figure 4.29 - Engine cycle with Rotational Speed Plateaus, Credits: (Nebelsiek, 2017)

This program, although being a simplified version of the first program, do not represent the oil pressure build up in the EST engine, a crucial parameter for the tribological analysis conducted so far and hence, will not represent the bearing wear process. Considering, however, that with sufficient stop time between the starts to break the fluid film, and that a start lasts less than the 3 seconds necessary for the oil film build up, TLPP can operate at all times either at boundary or elastohydrodynamic lubrication regime, when contact between counter bodies actually occur.

In that situation, the total energy input for the cylinder pairs 2 and 5, 4 and 3 and 1 and 6, which are represented respectively by the hydraulic cylinders 1, 2 and 3 during a start were calculated. Considering 100kN the highest load application of the hydraulic cylinders used, 80kN were stipulated as a safety load and the time each hydraulic cylinder would have to be maintained at 80kN to totalize the energy application for a cylinder pair was calculated. The new simplified test program will than simulate just one load application per hydraulic cylinder during a start, as the rotation increases to 750rpm, as shown in Figure 4.30. The time between loads applications are irrelevant and dependent on the program capability. The time for the engine to stop rotating after the completion of load applications is also irrelevant, as shown in previous RNT research. The most important in this program is the 5 second time between starts so that the lubricant can go back to the oil sump and that at each start the cylinder order is altered, so that the load application of each cylinder occurs in different rotational speeds.

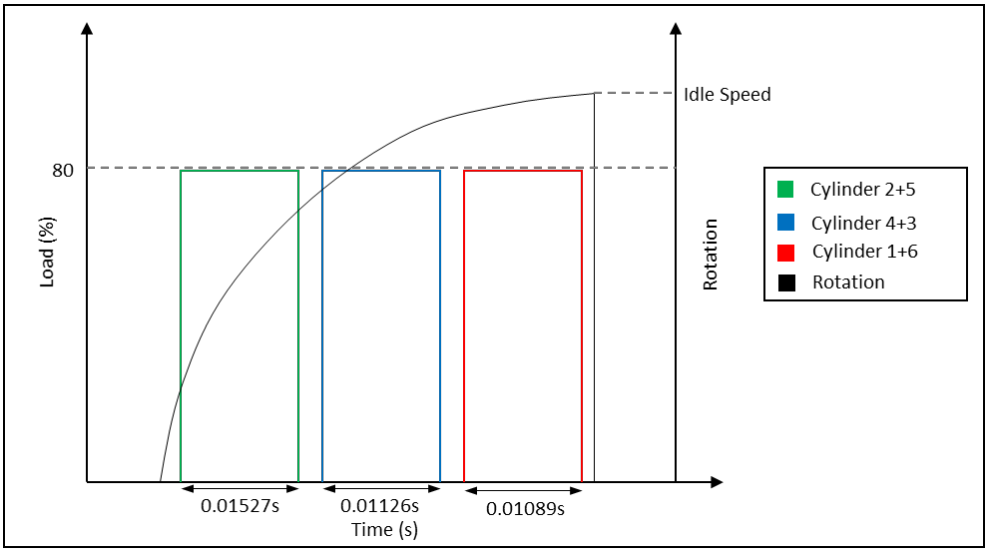


Figure 4.30 - Simplified TLPP Test Program 1

Using the energy input idea developed in Figure 4.30, and aiming to reduce testing time, as more number of starts should be tested so that the measurement inaccuracy of the measuring instruments will not impact on the results, Figure 4.31 presents the suggested new test program. The idea of this test is that a start can simulate 20 engine starts. In this concept the start time can be determined and for each cycle in each start one cylinder should start first, so that all bearings could experience the same wear levels, as also proposed for the other test programs.

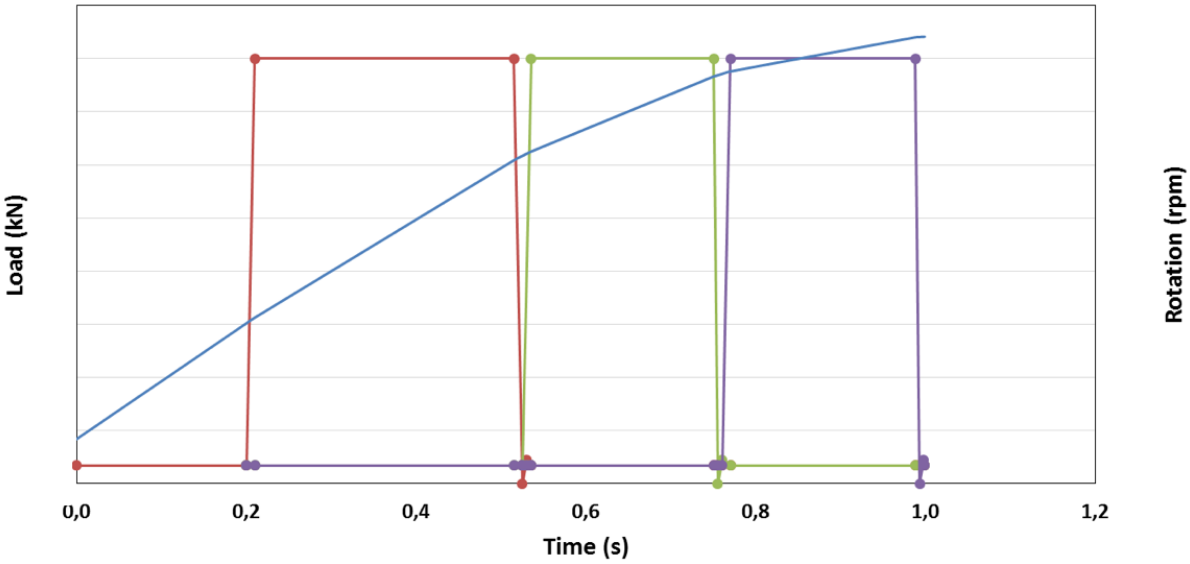


Figure 4.31 -Simplified TLPP Test Program 2

5 CONCLUSION

The main objectives stablished in the beginning of this work, regarding the acknowledgement of the component test bench importance, comparison of ICE and TLPP results and determination of development strategies for these new systems were accomplished.

During the test program development, the main conclusion was about the importance to create a test program capable to simulate Elastohydrodynamic or boundary lubrication in the drive train bearings. The regular engines take longer for being started and stopped, and in order to safe time in the component test benches, the first program operating in TLPP did not consider the stop time between starts. This program design, although decreased sensibly the overall test time, did not produce the expected wear, as the lack of this stop time does not leave time for the lubricant oil to flow back to the oil sump, as it generally occurs in a regular engine, causing the break of the fluid film and consequently increased wear.

After discovering the importance of the stop time between starts, a new simplified test program, based on the first program was developed, in order to reduce testing time and facilitate the data acquisition, based on the energy input given by each cylinder during a start, considering now, that the bearing-shaft contact would starve on lubrication during the whole operation time.

The results obtained in the first stage of the test bench implementation lead to the conclusion that the measuremnt equipment used in the work is not appropiate, as it presents the measuremnt incurancy in the same order of magnitude as the wear observed. That appoints to either the use of more accurate measuremnt equipment or the increase of test time, so that the wear observed increases and can be duly measured with the equipment availabe. The bearing materials, lubrication, operation temperatures and test bench instrumentation used in this research are however satisfactory and recommended for further testing.

Moreover, the work discusses the importance to use more appropriate tools and instrumentation to measure wear and the fluid film thickness during the test bench operation and associate this data to numerical simulation. With this association, the lubrication regime would be easily determined and methods such as the determination of the dimensional wear coefficient could be used to qualify the best bearing materials for the start-stop applications. Thus, the limitations of the system so far were discussed and strategies to minimize them were explored, completing the objectives stablished for the present work.

In general, despite the TLPP need for several further improvements, its use can be very important in the future for research in component wear not only in bearings, and simulating not only the start-stop systems, but also hybrid systems demanding less time and expenses than regular combustion engine tests.

6 SUGGESTIONS FOR FUTURE RESEARCH

In relation to the continuity of this work, the following activities are suggested:

- Variation of the stop time in the TLPP program and compare the wear results obtained by these other programs and the one tested in this work;
- Testing of other programs, that include more than just the start of an engine until idle, but take TLPP to different rotations and operation points during a start, and compare the wear results obtained by these other programs and the one tested in this work;
- Perform TLPP and EST test with similar configuration and with more frequent stops to dimensional analysis, in order to trace a wear profile of the bearings, validating TLPP. The data could be also compared to the data to the obtained during the previous RNT research;
- Work in parallel with the EST engine and TLPP
- Variate oil types and operation temperatures, to analyze their real impact in wear. In parallel, discuss the benefits brought by the use of oil with better behaviors concerning wear, also considering its use to the whole engine operation life time;
- Study the impact of the oil bores and channels in the shaft used in TLPP and what will be an optimum design to best simulate the same oil distribution of an engine crankshaft;
- Compare bearing materials using TLPP;
- Study wear in different engine components using TLPP;
- Association of TLPP results to computational simulations.

7 REFERENCES

AFFENZELLER, J.; GLÄSER, H. **Lagerung und Schmierung von Verbrennungsmotoren**. Springer-Verlag, 2013. ISBN 3709165687.

ALLMAIER, H. et al. Predicting friction reliably and accurately in journal bearings–The importance of extensive oil-models. **Tribology international,** v. 48, p. 93-101, 2012. ISSN 0301-679X.

Predicting friction reliably and accurately in journal bearings—extending the EHD simulation model to TEHD. **Tribology international,** v. 58, p. 20-28, 2013. ISSN 0301-679X.

Predicting friction reliably and accurately in journal bearings—A systematic validation of simulation results with experimental measurements. **Tribology International,** v. 44, n. 10, p. 1151-1160, 2011. ISSN 0301-679X.

ANTRIEBSTECHNIK, I. **Verschleißanalysen an den lagern der Daimler MDEG-Motoren für Motorstart-Stopp-Automatik (Bericht 0110010170053)** IAVF Antriebstechnik 2013.

ARCHARD, J. Contact and rubbing of flat surfaces. **Journal of applied physics,** v. 24, n. 8, p. 981-988, 1953. ISSN 0021-8979.

BARTEL, D. et al. Simulating transient wear characteristics of journal bearings subjected to mixed friction. **Proceedings of the Institution of Mechanical Engineers, Part J: Journal of Engineering Tribology,** v. 226, n. 12, p. 1095-1108, 2012. ISSN 1350-6501.

BARWELL, F. Theories of wear and their significance for engineering practice. In: (Ed.). **Treatise on Materials Science & Technology**: Elsevier, v.13, 1979. p.1-83. ISBN 0161-9160.

BATES, T. VISCOSITY CLASSIFICATION: with special reference to SAE J300. **Industrial Lubrication and Tribology,** v. 38, n. 1, p. 4-40, 1986. ISSN 0036-8792.

BAUMANN, B. M. et al. Mechatronic design and control of hybrid electric vehicles. **IEEE/ASME Transactions On Mechatronics,** v. 5, n. 1, p. 58-72, 2000. ISSN 1083-4435.

BAÊTA, J. G. C. **Metodologia Experimental para a Maximização do Desempenho de um Motor**
Multicombustível Turboalimentado sem Prejuízo à Eficiência Energética Global. 2006: Departamento de Engenharia Mecânica, Universidade Federal de Minas Gerais 2006.

BECKER, E. P. Trends in tribological materials and engine technology. **Tribology International,** v. 37, n. 7, p. 569-575, 2004. ISSN 0301-679X.

BOVINGTON, C.; KORCEK, S.; SORAB, J. The importance of the Stribeck curve in the minimisation of engine friction. **Tribology Series,** v. 36, p. 205-214, 1999. ISSN 0167-8922.

BOWDEN, F. P.; TABOR, D. **The friction and lubrication of solids**. Oxford university press, 2001. ISBN 0198507771.

CANOVA, F.; SALA, L. Back to square one: Identification issues in DSGE models. **Journal of Monetary Economics,** v. 56, n. 4, p. 431-449, 2009. ISSN 0304-3932.

CHAN, C. C. The state of the art of electric, hybrid, and fuel cell vehicles. **Proceedings of the IEEE,** v. 95, n. 4, p. 704-718, 2007. ISSN 0018-9219.

CLAUSTHAL, T. **Pin-on-disc Test**: TU Clausthal 2018.

CZICHOS, H. Failure criteria in thin film lubrication: investigation of the different stages of film failure. **Wear,** v. 36, n. 1, p. 13-17, 1976. ISSN 0043-1648.

DAIMLER. **Under the Microscope: ECO Start/Stop: Sophisticated technology gives the highest levels of efficiency** 2011.

DANIEL, G. B.; CAVALCA, K. L. Analysis of the dynamics of a slider–crank mechanism with hydrodynamic lubrication in the connecting rod–slider joint clearance. **Mechanism and Machine Theory,** v. 46, n. 10, p. 1434-1452, 2011. ISSN 0094-114X.

DE OLIVEIRA AGUIAR, S. et al. Avaliação das emissões de escapamento veicular em condições específicas do motor: partida e marcha-lenta. **Transportes,** v. 23, n. 3, p. 35-43, 2015. ISSN 2237-1346.

DOWSON, D.; HIGGINSON, G.; WHITAKER, A. Elasto-hydrodynamic lubrication: a survey of isothermal solutions. **Journal of Mechanical Engineering Science,** v. 4, n. 2, p. 121-126, 1962. ISSN 0022-2542.

FAIZ, A.; WEAVER, C. S.; WALSH, M. P. **Air pollution from motor vehicles: standards and technologies for controlling emissions**. The World Bank, 1996. ISBN 0821334441.

FANG, L.; QIN, S. Optimal control of parallel hybrid electric vehicles based on theory of switched system. **Asian Journal of Control,** v. 8, n. 3, p. 274-280, 2006. ISSN 1561-8625.

FILLON, M.; BOUYER, J. Thermohydrodynamic analysis of a worn plain journal bearing. **Tribology international,** v. 37, n. 2, p. 129-136, 2004. ISSN 0301-679X.

FLORADAY, P. **"Want stop-start technology on your next vehicle? Lobby the EPA"**: Automobile Magazine 2009.

FONSECA, N.; CASANOVA, J.; VALDES, M. Influence of the stop/start system on CO2 emissions of a diesel vehicle in urban traffic. **Transportation Research Part D: Transport and Environment,** v. 16, n. 2, p. 194-200, 2011. ISSN 1361-9209.

GEBRETSADIK, D. W.; HARDELL, J.; PRAKASH, B. Friction and wear characteristics of different Pb-free bearing materials in mixed and boundary lubrication regimes. **Wear,** v. 340, p. 63-72, 2015. ISSN 0043-1648.

Seizure behaviour of some selected Pb-free engine bearing materials under lubricated condition. **Tribology International,** v. 111, p. 265-275, 2017. ISSN 0301-679X.

GLOBAL, G. **Connecting rods**: Garima Global Website 2018.

GMBH, M. Gleitlager. **Zylinderkomponenten: Eigenschaften, Anwendungen, Werkstoffe**, p. 49-69, 2009. ISSN 3834804371.

GRÜN, F. et al. Tribological performance of thin overlays for journal bearings. **Tribology International,** v. 44, n. 11, p. 1271-1280, 2011. ISSN 0301-679X.

GURKAYNAK, Y.; KHALIGH, A.; EMADI, A. State of the art power management algorithms for hybrid electric vehicles. Vehicle Power and Propulsion Conference, 2009. VPPC'09. IEEE, 2009, IEEE. p.388-394.

HAMROCK, B. J.; SCHMID, S. R.; JACOBSON, B. O. **Fundamentals of fluid film lubrication**. CRC press, 2004. ISBN 1135537763.

HANEEF, M. et al. Vibration and wear prediction analysis of IC engine bearings by numerical simulation. **Wear,** v. 384, p. 15-27, 2017. ISSN 0043-1648.

HERKERT, B. Verschleißmessungen mit Hilfe von Radionukliden nach dem Durchflußmeßverfahren. 1975.

HEXAGON. **Visualise This! Design and Inspection Go Hand-in-Hand**: Hexagon Website 2018.

HEYWOOD, J. B. **Internal combustion engine fundamentals**. Mcgraw-hill New York, 1988.

HUTCHINGS, I.; SHIPWAY, P. **Tribology: friction and wear of engineering materials**. Butterworth-Heinemann, 2017. ISBN 0081009518.

HÄRING, J. **IROX II - Neue Hochleistungspollymerbeschichtung für Gleitlager**: VDI Wissenforum 2018.

JUNG, D.-H. et al. Reliability prediction of the fatigue life of a crankshaft. **Journal of mechanical science and technology,** v. 23, n. 4, p. 1071-1074, 2009. ISSN 1738-494X.

KAGOHARA, Y. et al. Tribological property of plain bearing with low frictional layer. **Tribology International,** v. 42, n. 11-12, p. 1800-1806, 2009. ISSN 0301-679X.

KATAFUCHI, T.; KASAI, M. Effect of base stocks on the automobile engine bearing. **Tribology International,** v. 42, n. 4, p. 548-553, 2009. ISSN 0301-679X.

KATAOKA, K.; TSUJI, K. **Crankshaft positioning utilizing compression force and fast starting with combustion assist for indirect injection engine**. SAE Technical Paper. 2005. (0148-7191)

KERIMOV, N. A.; MEKTIEV, R. I. **Engines with Stratified Charge**. SAE Technical Paper. 1978. (0148-7191)

KING, A. **Non friction**: Chemistry & Industry News 2012.

KUANG, M. L. **An investigation of engine start-stop NVH in a power split powertrain hybrid electric vehicle**. SAE Technical Paper. 2006. (0148-7191)

LEET, K. M.; UANG, C. M.; GILBERT, A. M. **Fundamentos da Análise Estrutural-3**. AMGH Editora, 2014. ISBN 8563308343.

LTD, F. J. E. **Perkins 6.354 Crankshaft**: F&J Export Ltd Website 2019.

MAHLE. Gleitlager. **Zylinderkomponenten: Eigenschaften, Anwendungen, Werkstoffe**, p. 49-69, 2009. ISSN 3834804371.

MAHR. **Marsurf VD 280 Roughness and Contour Measuring Station**: Mahr website 2019.

MANUAL, B. Bearing Group Miba. **Miba Gleitlager AG**, 2000.

MARTINEZ, J. S. et al. Practical control structure and energy management of a testbed hybrid electric vehicle. **IEEE Transactions on Vehicular Technology,** v. 60, n. 9, p. 4139-4152, 2011. ISSN 0018-9545.

MATERIALS, O. R. G. O. W. O. E. **Friction, Wear and Lubrication - Tribology of Terms and Definition**: OECD 1969.

MEDEIROS DE ARAÚJO NUNES, V.; PAIVA DE MENEZES, R. M.; ALCHIERI, J. C. Avaliação da qualidade de vida em idosos institucionalizados no município de Natal, Estado do Rio Grande do Norte. **Acta Scientiarum. Health Sciences,** v. 32, n. 2, 2010. ISSN 1679-9291.

MEYER, C. **The Council of Europe, Conservation, and Environmental Concern**: Cambridge University Press 1990.

NEBELSIEK, S. **Auslegung einer Methodik zur Verschleißermittlung an Triebwerkslagern**: Hochschule Esslingen - University of Applied Sciences 2017.

NIKOLIC, N.; TOROVIC, T.; ANTONIC, Z. A procedure for constructing a theoretical wear diagram of IC engine crankshaft main bearings. **Mechanism and Machine Theory,** v. 58, p. 120-136, 2012. ISSN 0094-114X.

NORMUNG, D. I. F. **DIN 50320: Verscheiss - Begriff, Analyse von Verschleissvorgängen, Gliederung des Verschleissgebietes**: Beuth Verlag 1979.

OLYAEI, A. A.; GHAZAVI, M. R. Stabilizing slider-crank mechanism with clearance joints. **Mechanism and Machine Theory,** v. 53, p. 17-29, 2012. ISSN 0094-114X.

OTHERS, W. H. O. A. U. A. **Air quality guidelines: global update 2005**: World Health Organization 2006.

OZDEMIR, A.; MUGAN, A. Stop/Start System Integration to Diesel Engine and System Modelling & Validation. **IFAC Proceedings Volumes,** v. 46, n. 25, p. 95-100, 2013. ISSN 1474-6670.

POWERTRAIN, F. M. **Application Engineering FM Bearings**: Federal Mogul Powertrain 2010.

Application Engineering Bearings: Federal Mogul Powertrain 2016.

PRATT, G. C. Materials for plain bearings. **International Metallurgical Reviews,** v. 18, n. 2, p. 62-88, 1973. ISSN 0367-9020.

PRIEST, M.; TAYLOR, C. Automobile engine tribology—approaching the surface. **Wear,** v. 241, n. 2, p. 193-203, 2000. ISSN 0043-1648.

PRIESTNER, C. et al. Refined simulation of friction power loss in crank shaft slider bearings considering wear in the mixed lubrication regime. **Tribology International,** v. 46, n. 1, p. 200-207, 2012. ISSN 0301-679X.

RETTER. **Probe Test Unit**: Retter Website 2018.

RIZZONI, G.; GUZZELLA, L.; BAUMANN, B. M. Unified modeling of hybrid electric vehicle drivetrains. **IEEE/ASME transactions on mechatronics,** v. 4, n. 3, p. 246-257, 1999. ISSN 1083-4435.

ROGOWSKI, A. R. **Elements of Internal Combustion Engines**: McGraw-Hill 1953.

RUEGER, J. Clean Diesel-Real Life Fuel Economy and Environmental Performance. SAE Government and Industry Meeting, Washington, DC, 2008.

RYK, G.; KLIGERMAN, Y.; ETSION, I. Experimental investigation of laser surface texturing for reciprocating automotive components. **Tribology Transactions,** v. 45, n. 4, p. 444-449, 2002. ISSN 1040-2004.

SALMASI, F. R. Control strategies for hybrid electric vehicles: Evolution, classification, comparison, and future trends. **IEEE Transactions on vehicular technology,** v. 56, n. 5, p. 2393-2404, 2007. ISSN 0018-9545.

SALVINDER, S.; SHAHRUM, A.; MOHAMED, N. A. N. Discretized Markov chain in damage assessment using Rainflow cycle with effects of mean stress on an automobile crankshaft. **Journal of Mechanical Science and Technology,** v. 30, n. 8, p. 3539-3551, 2016. ISSN 1738-494X.

SCHERGE, M.; PÖHLMANN, K.; GERVÉ, A. Wear measurement using radionuclide-technique (RNT). **Wear,** v. 254, n. 9, p. 801-817, 2003. ISSN 0043-1648.

STACHOWIAK, G.; BATCHELOR, A.; STOLARSKI, T. **Engineering tribology: Elsevier, 1993, ISBN 0-444-89235-4, 960 pp,£ 156.00**: Elsevier 1994.

SUN, J. et al. Effect of surface roughness, viscosity-pressure relationship and elastic deformation on lubrication performance of misaligned journal bearings. **Industrial Lubrication and Tribology,** v. 66, n. 3, p. 337-345, 2014. ISSN 0036-8792.

SUN, S.-S. et al. Component structural equivalent research based on different failure strength criterions and the theory of critical distance. **Engineering Failure Analysis,** v. 70, p. 31-43, 2016. ISSN 1350-6307.

TAMBELLINI, L.; OLIVEIRA, L.; TSUBOUCHI, M. **Bearing Fundamentals**: MAHLE Metal Leve S.A., GEA-B 2007.

TAYLOR, C. Automobile engine tribology—design considerations for efficiency and durability. **Wear,** v. 221, n. 1, p. 1-8, 1998. ISSN 0043-1648.

TAYLOR, C. F. **The Internal-combustion Engine in Theory and Practice: Combustion, fuels, materials, design**. MIT press, 1985. ISBN 0262700271.

TAYLOR, R. Transient effects in engines operating at steady speeds & loads. In: (Ed.). **Tribology Series**: Elsevier, v.43, 2003. p.123-131. ISBN 0167-8922.

TUNG, S. C.; MCMILLAN, M. L. Automotive tribology overview of current advances and challenges for the future. **Tribology International,** v. 37, n. 7, p. 517-536, 2004. ISSN 0301-679X.

UICKER, J. J.; PENNOCK, G. R.; SHIGLEY, J. E. **Theory of machines and mechanisms**. Oxford University Press New York, NY, 2011.

VAN BASSHUYSEN, R.; SCHÄFER, F. **Internal combustion engine handbook-basics, components, systems and perspectives**. 2004. ISBN 0768011396.

VAN BERKEL, K. et al. Optimal control of a mechanical hybrid powertrain. **IEEE Transactions on Vehicular Technology,** v. 61, n. 2, p. 485-497, 2012. ISSN 0018-9545.

WALKER, J.; KAMPS, T.; WOOD, R. The influence of start–stop transient velocity on the friction and wear behaviour of a hyper-eutectic Al–Si automotive alloy. **Wear,** v. 306, n. 1-2, p. 209-218, 2013. ISSN 0043-1648.

WILLIAMS, M. A. M., R. **A Technical Summary of Euro 6/VI Vehicle Emission Standards**: ICCT International council on clean transportation 2016.

WORLD, C. **Crankshaft and piston assembly**: Cycle World Website 2018.

WU, L. J.; LI, A. P.; LIU, X. M. Modeling and simulation of a slider-crank mechanism with clearance and lubricant joint. Advanced Materials Research, 2012, Trans Tech Publ. p.458-466.

XU, L. X.; HAN, Y. C. A method for contact analysis of revolute joints with noncircular clearance in a planar multibody system. **Proceedings of the Institution of Mechanical Engineers, Part K: Journal of Multi-body Dynamics,** v. 230, n. 4, p. 589-605, 2016. ISSN 1464-4193.

ZADOROZHNAYA, E.; LEVANOV, I.; OSKINA, O. Study of HTHS Viscosity of modern motor oils. **Procedia Engineering,** v. 150, p. 602-606, 2016. ISSN 1877-7058.

ZHANG, Y. et al. High strength tin-based overlay for medium and high speed diesel engine bearing tribological applications. **Tribology International,** v. 93, p. 687-695, 2016. ISSN 0301-679X.

ZUM-GAHR, K. H. Microstructure and wear of materials. Institute of Materials Technology. **University of Siegen, Siegen, Federal Republic of Germany,** v. 10, 1987.

ZUMBÜHL, H. **Motoren - Ein Buch über Wärmekraftmaschinen und ihre Brennstoffe**: SDV-Fachbücher 1946.

ANNEX 1

Bearing description

This annex presents the specifications of the bearings used in this work

A370

Bearing manufactured by Federal Mogul, with average cost. Figure 7.2 presents a metallographic analysis of the bearing and highlights its 2 layers deposited in a steel back. The composition and width of each layer are presented in Table 7.1. The thickness of the aluminum layer is 0.2-0.3 mm.

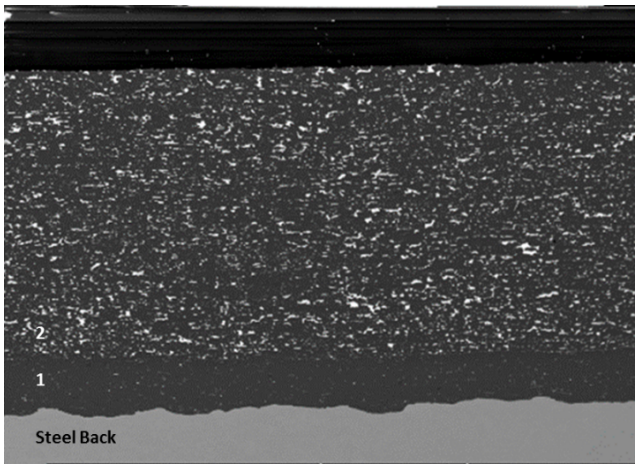


Figure 7.1 - Bearing A370 Composition

Table 7.1 - Bearing A370 Composition

Bearing layer	Composition
1	Al
2	$AlSn_{20}CuMn$

G488

Bearing manufactured by Federal Mogul, with average cost. Figure 7.3 presents a metallographic analysis of the bearing and highlights its 4 layers deposited in a steel back. The composition of each layer is presented in Table 7.2. The coating has an average width of 11-12 μm for MB, 10-11μm for CB. The thickness of the bronze layer is 0.2-0.3 mm and the galvanic coating is 20±4μm.

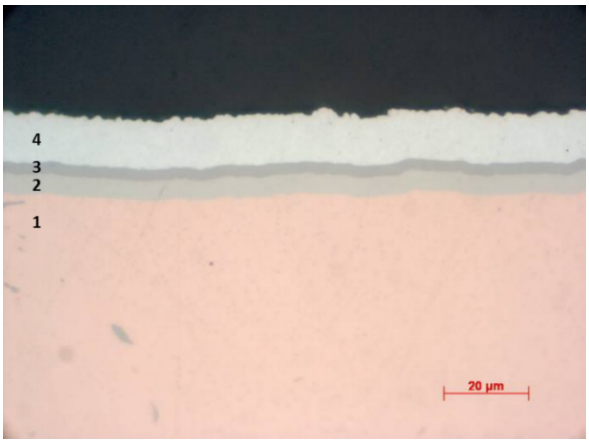


Figure 7.2 - Bearing G488 Composition

Table 7.2 - Bearing G488 Composition

Bearing layer	Composition
1	$CuNi_2Si$
2	Ni
3	NiSn
4	$SnCu_6$